acta physica slovaca vol. 64 No. 4, 401 – 466 **August 2014**

TOP QUARK PHYSICS AFTER THE FIRST PHASE OF LHC[1]

Stanislav Tokár[2]
Department of Nuclear Physics and Biophysics, Comenius University, Bratislava, Slovakia

Received 19 May 2015, in final form 26 May 2015, accepted 27 May 2015

The latest experimental results concerning the top quark physics obtained by the experiments at Large Hadron Colliders using the data produced in proton-proton collisions at $\sqrt{s} = 7$ and 8 TeV are shown. The data were collected by the ATLAS detector in 2011 (7 TeV) and 2012 (8 TeV) with the integrated luminosity of 4.9 fb^{-1} and 21 fb^{-1} and the CMS detector at the same collision energies with the integrated luminosity of 5 fb^{-1} and 20 fb^{-1}, respectively. The results on different aspects of the top quark studies including searches of physics beyond the Standard Model are also reported. No signs of physics beyond the Standard Model has been found so far.

DOI: 10.2478/apsrt-2014-0004

PACS: 14.65.Ha, 14.70.Dj, 14.70.Fm, 12.60.Jv

KEYWORDS: Top Quark, Single Top Quark, Higgs Boson, Vacuum Instability, Anomalous Couplings, Forward-Backward Asymmetry, Flavour Changing Neutral Currents, Jet Charge

Contents

[1]Post-processing corrections were made by the author in the title.
[2]E-mail address: Stanislav.Tokar@cern.ch

1 Introduction

The Large Hadron Collider (LHC) project [1] has started a new era of particle physics. The high collision energy available at LHC (7-14) GeV together with the high luminosity ($\sim 10^{34}$ cm^{-2}s^{-1}) allow progress to be made in investigation of the main challenges of particle physics such as the status of the Higgs boson, precision tests of the Standard Model (SM) [2, 3, 4, 5], searches for physics beyond the Standard model (BSM). In the era before LHC in the elementary particle physics there exist a very good agreement between the experiment and the theoretical prediction of the SM. The existence of all fundamental fermions as well of all vector bosons mediating the electromagnetic, weak and strong interactions has been experimentally confirmed in perfect agreement with the hypothesis that there are just three generations of particles. The only missing part of the SM was the so-called Higgs sector which in the SM is represented by one neutral particle – Higgs boson. On the other hand existence of the Higgs boson is a critical part of the SM as according the SM the fundamental particles acquire their masses through interaction with the Higgs field which has a non-zero vacuum expectation value (VEV). It is just the non-zero VEV which is responsible for non-zero particle masses. Mechanism of the mass acquirement through interaction of particle fields with Higgs field which has non-zero VEV, called Brout-Englert-Higgs mechanism (or shortly Higgs mechanism) [6, 7, 8, 9], is responsible for breaking of electroweak symmetry (EWSB). The EWSB along with gauge symmetries (see e.g. [10]) is a base of the SM and many theoretical models going beyond the SM. Discovery of a new boson with properties compatible with the SM Higgs boson announced in July 2012 by the ATLAS [11] and the CMS [12] collaborations, not only has fulfilled the last missing part of the SM, but it is one of the most significant discoveries of particle physics and physics as a whole.

With the Higgs boson being experimentally confirmed, the SM is firmly established as the dominant theory of particle physics. The prediction of the SM are in excellent agreement with experiment – deviations of observables of the quantum chromodynamics (QCD) and electroweak (EW) theory, from their measured values are within the theoretical and experimental uncertainties [13]. Nonetheless, despite of its great success, the SM is generally considered as only an effective theory valid at presently available energies. The reason is that it has a range of shortcomings. The SM does not have answers to global questions like the questions concerning the dark matter, the baryon asymmetry or dark energy, it does not include gravitation, it does not explain the hierarchy of the fundamental fermion masses, the number of generations and moreover it has some conceptual problems, like the naturalness problem of the Higgs boson mass, which cannot be satisfactorily solved within the SM frame. As a consequence a series of theoretical conceptions going beyond the SM have been created. The most important among them are models based on supersymmetry (SUSY) [14, 15, 16], on models with extra dimensions [17, 18] and technicolors models [19].

The first phase of LHC, which studied proton-proton (pp) collisions at centre-of-mass energies of 7 and 8 TeV, has finished accumulating data with size of around 5 fb^{-1} at $\sqrt{s}$ = 7 TeV and with size of around 20 fb^{-1} at $\sqrt{s}$ = 8 TeV. The obtained experimental information has enabled not only the discovery of the Higgs boson but also significantly expanded the limits of the validity of the SM and thereby to widen the region of exclusion of new physics, i.e. Beyond the Standard Model (BSM) physics.

In the search for a manifestation of a BSM physics, a special role is played by processes with top quarks. Many BSM physics scenarios, if occur, could change significantly these processes.

The BSM physics could significantly modify the forward - backward asymmetry and the spin correlation in $t\bar{t}$ production, the size of the top quark decay width, the polarization of W bosons from the top quark decays, the coupling of top quark to W boon and b-quark (Wtb coupling), etc. The description of the results of the ATLAS and CMS studies of processes with top quarks is the main goal of this contribution.

The present paper is organized as follows: in Sec. 2 is presented a basics information about the Standard Model with an emphasis on the top quark physics. Within this section is also discussed the heritage of the Tevatron experiments. A short description of the LHC accelerator and the ATLAS and CMS experiments is given in Sec. 3. In Sec. 4, which has seven subsections, are discussed the main top quark physics topics starting with the importance of top quark physics for tests of the SM and for searches of a new physics. The core of this paper is survey of the latest results of the ATLAS and CMS experiments, obtained in the first phase of LHC at centre-of-mass energies 7 and 8 TeV, and also the Tevatron experiments on the top quark cross sections, the top quark mass and other top quark properties. Finally, Sec. 5 contains a short summary of the paper topics.

2 Standard model – present status

At present the Standard Model, developed mostly in the seventies, is the theory describing the fundamental particles and their interactions. The SM comprises of two basic components:

- theory of electroweak interactions describing electromagnetic and weak processes,
- quantum chromodynamics (QCD) which is theory of strong interactions describing interactions between hadron components.

In both the cases one has to do with gauge theories, in base of which are Lagrangians with $SU(2)_{\rm L} \otimes U(1)_{\rm Y}$ symmetry[3] (theory of electroweak interactions) and with $SU(3)_{\rm c}$ symmetry[4] (theory of strong interactions). Hence, the SM includes processes with the electromagnetic, weak and strong interactions but does not include processes with gravitational force. Within the SM description of basic processes in the nature is based on existence of three sectors of particles:

- Fundamental fermions – three generations of leptons and quarks which are basic constituents of the nature discrete structures like nucleons, atoms, etc.
- Intermediate bosons, i.e. force-carrier particles – the fundamental forces present in the nature result from the exchange of these boson between interacting particles.
- Higgs particles – Importance of the Higgs sector is in the fact that after spontaneously symmetry breaking the vacuum mean value of Higgs field has non-zero value (Higgs condensate is created) and it is just interaction of particle fields with the Higgs condensate which gives masses to particles.

The fundamental particles of the SM are shown in Fig. 2.1. As it has been already mentioned from experimental point of view the SM is remarkably successful. The cross sections of the mentioned fundamental interactions are described very well. All the expected particles of the SM, including Higgs boson, are experimentally confirmed. In the first phase of LHC the Higgs boson, its properties – mainly its couplings to other SM particles, were of a predominant interest of the studies at the LHC. It is really very important to find out if the Higgs boson is really the particle of the SM which introduces a new non-gauge interaction leading to spontaneous symmetry breaking or it is something else - e.g. an composed object. The studies carried out up to now suggest that the new boson discovered by ATLAS and CMS has its properties fully compatible with the SM Higgs boson. An important task is to continue in tests of the SM - refinement of its parameters, study of the CP-violating phenomena, etc. Such tests require predominantly to study the physics of heavy quarks (b, t) and are closely connected with searches of BSM physics. As it has been already mentioned, the SM in spite of its success, has a series of deficiencies which should be overcome to get more proper picture of the nature. Among the deficiencies of the SM are:

- A big number of free parameters: the SM has in its minimal version, which assumes three generations of particles, non-zero neutrino masses and CP conservation in strong interactions, 25 free parameters.

[3]The index L means that symmetry is valid only for the left components of fermion fields, Y is the hypercharge.

[4]The index c means that its a colour charge mixing group of the strong interactions.

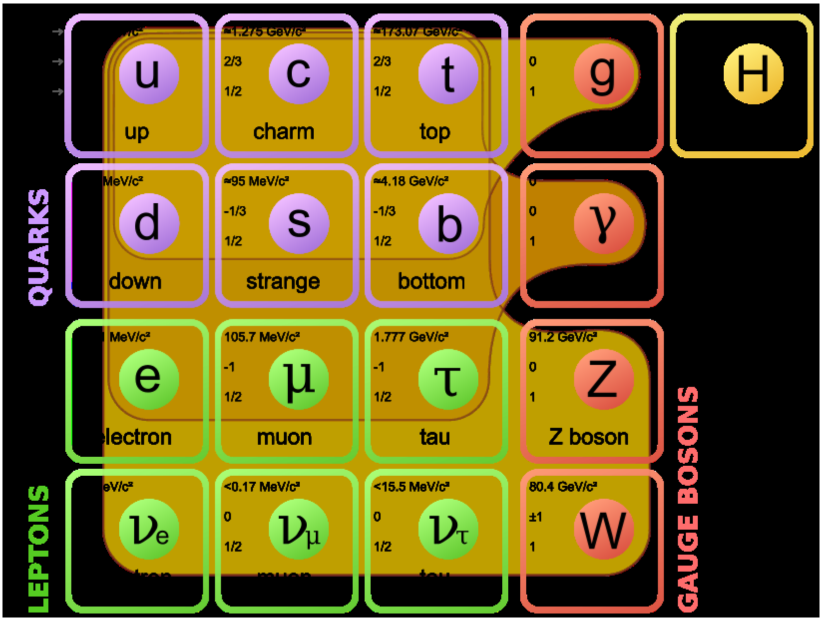

Fig. 2.1. Fundamental particles of the Standard model.

- It dos not explain hierarchy of particle masses. The ratio of the heaviest (*top*) and lightest quark (u) is about 10^5 and the ratio of the heaviest fermion and lightest fermion (neutrino) is more than 10^{11}.
- Question of the CP-violation origin is not explained satisfactorily.
- It has no answer to the question on the number of fundamental particle generations.
- It does not include gravitation - it means cannot give a full picture of nature.
- It has no explanation for dark matter, dark energy or baryon asymmetry.
- There is no natural explanation for the problem of naturalness of Higgs boson mass.

These deficiencies have led to creation of manifold extensions of the SM as well as to creation of completely new conceptions. Among them are so-called GUT-theories (Grand Unification Theories) which unify not only the electromagnetic and weak interactions but includes also the strong interactions [20, 21]. The most simple GUT is based on symmetry $SU(5)$ and contains the group of the SM symmetries ($SU(2)_{\mathrm{L}} \otimes U(1)\mathrm{Y} \otimes SU(3)_{\mathrm{c}}$) as its subgroup.

There are also theoretical conceptions which enable spontaneous violation of symmetry without Higgs mechanism (Technicolor). Quantum Technicolor Dynamics (QTD) [19] introduces new strong interactions and a new set of fermion fields – technifermions (doublet of fields as a minimum). Instead of the condensate of scalar Higgs field there is a condensate of the technifermion pairs which spontaneously breaks the symmetry and gives masses to particles. At present the main theoretical conceptions are models based on supersymmetry (SUSY) [14,15,16] and models based on the idea of extra dimensions (ED) [17, 18], which are inspired by the theory of superstrings [22, 23, 24]. The SUSY is based on fermion-boson symmetry and its goal is unification of all types of interaction including the gravitation. Unification of gauge forces with exchanged boson of spin 2 (graviton) with those of spin 1 (gluons, photon, W and Z bosons) is carried out within a supersymetry, i.e. the symmetry which generators transform bosons to fermions and *vice-versa*. A very fancy theory is supergravitation (SUGRA) [25]. It is a theory where the supersymmetry is a local (and not a global) symmetry. The ED models assumes existence of extra dimensions which are compactified. The compactification radius, R, can be very small, at a level of Planck length ($l_{\rm P} = \sqrt{\hbar/G_{\rm N}/c^3}$, $\hbar$ is Planck constant, c – speed of light, $G_{\rm N}$ – Newton gravitation constant), but they can be also sufficiently big to lower Planck scale ($M_{\rm P} = \sqrt{\hbar c/G_{\rm N}}$) for the space with extra dimensions to the level o 1 TeV [17]. An attractive features of both these approaches is the fact that they offer solution for the naturalness problem, they have candidate for the dark matter and they include the gravitation.

Probably the most ambitious theory in the elementary particle field is the theory of superstrings, first of all its latest variant – M-theory [24], which pretends to be theory of everything. The basic object of this theory is one- and more-dimensional object called superstring, which can be in different vibration modes (mass states in local quantum field theory). Base space of the superstrings is a 10^{th} or 11^{th} dimensional space. Wherein the extra dimensions give rise to gauge and other symmetries observed in our four-dimensional world.

2.1 Top quark physics and the Tevatron heritage

This paper deals with the top quark physics which appears as one of the most important front lines of the present particle physics. It is generally believed that study of the top quark processes is probably the most important pathway to test the SM and to search for a new physics. Before analyzing the results that have been obtained by the LHC experiments on the field of the top quark physics, it is inevitable to mention an excellent top quark physics heritage from the Tevatron experiments. The Tevatron collider was an accelerator with colliding beams of protons and antiprotons ($p\bar{p}$) collisions accelerating particles to centre-of-mass energy $\sqrt{s}$ = 1.8 TeV (Run I phase, 1986–1996) and $\sqrt{s}$ = 1.96 TeV (Run II phase, 2001–2011) and located at Fermilab (Batavia, near Chicago, USA). The Tevatron experiments CDF [26] and D0 [27] have given (and still give) a huge contribution to the top quark physics. These experiments not only discovered the top quark [28, 29] but also have measured basic characteristics of the top quark processes like the top quark mass, top quark production cross sections and other top quark properties. The survey of the top quark physics results as well as the results concerning other fields of particle physics (Higgs boson, electroweak processes, QCD, etc.) can be found at web sides of the CDF [30] and D0 [31] experiments.

3 The Large Hadron Collider

The Large Hadron Collider (LHC) [1] is the worlds largest and most powerful particle accelerator built from 1998 to 2008 at CERN, in the 27 km long circular underground tunnel on the France-Switzerland border near Geneva. It has been designed to collide two opposing particle beams either of protons, with a centre-of-mass energy $\sqrt{s} = 14$ TeV and a luminosity of 10^{34} cm^{2}s^{-1}, or lead ions with energy 2.8 TeV per nucleon and a peak luminosity of 10^{27}. Bunches of these particles interact at four interaction points along the collider, which correspond to the four main particle detectors (experiments): ATLAS, CMS, ALICE and LHCb.

To provide proton beams to the LHC a whole set of accelerators (Fig. 3.1) is used. Protons are obtained from molecular hydrogen by breaking it down into individual atoms and stripping the electrons. Afterwards they are passed into the linear accelerator LINAC2 and small circular accelerator Proton Synchrotron Booster (PSB), which has four separate rings. In each ring one bunch of approximately 10^{11} protons is accelerated by electric fields until it reaches energy 1.4 GeV per proton. Magnets are used to keep the beam in the circular trajectory. Bunches are then sent into the Proton Synchrotron (PS) and Super Proton Synchrotron (SPS) with 7 km circumference, where they reach energy of 450 GeV per proton.

After the acceleration in the SPS the proton bunches are injected into the LHC, half of them in one direction and half in the opposite (the LHC has two separate beam pipes). Unlike the SPS and smaller accelerators, the LHC has superconducting niobium-titanium magnets with field of 8.3 T. Together 1232 dipole magnets are used for bending the beam, another quadrupole, sextupole etc.

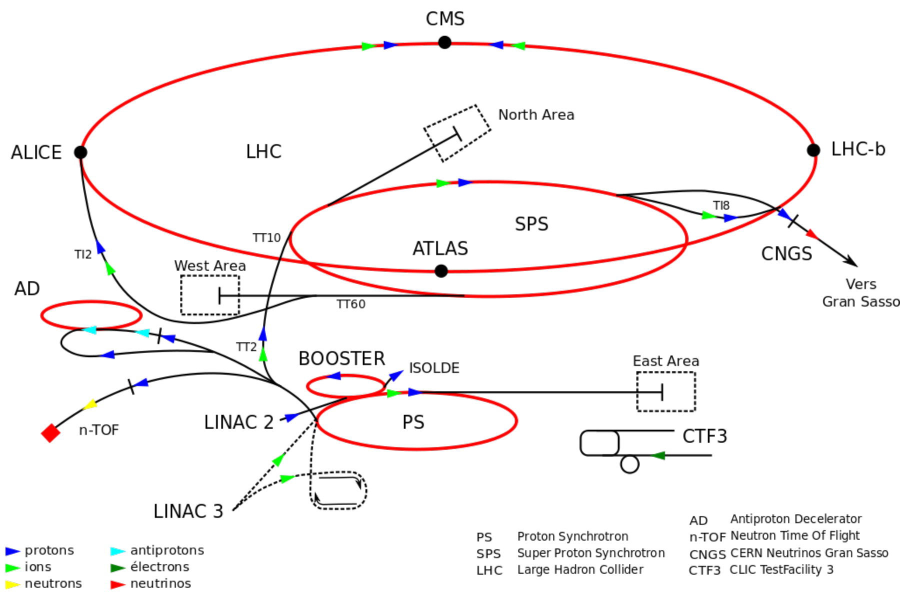

Fig. 3.1. LHC accelerator complex. Taken from [32].

magnets are used for beam focusation. Huge cryogenic system with 700 m^3 of liquid helium is needed to cool down the magnets to the temperature 1.9 K. When the accelerated particles reach the required energy, magnets near the interaction points switch the trajectories of the opposite beams so that they cross and start to collide. Typically tens of protons collide per each bunch crossing, while most of them do not interact at all and they continue to circulate for several hours, until the luminosity of the bunches becomes too small. The rest of the beam is deflected by a fast kicker magnet into the beam dump tunnel, where it is diluted and absorbed in a well shielded graphite beam dump block. The designed maximum instantaneous luminosity of LHC is 10^{34} cm^2s^{-1}.

3.1 The ATLAS Detector

The ATLAS detector [33] is a multipurpose particle physics apparatus operating at one of the beam interaction points of the LHC. It covers almost the entire solid angle around the collision point. ATLAS uses a right-handed coordinate system with its origin in the centre of the detector (the nominal interaction point and the z-axis along the beam pipe. The x-axis points from the coordinate system origin to the centre of the LHC ring, and the y-axis points upward.

The innermost part of this detector is an inner tracking detector (ID) comprised of a silicon pixel detector, a silicon microstrip detector, and a transition radiation tracker. The ID covers the pseudo-rapidity[5] range $\mid \eta \mid < 2.5$ and is surrounded by a thin superconducting solenoid providing a 2 T magnetic field, and by liquid-argon electromagnetic sampling calorimeters with high granularity (LAr). An iron-scintillator tile calorimeter provides hadronic energy measurements in the central pseudorapidity range ($\mid \eta \mid < 1.7$). The end-cap and forward regions are instrumented with LAr calorimetry for both electromagnetic (EM) and hadronic energy measurements up to $\mid \eta \mid = 4.9$. The calorimeter system is surrounded by a muon spectrometer incorporating three superconducting toroid magnet assemblies, with bending power between 2.0 and 7.5 Tm and the pseudorapidity coverage is: $\mid \eta \mid < 2.7$.

3.2 The CMS Detector

The central feature of the CMS detector [34] is a superconducting solenoid, 13 m in length and 6 m in diameter, which provides an axial magnetic field of 3.8 T. The bore of the solenoid is outfitted with various particle detection systems. Charged particle trajectories are measured by the silicon pixel and strip tracker, covering $0 < \phi < 2\pi$ in azimuth and $|\eta| < 2.5$ in pseudorapidity A crystal electromagnetic calorimeter (ECAL) and a brass/scintillator hadronic calorimeter surround the tracking volume – the calorimetry provides high resolution energy and direction measurements of electrons and hadronic jets[6]. Muons are measured in gas-ionisation detectors embedded in the steel return yoke outside the solenoid. The detector is nearly hermetic, allowing for energy balance measurements in the plane transverse to the beam directions. A two-level trigger system selects the most interesting pp collision events for use in physics analysis. A more detailed description of the CMS detector can be found in Ref. [34].

[5]The pseudorapidity is defined in terms of the polar angle θ as $\eta = -ln(tan(\theta/2))$

[6]By a jet is meant a narrow cone of particles (mostly hadrons) produced by the hadronization of a quark or gluon.

4 Top quark physics studies

Top quark physics is one of the most important subjects presently studied at LHC. The top quark properties are still not known properly and the top quark is in many respects an extraordinary particle:

- The mass of top quark ($m_{\rm t}$) is very big – it is close to the electroweak symmetry breaking (EWSB) scale. Its Yukawa coupling, $\lambda_{\rm t} = \sqrt{2}m_{\rm t}/v \approx 1$ (v = 246 GeV – is the vacuum mean value of the Higgs field), indicates the top quark can play a role in the EWSB.
- The top quark is an excellent perturbative object for testing QCD as it is produced at small distances ($\sim 1/m_{\rm t}$) characterized by low value of coupling constant $\alpha_{\rm S} \approx 0.1$.
- It decays before hadronization: the production time ($1/m_{\rm t}$) < lifetime ($1/\Gamma_{\rm t}$) < hadronization time ($1/\Lambda_{\rm QCD}$). This permits study of spin characteristics of the top quark as it is not diluted by hadronization (test of the top production mechanisms) or measurement of W boson helicity (test of the EW V-A structure).
- The $t\bar{t}$ production cross section is sensitive to new physics, e.g. resonant production of $t\bar{t}$ pairs would be a hint of existence of a new boson (KK-gravitons, etc.) or the decay $t \to H^+b$ would indicate presence of a charged Higgs boson.

In addition, the top quark processes are a very important background for the Higgs processes. It can be concluded that the top quark physics can provide stringent tests of the SM as well as it is an excellent platform for searches for new physics.

4.1 Top quark and the electroweak precision data

In the previous part it has been stressed that the top quark is in many respects an extraordinary fundamental particle. Among its virtues is that it can be used for very stringent consistency tests of the SM. One of them is an indirect determination of the Higgs boson mass. The idea is based on a capability of present experiment to do precision electroweak measurements, which are able to measure the contributions from radiative corrections. Taking into account a process mediated by W boson, e.g. muon decay ($\mu^- \to \nu_\mu W^- \to \nu_\mu \ell^- \bar{\nu}_e$), the one loop corrections to W boson propagator will contain contributions from the top quark and Higgs boson (see Fig. 4.1). Assuming that the dominant virtual contributions arise through vacuum polarisation loops, one can write:

$$M_W^2\left(1-\frac{M_W^2}{M_Z^2}\right) = \frac{\pi\alpha}{\sqrt{2}G_F}\left(1+\Delta r\right), \quad \Delta r = \Delta\alpha + \frac{s_W}{c_W}\Delta\rho + (\Delta r)_{nl}, \tag{4.1}$$

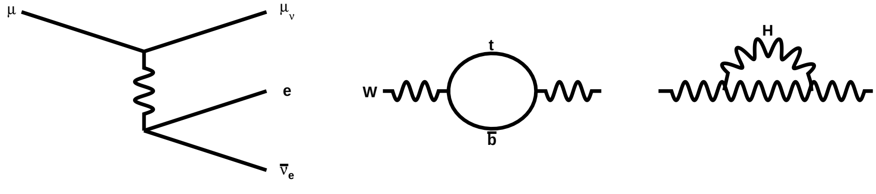

Fig. 4.1. Muon decay diagram (left) and one loop corrections to W boson propagator - the loop containing top quark (middle) and Higgs boson (right).

where M_W (M_Z) is the mass of W (Z) boson, α is the electromagnetic coupling constant, G_F is the Fermi constant, Δr is the higher order correction, $s_W = sin\theta_W$ and $c_W = cos\theta_W$, where θ_W is the electroweak mixing angle, $\Delta\alpha$ is the hadronic contribution to the running electromagnetic coupling strength and $\Delta\rho$ reads

$$\Delta\rho = N_C \frac{\alpha}{16\pi s_W^2 c_W^2} \frac{m_t^2}{M_Z^2}, \tag{4.2}$$

and in Δr_{rem} is comprised the contribution of vacuum polarization loop with the Higgs boson:

$$\Delta r_{rem}^{Higgs} = \frac{\alpha}{16\pi s_W^2} \frac{11}{3} \left(\ln \frac{M_H^2}{M_W^2} - \frac{5}{6} \right), \tag{4.3}$$

where M_H is the Higgs boson mass.

From Eq. 4.1, 4.2 and 4.3 it follows that Eq. 4.1 bounds the Higgs boson mass (M_H) with that of the W boson (M_W), top quark (m_t) and Z boson(M_Z) and with other quantities like electromagnetic coupling strength, etc. In such a way this equation can be used to constraint the Higgs boson mass M_H provided that the above mentioned quantities are precisely measured.

Taking into account that M_Z, G_F and α are known with high precision [13] ($M_Z = 91.1876$ $\pm$ 0.0021 GeV, G_F = 1.166378 7(6)$\times 10^{-5}$ GeV^{-2} and α = 1/137.035999679(94)) and the correction $\Delta\alpha$ is calculated reliably [35], it can be concluded that precision measurement of M_{W} and m_{t} is critical for determination of the Higgs mass. On the other hand for the Higgs boson mass constraint can be used not only precise measurement of M_{W} and m_{t}, but also a series of other precision electroweak observables [36]. Taking into account all the EW observables and doing a fit using higher order expressions between the observables for the Higgs boson mass has been extracted [36]: $M_H = 94^{+25}_{-22}$ GeV. In Fig. 4.2a are shown the results of fits with fixed values of M_{W} and m_{t} which are scanned in the (M_{W}, m_t) plane. Contours of 68% and 95% confidence level (C.L.) are the results of the fit including (blue regions) and excluding (grey regions) the M_{H} measurements, respectively. The horizontal (vertical) bands indicate the 1σ regions of the M_{W} (m_{t}) measurements. In Fig. 4.2a is shown χ^2 as a function of Higgs boson mass M_{H} with (blue band) without (grey band) inclusion the M_{H} measurements. From Fig. 4.2 it follows that the results of the direct M_{H} measurement is in good agreement with that obtained by the EW precision fit.

4.2 Top quark and stability of vacuum

Higgs boson looks to be firmly established by LHC ([38, 39]). Under the SM its vacuum has nonzero Higgs field component (Higgs condensate) and question of its stability can be raised. The Higgs field potential is

$$V(\phi) = m^2 \phi^* \phi + \lambda \left(\phi^* \phi\right)^2, \quad \phi = \frac{\phi_1 + i\phi_2}{\sqrt{2}} \tag{4.4}$$

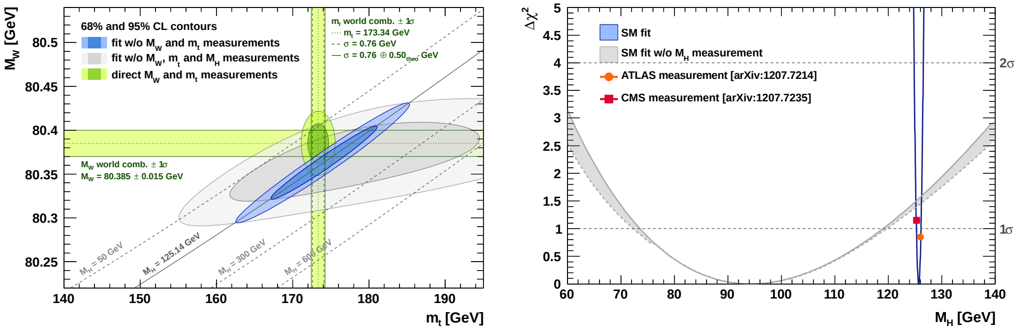

Fig. 4.2. (a) Contours of 68% and 95% C.L. obtained from scans of fits with fixed variable pairs M_W vs. m_t. The narrower blue and larger grey allowed regions are the results of the fit including and excluding the M_H measurements, respectively. The horizontal bands indicate the 1σ regions of the M_{W} and m_{t} measurements; (b) χ^2 as a function of Higgs boson mass M_{H}, shown for the fit case with (blue band) and without the M_{H} measurements (grey band). The solid and dashed lines give the results when including and ignoring theoretical errors, respectively (taken from [37]).

where the potential parameters fulfill the conditions: $m^2 < 0$ and the quartic parameter $\lambda > 0$. These conditions provide that this potential has the known "mexican hat" shape and the minimum of this potential corresponds to the SM vacuum $v = \sqrt{-m^2/\lambda}$. In connection with the expected new physics, though it is not clear what is its scale or if there is any new physics bellow Planck scale M_{P} (= 1.22×10^{19} GeV), the question of the SM vacuum stability is of high importance [40, 41, 42]. We need to know if the EW minimum of our world is really the true minimum of the SM effective potential, i.e. the radiatively corrected Higgs scalar potential. In the first approximation this effective potential, $V^{\mathrm{eff}}(\phi)$ has the form of Eq. 4.4 but the potential parameter are running constants dependent on an energy scale μ (renormalization scale). At large values of the Higgs field, $\phi(\mu) >> v$, the dominant contribution to the potential is from the quartic term $(\lambda(\phi^*\phi)^2)$ and possible change of sign of the quartic coupling λ would have a critical impact on the stability of the EW vacuum.

The search for the instability scale, Λ_{I}, is looking for the scale where V^{eff} becomes smaller than its value at the EW minimum (v), practically the scale is looked for where $\lambda(\mu) = 0$. A special feature of the Higgs quartic coupling, λ, is that it is the only SM coupling that is allowed to change sign during the renormalization group evolution because it is not multiplicatively renormalized [40]. The quartic β-function ($\beta_\lambda \equiv d\lambda/d\ln\mu$) contains, at the one loop level, the part not proportional to λ that contains the top quark Yukawa coupling at the fourth power and with a negative sign. This term dominates in β_λ for small values of λ and λ can evolve towards smaller values and eventually cross zero. The running of the three gauge couplings and the top quark Yukawa coupling has been determined using three-loop beta functions [43] and two-loop matching conditions [44]. Assuming only the SM interactions the Higgs quartic coupling decreases with energy crossing $\lambda = 0$, for the central values of top quark mass, m_t, the strong coupling, α_{S}, and the Higgs mass, M_{H}, at a scale of about 10^{10} GeV, i.e. deeply below M_{P} (see Fig. 4.3). The fact that λ, assuming the SM physics, becomes negative at a scale below M_{P} indicates that the Higgs effective potential is unstable, i.e. at a scale above Λ_{I} is either not bounded from below

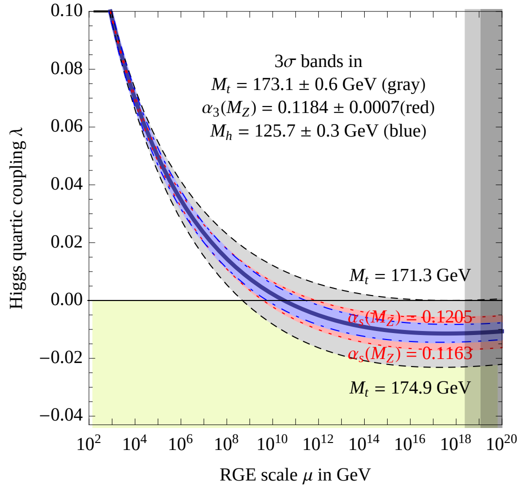

Fig. 4.3. Evolution of the Higgs quartic constant taking into account uncertainties in $m_{\rm t}$, $\alpha_{\rm S}$ and $M_{\rm H}$, the plot is taken from ref. [41].

or it develops a second minimum that can be deeper than the EW one [40]. In connection with this fact, the idea that the SM can be considered as a valid theory up to $M_{\rm P}$ appears problematic as the EW vacuum is the false one (the mean expected vacuum value v is not the true minimum of the Higgs potential) and a tunneling from our (false) vacuum to the true vacuum at high field values is possible. A new physics, if exists, can cure the situation if its characteristic scale is below $\Lambda_{\rm I}$. The rate of quantum tunneling out of the EW vacuum can be calculated – the basic idea of this calculation can be found in ref. [45].

Analyses of the two-loop Higgs effective potential have revealed that stability of the EW vacuum depends critically on the Higgs and top quark pole masses [46, 47]. The phases of the EW vacuum in the $M_{\rm H} - m_{\rm t}$-plane are shown in Fig. 4.4, where the region of stability, metastability and instability of the EW vacuum are shown for a broad range of $M_{\rm H}$ and $m_{\rm t}$. As it follows from Fig. 4.4 the question of the vacuum stability is critically dependent on the measured values of $M_{\rm H}$ and $m_{\rm t}$. The stability condition can be approximated by [40]:

$$H_{\rm M} > 129.1\,{\rm GeV} + 2\,(m_{\rm t} - 173.1\,{\rm GeV}) - 0.5\,{\rm GeV}\frac{\alpha_{\rm S}(M_{\rm Z}) - 0.1184}{0.0007} \pm 0.3\,{\rm GeV}, \quad (4.5)$$

Since the experimental uncertainty on the Higgs boson mass is already very small and in future will be further reduced, it is becoming more appropriate to express the stability condition in terms of the pole top quark mass:

$$m_t < (171.53 \pm 0.15 \pm 0.23_{\alpha_{\rm S}} \pm 0.15_{M_{\rm H}})\,{\rm GeV}, \quad (4.6)$$

where the second and the third uncertainty term correspond to the uncertainties connected with $\alpha_{\rm S}$ and $M_{\rm H}$.

From Eq. 4.6 it follows that the precise measurement of top quark pole mass is extremely important for the correct understanding of the vacuum stability. Another consequence stemming

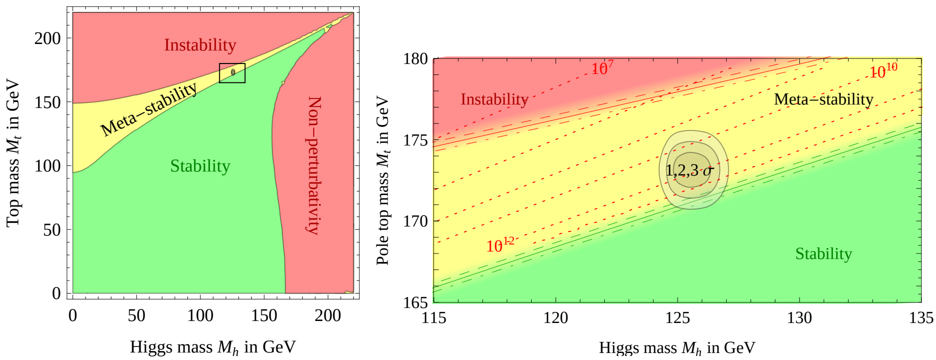

Fig. 4.4. SM phase diagram in terms of Higgs and top quark pole masses. The plane is divided into regions of absolute stability, meta-stability, instability of the SM vacuum, and non- perturbativity of the Higgs quartic coupling. The plot is taken from ref. [41].

from this equation is that we live in a metastable world as the measured value of $m_{\rm t}$ appears bigger than 171.53 GeV. Taking into account the present values of $M_{\rm H}$ and $m_{\rm t}$ our vacuum is metastable but probability of tunneling is extremely small (less than 10^{-100}), i.e. the lifetime of the EW vacuum is extremely long much larger than the age of Universe. In addition, from the right plot in Fig. 4.4 it follows that it is the exact value of the top mass which is the main factor that can discriminate between a stable and a metastable EW vacuum. In connection with the question of the top quark pole mass, $m_{\rm t}^{\rm pole}$, can be raised as measured top quark mass, $m_{\rm t}^{\rm MC}$, can differ from $m_{\rm t}^{\rm pole}$. This issue will be discussed later (see sec. 4.5).

4.3 Top quark decay

The top quark decays rapidly (the decay width is $\Gamma(t \to Wb)$ = 1.32 GeV [48]) without forming hadrons and almost exclusively through the mode $t \to Wb$, where the b-quark hadronizes producing shower of particles called b-jet and the W boson decays leptonically or hadronically. The total top quark decay width assuming a Cabbibo-Kobayashi-Maskawa matrix element $|V_{tb}|$ and the b-quark mass $m_b = 0$, at leading order (LO) [49] is given by

$$\Gamma_{\rm t}^{(0)} = \frac{G_{\rm F} m_t^3}{8\pi\sqrt{2}} \left[1 - 3\left(\frac{m_W^2}{m_t^2}\right)^2 + 2\left(\frac{m_W^2}{m_t^2}\right)^3\right], \tag{4.7}$$

where m_t is the top quark mass, m_W is the W boson mass and $G_{\rm F}$ is the Fermi constant. Presently considered corrections to the LO width include finite b-quark mass and W boson width effects, δ_f^b and δ_f^W, the Next-to-Leading Order (NLO) electroweak corrections, $\delta_{\rm EW}$, NLO and NNLO QCD corrections, $\delta_{\rm QCD}^{(1)}$ and $\delta_{\rm QCD}^{(2)}$. The total decay width with the electroweak and QCD corrections included [48] reads

$$\Gamma_{\rm t} = \Gamma_{\rm t}^{(0)} \left(1 + \delta_f^b + \delta_f^W + \delta_{\rm EW} + \delta_{\rm QCD}^{(1)} + \delta_{\rm QCD}^{(2)}\right), \tag{4.8}$$

where $\Gamma_{\rm t}$ is the total corrected top quark decay rate.

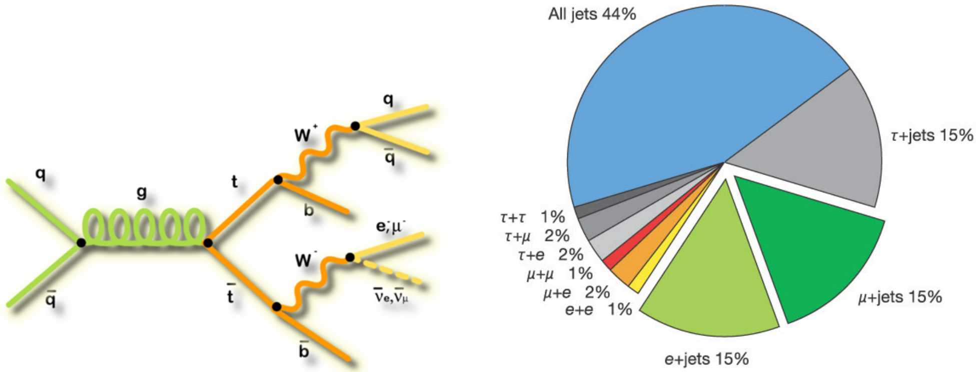

Fig. 4.5. Decay of top quark pair $t\bar{t} \to W^+bW^-\bar{b} \to b\bar{b}\ell^+\nu q_1\bar{q}_2$ (left) and the $t\bar{t}$ decay branchings (right).

All the corrections along with the LO decay width, $\Gamma_{\rm t}^{(0)}$ are shown in Table 4.1 for three different values of the top quark mass. From Eq. 4.8 and the corresponding top quark lifetime is: $\tau_{\rm top} \approx 5 \times 10^{-25}$ sec which is much shorter than the hadronization time $\tau_{\rm hadr} \approx 5 \times 10^{-23}$ sec. It should be stressed that at the top-quark decay the top quark is considered as a "free" particle i.e. a narrow width approximation is assumed. In this approximation the top-quark production and decay (see Fig. 4.5) are considered as two independent processes. Hence, the narrow width approximation assumes that the t-lines in Fig. 4.5 (left) are cut: (polarized) top quarks are produced on-mass shell and then these on-mass shell top quarks decay. In Fig. 4.5 is shown an example of a produced top-quark pair ($t\bar{t}$). The full set of $t\bar{t}$ branchings are depicted in Fig. 4.5 (right).

From the experimental point of view the $t\bar{t}$ events are classified according to the W bosons decays dividing them into three basic channels: the dilepton channel (D-L) – both W bosons decay leptonically, the lepton+jets channel (L+J) – one W boson decays leptonically and the other one hadronically, and the all-hadronic channel (A-H) – both W bosons decay hadronically. Though tau leptons are also leptons, the $t\bar{t}$ decays containing taus are usually consider separately taking into account peculiarities of the tau-lepton decays.

Tab. 4.1. Total top-quark width with all corrections in GeV for different values of the top-quark mass (GeV) *vs* top-quark total width (GeV) at LO and corrections in percentage (%) from finite W boson width, finite b-quark mass, and high orders, including NLO in EW couplings and NLO and NNLO in QCD coupling.

m_t	$\Gamma_{\rm t}^{(0)}$	δ_f^b	δ_f^W	$\delta_{\rm EW}$	$\delta_{\rm QCD}^{(1)}$	$\delta_{\rm QCD}^{(2)}$	$\Gamma_{\rm t}$
172.5	1.4806	-0.26	-1.49	1.68	-8.58	2.09	1.32
173.5	1.5109	-0.26	-1.49	1.69	-8.58	2.09	1.35
174.5	1.5415	-0.25	-1.48	1.69	-8.58	2.09	1.38

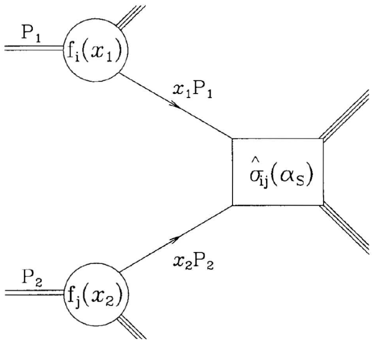

Fig. 4.6. Scheme of hadron-hadron interaction in partonic picture.

4.4 Top quark pair production cross section

As it has been already mentioned the top quark is an excellent perturbative object. Being produced at small distances ($\sim 1/m_{\mathrm{t}}$) with a small strong force coupling constant ($\alpha_{\mathrm{S}} \approx 0.1$) its perturbative expansion converges rapidly. For this reason the top quark is an ideal tool for the tests of QCD. As LHC is a top-quark factory with an abundant top-quark production, many aspect of the top-quark production including differential distributions can be used for the SM tests and alternatively for searches of physics beyond the SM (BSM). Taking into account the progress made in theory and the excellent resolution of the LHC experiments, a deeper understanding of fundamental laws of the nature is anticipated.

4.4.1 Progress in the calculation of the top quark pair production cross section

The top quark production cross section in *pp* collisions, or in general in hadron-hadron collisions, is calculated using the so-called factorization theorem which is based on the idea that interacting hadrons can be considered as systems of free partons as is schematically shown in Fig. 4.6. This assumption is justified if deep hadron-hadron inelastic interaction occurs. In such a case the factorization formula reads:

$$\sigma = \sum_{i,j} \int dx_1 dx_2 F_i^{(1)}\left(x_1, \mu_{\mathrm{F}}\right) F_j^{(2)}\left(x_2, \mu_{\mathrm{F}}\right) \hat{\sigma}_{ij}\left(s; \mu_{\mathrm{F}}, \mu_{\mathrm{R}}\right), \tag{4.9}$$

where $F_i^{(\lambda)}\left(x_1, \mu_{\mathrm{F}}\right)$ is the Parton Density Function (PDF), i.e. the probability density to observe a parton i with longitudinal momentum fraction x_λ in incoming hadron λ, when probed at a scale μ_{F}, μ_{F} is the factorization scale (a free parameter) – it determines the proton structure if probed (by virtual photon or gluon) with $q^2 = -\mu_{\mathrm{F}}^2$, μ_{R} is the renormalization scale defining size of the strong coupling constant and $\hat{\sigma}_{ij}(s)$ is the partonic cross section. Eq. 4.9 connects the experimentally measured cross section with the theoretical one and the proton structure functions, i.e. with PDFs. The factorisation theorem assumes that the incident hadrons consist of partons and the hadron-hadron cross section is a sum of the parton-parton cross section.

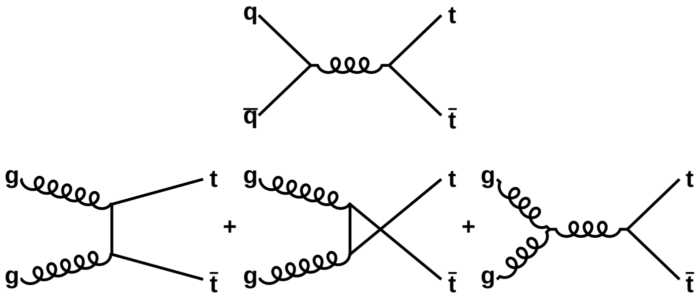

Fig. 4.7. Leading order top quark pair production diagrams: the quark anihilation (upper plot) and gluon fusion (bottom row plots).

The theoretical $t\bar{t}$ partonic cross section is now calculated at NNLO (Next-to-Next-to-Leading-Order) approximation with resummation of soft gluon contributions in NNLL (Next-to-Next-to-Leading-Logarithm) approximation [50]. Expanding the partonic cross section, σ_{ij}, into series of the strong coupling constant α_S, one gets

$$\hat{\sigma}_{ij}\left(\beta, \frac{\mu^2}{m_t^2}\right) = \frac{\alpha_\mathrm{S}^2}{m_t^2}\left[\hat{\sigma}_{ij}^{(0)} + \alpha_\mathrm{S}\left(\hat{\sigma}_{ij}^{(1)} + L\hat{\sigma}_{ij}^{(2)}\right)\right. \\ \left. + \alpha_\mathrm{S}^2\left(\hat{\sigma}_{ij}^{(2)} + L\hat{\sigma}_{ij}^{(2,1)} + L^2\hat{\sigma}_{ij}^{(2,2)}\right) + O\left(\alpha_\mathrm{S}^3\right)\right], \quad (4.10)$$

where i, j are the initial state parton indices, $\beta = \sqrt{1 - 4m_t^2/s}$ is the top quark velocity, μ $(= \mu_\mathrm{R} = \mu_\mathrm{F})$ is the process characteristic scale, m_t is the top quark mass, $L = \ln\left(\mu^2/m_t^2\right)$ and $\hat{\sigma}_{ij}^{(x)}$ depend only on β but can contain big logarithmic term which is a consequence of the incomplete cancellation between graphs with gluon emission and virtual gluon corrections.

Remark. The terms in the $\hat{\sigma}_{ij}$ expansion in α_S (see Eq. 4.10) can be categorized as follows: the first term in the expansion, which is proportional to α_S^2, is called the leading order (LO), the second term (proportional to α_S^3) is the Next-to-Leading Order (NLO) and the third term (proportional to α_S^4) is the Next-to-Next-to-Leading Order (NNLO). In addition, at the $t\bar{t}$ cross section calculation contribution of the soft gluon emission, which leads to logarithmic terms, needs be taken into account. The leading logarithms (LL) for the $t\bar{t}$ production arise from soft gluon emission from the quarks and gluons in the incoming protons. Procedure of calculation of the soft gluon contribution, the resummation procedure, is now extended to gluon resummation up to the Next-to-Next-to-Leading Logarithms (NNLL) – the details can be found in Refs. [50, 51].

The top quark is produced via strong interactions mediated through gluon (production of $t\bar{t}$ pair) and in the electroweak ones (single top quark production). In the former case the main production mechanisms are the quark annihilation ($q\bar{q} \to t\bar{t}$) and gluon fusion ($gg \to t\bar{t}$) (see Fig. 4.7). The latter case where the production is mediated by W boson will be discussed later (see Sec. 4.6).

The predicted $t\bar{t}$ production cross sections [50] are summarized in Table 4.2. The uncertainty of the theoretical calculations is 4%.

Tab. 4.2. Top quark pair ($t\bar{t}$) production cross section in NNLO + NNLL approximation for the energies: 2 TeV (Tevatron) and 7, 8 and 14 TeV (LHC).

Energy	σ_{tot} [pb]	scales [nb]	pdf [nb]
1.96 [TeV]	7.2	+0.110(1.5%)	+0.169(2.4%)
		-0.200(2.8%)	-0.122(1.7%)
7 [TeV]	172.0	+4.4(2.6%)	+4.7(2.7%)
		-5.8(3.4%)	-4.8(2.8%)
8 [TeV]	245.8	+6.2(2.5%)	+6.2(2.5%)
		-8.4(3.4%)	-6.4(2.6%)
14 [TeV]	953.6	+22.7(2.4%)	+16.2(1.7%)
		-33.9(3.6%)	-17.8(1.9%)

4.4.2 Measurement of the top quark pair production cross section

The $t\bar{t}$ cross section analysis is carried out in all three above mentioned channels. The most precise results are obtained for the lepton + jet and dileptons channels.

The measured cross section, $\sigma_{t\bar{t}}$, is determined using the likelihood discriminant employed to separate signal events from the background ones and then a procedure is used based on the relation:

$$\sigma_{t\bar{t}} = \frac{\sum_i N_{\rm obs} - N_{\rm bkg}}{A \cdot \epsilon \cdot \int L.dt}, \tag{4.11}$$

where $N_{\rm obs}$ ($N_{\rm bkg}$) is the number of the observed candidate (expected background) events, A is the acceptance, ϵ is the trigger efficiency and $\int Ldt$ is the integrated luminosity.

An example of a precise ATLAS $t\bar{t}$ cross section measurement is the analysis carried out using the data samples of 4.6 fb^{-1} at 7 TeV and 20.3 fb^{-1} at 8 TeV [53]. At the both collision energies the dilepton $t\bar{t}$ events with an opposite-charge electron-muon pair in the final state have been taken. The events were required to pass either a single-electron or single-muon trigger and only the events with exactly one and exactly two b-tagged jets have been counted and used to determine simultaneously the $t\bar{t}$ cross section and the efficiency to reconstruct and b-tag a b-jet from top quark decay. If a jet is denoted as b-tagged, it means that with high probability it comes from hadronization of a b- or $\bar{b}$-quark. Procedure of b-tagging exploits the fact that b-quark has quite a long lifetime ($\sim 10^{-12}$ sec and its mass is big (in comparison with light quarks). In this channel the main background arises from the associated production of a W boson and a single top quark (Wt) and the other sources of background come from $Z \to \tau\tau \to e\mu$+jets production, diboson production with at least one lepton not arising from W or Z boson decay. The cross section has been measured to be:

$$\sigma_{t\bar{t}} = 182.9 \pm 3.1\ (\text{stat.}) \pm 4.2\ (\text{syst.}) \pm 3.6\ (\text{lumi.}) \pm 3.3\ (\text{beam})\text{pb}\ (7\ \text{TeV}),$$
$$\sigma_{t\bar{t}} = 242.4 \pm 1.7\ (\text{stat.}) \pm 5.5\ (\text{syst.}) \pm 7.5\ (\text{lumi.}) \pm 4.2\ (\text{beam})\text{pb}\ (8\ \text{TeV}).$$

The uncertainties arise from data statistics (stat.), experimental and theoretical systematic effects (syst.), knowledge of the integrated luminosity (lumi.) and of the LHC beam energy (beam). The result of the analysis assumes a fixed top mass of 172.5 GeV and the main systematic arises from $t\bar{t}$ modeling, PDFs, single-top Wt cross-section and lepton isolation. This result is in excellent agreement with the theoretical prediction [50]: $\sigma_{t\bar{t}}^{\mathrm{theo}} = 245.8^{+6.2}_{-8.4}$ (stat.) $^{+6.2}_{-8.4}$ (pdf) pb as well as with the CMS results obtained in dilepton channel [54]. This CMS $t\bar{t}$ cross section measurement has been carried out at $\sqrt{s}$ = 8 TeV using a data sample corresponding to an integrated luminosity of 5.3 fb^{-1}. The analysis, based on dilepton trigger, selects final states containing two leptons of opposite electric charge (electrons or muons), with missing transverse momentum associated to the neutrinos from the W boson decays, and two jets resulting from the hadronisation of two b-quarks. The main background arise from Drell-Yan, single-top-quark and diboson processes. The $t\bar{t}$ cross section was measured for each of the three final states, e^+e^-, $\mu^+\mu^-$, and $e^{\pm}\mu^{\mp}$ which give compatible results and the final result is obtained using the BLUE method [55] yielding a measured cross section of $\sigma_{t\bar{t}}$ = 239.0 $\pm$ 2.1 (stat.) $\pm$ 11.3 (syst.) $\pm$ 6.2 (lumi.) pb for a top-quark mass of 172.5 GeV.

The $t\bar{t}$ cross section measurement of ATLAS and CMS at 8 TeV have been combined resulting in $\sigma_{t\bar{t}} = 240.6 \pm 1.4$(stat.) $\pm$ 5.7(syst.) $\pm$ 6.2(lumi.) pb

The $t\bar{t}$ cross section measurements were carried out by ATLAS and CMS also in other channels mostly at $\sqrt{s}$ = 7 TeV. The analyses performed at 7 TeV in the lepton + jets channel can be found in Ref. [56] (ATLAS) and in Ref. [57] (CMS) and for channel containing τ leptons in Ref. [58] (ATLAS) and in Ref. [59] (CMS). The measured $t\bar{t}$ cross sections performed by ATLAS and CMS at 7 and 8 TeV are summarized in Figure 4.8, where they are compared to the exact NNLO QCD calculation complemented with NNLL resummation [60]. Measurement the total $t\bar{t}$ cross sections at different energies, including the Tevatron measurement carried out by the CDF a D0 collaborations, are compared in Figure 4.9 with the full NNLO QCD calculation with NNLL resumations [50].

4.4.3 Top quark pair differential cross section

The large number of $t\bar{t}$ events available at the LHC experiments makes it possible to measure precisely the $t\bar{t}$ production cross sections, $\sigma(t\bar{t})$, differentially, providing precision tests of current perturbative QCD predictions in different regions of phase space. At differential cross section measurement we need to measure the $\sigma(t\bar{t})$ as a function of kinematic distributions of top quark, top quark pairs, (b)-jets, leptons. etc. Main ingredients of corresponding analysis are:

- event selection (trigger and off-line selections);
- $t\bar{t}$ kinematic reconstruction – the analysis objects should be reconstructed to parton or particle level;
- bin cross section measurement;
- the obtained distribution should be unfolded to parton or particle level taking into account detector effects and acceptance in the full or fiducial phase space.

Within the unfolding procedure a correct regularisation should be performed to remove large statistical fluctuations and also bins should be chosen optimally to limit migration effects. Taking

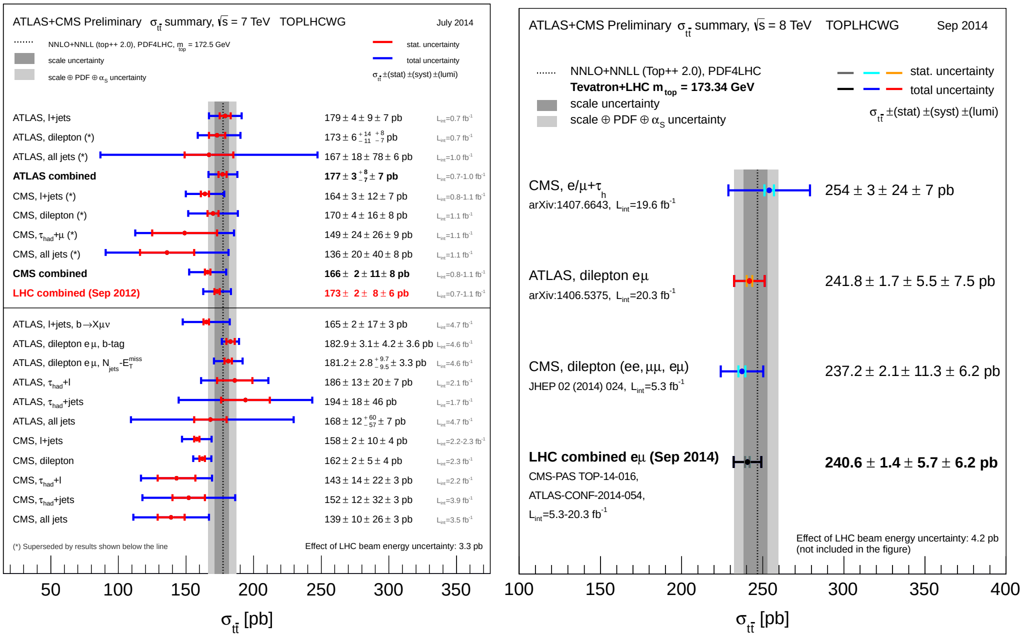

Fig. 4.8. Summary of measurements of the $t\bar{t}$ production cross-section at 7 TeV (left) and 8 TeV (right) compared to the exact NNLO QCD calculation complemented with NNLL resummation. The theory band represents uncertainties due to renormalisation and factorisation scale, parton density functions and the strong coupling. The measurements and the theory calculation is quoted at the current world average m_t=173.34 GeV.

in to account the above mentioned the differential cross section can be expressed as follows:

$$\frac{d\sigma_{t\bar{t}}}{dX_i} = \frac{\sum_i A^{-1}_{\mathrm{i,j}} \left(N_{\mathrm{data,j}} - N_{\mathrm{bkg,j}}\right)}{\Delta_{X_i} \cdot \int L.dt}, \tag{4.12}$$

where X is the considered kinematic variable (e.g. top quark p_{T}), A is the response matrix, $N_{\mathrm{data,j}}$ – the number of candidate $t\bar{t}$ events in j^{th} bin, $N_{\mathrm{bkg,j}}$ – the number of background events in j^{th} bin, $\int L.dt$ is the integrated luminosity and Δ_{X_i} is the X variable bin size.

A series of measurements of the differential $t\bar{t}$ cross sections at $\sqrt{s}$ = 7 TeV and 8 TeV were carried out by ATLAS and CMS. An example of a measurement carried out by ATLAS at $\sqrt{s}$ = 7 TeV is the analysis described in Ref. [61]. In this analysis measurements of normalized differential cross sections for $t\bar{t}$ production are presented as a function of the top-quark transverse momentum (p^t_{T}), and of the mass ($m_{t\bar{t}}$), transverse momentum ($p^{t\bar{t}}_{\mathrm{T}}$), and rapidity of the $t\bar{t}$ system. The used data set corresponds to an integrated luminosity of 4.6 fb^{-1} and events are selected in the lepton + jets channel, requiring exactly one lepton and at least four jets with at least one of the jets tagged as originating from a b-quark. The measured spectra are corrected for detector efficiency and resolution effects. Kinematic reconstruction of the $t\bar{t}$ system is per-

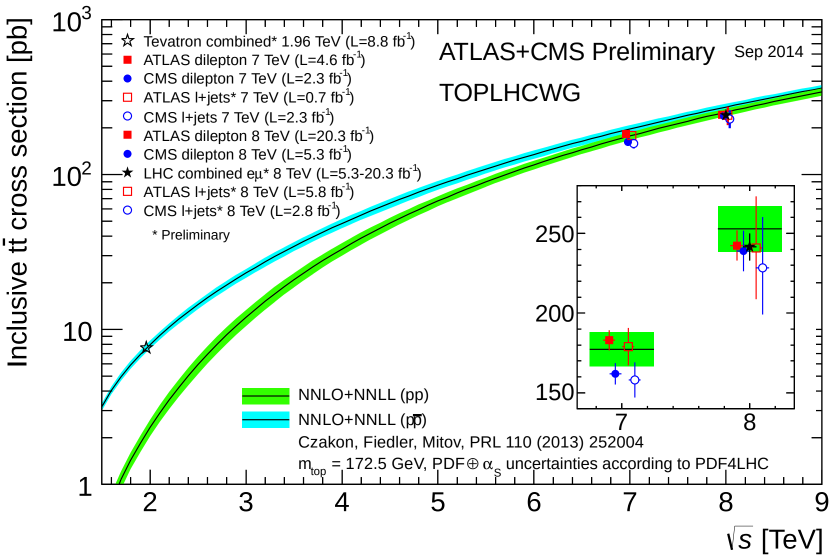

Fig. 4.9. Summary of LHC and Tevatron measurements of the $t\bar{t}$ production cross-section as a function of the centre-of-mass energy compared to the NNLO QCD calculation complemented with NNLL resummation. The theory band represents uncertainties due to renormalisation and factorisation scale, parton density functions and the strong coupling. The measurements and the theory calculation is quoted at m_t = 172.5 GeV. Measurements made at the same centre-of-mass energy are slightly offset for clarity.

formed using a likelihood fit. Systematic uncertainties arise from detector effects as well as from theoretical uncertainties. The systematic uncertainties are evaluated by varying each source of uncertainty by one standard deviation (up and down). The dominant uncertainties arise from the jet energy scale, b-tagging efficiency, lepton selection and momentum scale, MC generator, and uncertainties arising from background. As an example, in Fig. 4.10 are shown the distributions (the normalised cross sections) of the top-quark p_{T}^{t} and the top-quark-pair invariant mass, $m_{t\bar{t}}$, in the lepton + jets channels.

In a similar study CMS measured the differential $t\bar{t}$ cross sections at $\sqrt{s}$ = 7 TeV in the lepton + jets decay channels and also in the dilepton decay channels (lepton $\equiv$ electron, muon) using the data set corresponding to an integrated luminosity of 5.0 fb^{-1}. In the lepton + jets channels a single isolated lepton and at least four jets in the final state are required and in the dilepton channels two oppositely charged leptons are required and at least two jets. Sources of the systematic uncertainties are similar to those in the ATLAS case. Each systematic uncertainty is investigated separately, and determined individually in each bin of the measurement, by variation of the corresponding efficiency, resolution, or scale within its uncertainty. The dominant uncertainties on the normalized differential cross section originate from the lepton selection, the b-tagging, and from model uncertainties. An example of the differential cross sections obtained by CMS at $\sqrt{s}$ = 7 TeV in the lepton + jets decay channels are shown in Fig. 4.11, where the the normalized cross sections as a function of the top-quark p_{T}^{t} and the top-quark-pair invariant mass, $m_{t\bar{t}}$, are compared with the MC predictions from MadGraph [62], Powheg [63], and

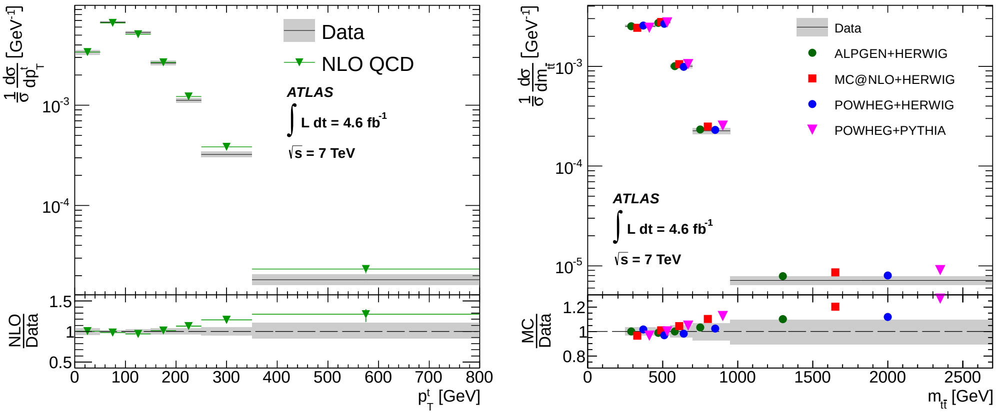

Fig. 4.10. Normalized differential cross-sections for the transverse momentum of the hadronically decaying top-quark, p_{T}^{t}, (left) and the mass, $m_{t\bar{t}}$, of the $t\bar{t}$ system. The distributions are compared to NLO QCD predictions (based on MCFM with the CT10 PDF). The error bars correspond to the PDF and fixed scale uncertainties in the theoretical prediction. The gray bands indicate the total uncertainty on the data in each bin. The lower part of each figure shows the ratio of the NLO QCD predictions to data.

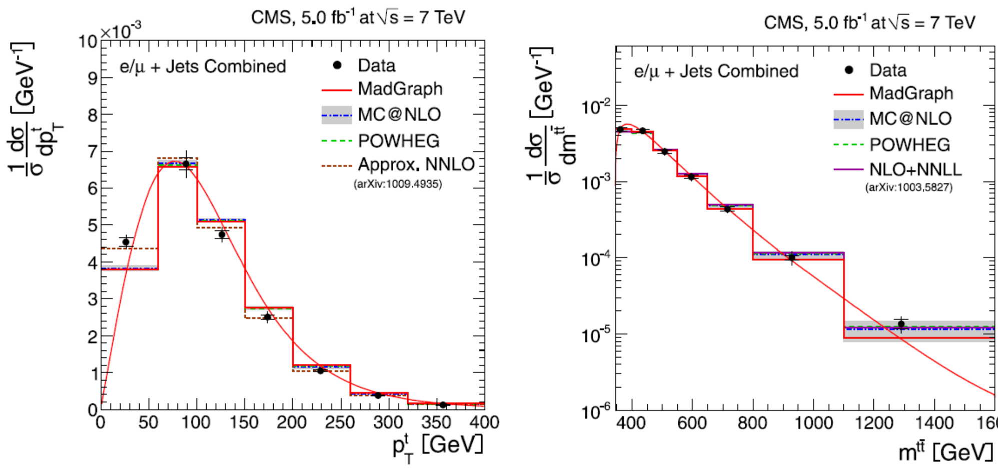

Fig. 4.11. Normalized differential $t\bar{t}$ cross-sections in the lepton + jets channels for the top-quark transverse momentum, p_{T}^{t}, (left) and the mass, $m_{t\bar{t}}$, of the $t\bar{t}$ system. The inner (outer) error bars indicate the statistical (combined statistical and systematic) uncertainty. The measurements are compared to predictions from MadGraph, Powheg, and MC@NLO, and to NLO + NNLL [67] and approximate NNLO [65, 66] calculations.

MC@NLO [64] [7]. In addition, the top-quark results are compared to the approximate NNLO calculations from Refs. [65, 66], while the $m_{t\bar{t}}$ distribution is compared to the NLO + NNLL prediction in Ref. [67]. Fig. 4.11 shows the measured differential $t\bar{t}$ cross section at $\sqrt{s} = 7$ TeV

[7] MadGraph, Powheg and MC@NLO are different parton level generators which simulate parton-parton interactions.

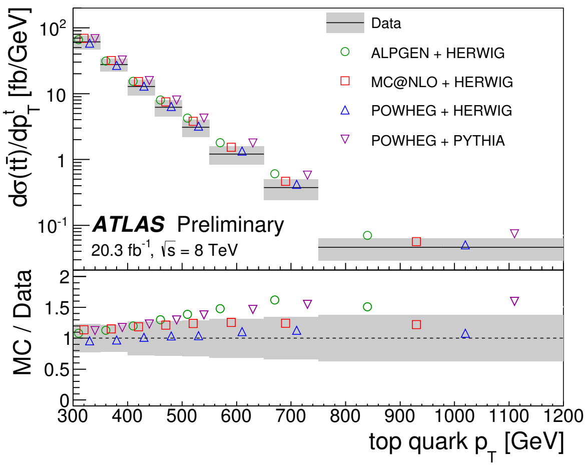

Fig. 4.12. Normalised differential cross-section as a function of jet multiplicity for jets with $p_{\mathrm{T}} > 30$ GeV. The data are compared with predictions from MadGraph+Pythia, MC@NLO+Herwig and Powheg+Pythia, as well as with predictions from MadGraph with varied Q^2 scale and jet-parton matching threshold. The errors on the data points indicate the statistical (inner bars) and the total uncertainties.

as a function of the top quark p_{T}^t (left) and the mass of the $t\bar{t}$ system, $m_{t\bar{t}}$, (right) measured by CMS.

Differential cross sections have been measured also at $\sqrt{s}$ = 8 TeV. The ATLAS results can be found in [71] and the CMS ones in Refs. [72, 73, 74, 75]. At $\sqrt{s}$ = 8 TeV, in comparison with the $\sqrt{s}$ = 7 TeV case, there is not only higher cross section but also higher integrated luminosity – 20.3 fb^{-1} and 19.6 fb^{-1} collected by ATLAS and CMS, respectively. It enables to perform more advanced studies. In connection with this, ATLAS has studied the differential cross-section for boosted top quark pair production. The measurement is performed for $t\bar{t}$ events in the lepton+jets channel, where the hadronically decaying top quark has a transverse momentum above 300 GeV. Jet substructure techniques are employed to identify top quarks, which are reconstructed with an anti-k_t jet with radius parameter $R = 1.0$. The cross-section is reported as a function of the hadronically decaying top quark transverse momentum. In Fig. 4.12 (left) is shown this parton-level differential cross-section as a function of the top quark p_{T}^t measured by ATLAS and is compared with Powheg+Pythia, Powheg+Herwig, MC@NLO+Herwig and Alpgen+Herwig predictions for details see Ref. [71].

Remark. The generators Pythia [68] and Herwig [69] are two different parton shower generators which simulate hadronization process of partons (quarks and gluons) and usually they are used in combination with parton level generators (like Powheg or MC@NLO). The generator Alpgen [70] is an additional parton level generator proposed to simulate the parton-parton interactions with multi-parton production in the final state).

In the CMS analysis at $\sqrt{s} = 8$ TeV described in Ref. [74] the $t\bar{t}$ cross section is investigated as a function of jet multiplicity for different p_{T}^t threshold. Such study is important as at LHC ener-

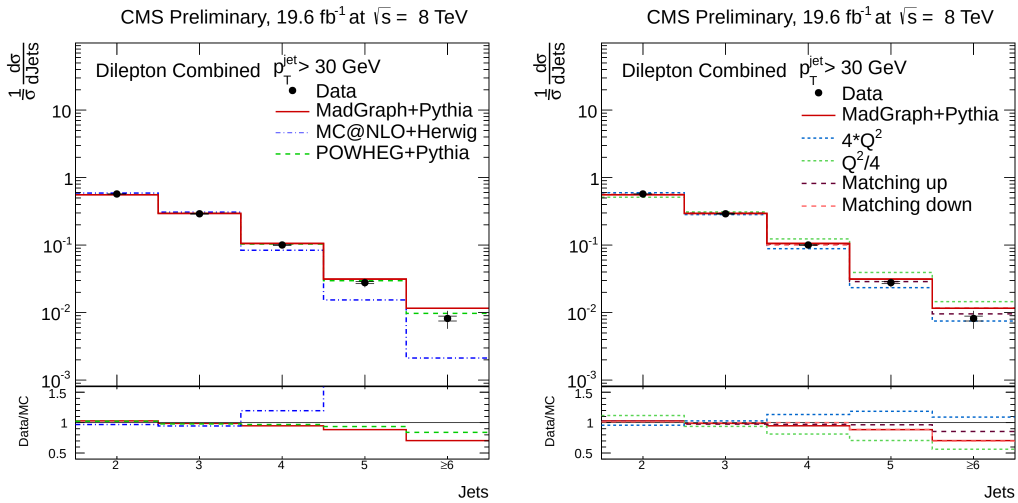

Fig. 4.13. Parton-level differential cross-section as a function of the top quark p_{T}^{t} and is compared with POWHEG+PYTHIA, POWHEG+HERWIG, MC@NLO+HERWIG and ALPGEN+HERWIG predictions (left) and for MADGRAPH one (right). MC samples are normalized to the NNLO+NNLL inclusive cross-section $\sigma_{t\bar{t}}= 253^{+13}_{-15}$ pb. The lower part of the figure shows the ratio between the MC prediction and the data. The shaded area include the total statistical plus systematic uncertainties.

gies, the fraction of $t\bar{t}$ events with additional hard jets in the final state is large. The understanding of these processes is relevant to test higher order QCD calculations, in which contributions from initial and final state radiation are taken into account to achieve a good quantitative description of multijet processes. CMS has measured the differential cross sections for three jet p_{T}^{t} threshold values (30, 60 and 100 GeV) and compared with different MC predictions. As an example in Fig. 4.13 are shown the differential cross section for the jet p_{T}^{t} threshold 30 GeV compared with POWHEG+PYTHIA, POWHEG+HERWIG, MC@NLO+HERWIG and ALPGEN+HERWIG predictions (left) and MADGRAPH one (right). The MC samples are normalized to the NNLO+NNLL inclusive cross-section $\sigma_{t\bar{t}} = 253^{+13}_{-15}$ pb.

Comparing the results measured by ATLAS and CMS at different energies (7 and 8 TeV) in different channels, one can conclude that there is good compatibility between the ATLAS and CMS results as well as between the results of different channels. In general the MC predictions and the QCD calculations agree with data in a wide kinematic region. However, the ATLAS data are softer than all predictions in the tail of the p_{T}^{t} spectrum, particularly in the case of the ALPGEN+HERWIG and POWHEG+PYTHIA generators. The same trend is observed for both ATLAS and CMS for the NLO + NNLL predictions of the $m_{t\bar{t}}$ and p_{T}^{t} spectra which tend to be above the data in the tail of the distributions. From this view point calculations of the differential cross sections at full NNLO with gluon resummation at NNLL are needed.

4.4.4 Measurement of the top quark pair production with other particles

Among the basic top quark properties are the couplings between the top quark and the vector bosons. The existence of non-zero couplings between the top quark and the neutral vector bosons can be inferred through the analysis of direct production of $t\bar{t}$ pairs in association with a γ or a Z boson. The LHC allows these two processes to be disentangled and the corresponding couplings to be measured. The associated production of $t\bar{t}$ pairs with a W boson, the $t\bar{t}W$ process, has a cross section similar to $t\bar{t}Z$ and $t\bar{t}\gamma$ production. All three processes can be used to test the internal consistency of the SM.

CMS has carried out a measurement of the cross section for the production of $t\bar{t}$ pairs in association with a vector boson *V* (*W* or *Z*) (pp collisions at $\sqrt{s}$ = 8 TeV) – details can be found in Ref. [76]. The results are based on a dataset corresponding to an integrated luminosity of 19.5 fb^{-1}. For all the channels considered in this analysis, the data are selected online by dilepton (ee, $e\mu$, and $\mu\mu$) triggers that demand a transverse momentum (p_{T}) larger than 17 GeV for the highest p_{T} lepton and 8 GeV for the second-highest scalar transverse momentum of the event. The selection, assuming the process $pp \rightarrow t\bar{t}W \rightarrow (t \rightarrow b\ell\nu)(t \rightarrow bq\bar{q})$, requires: two the same charge isolated leptons with $p_{\mathrm{T}} > 40$ GeV, at least three jets – one of them with b-tagging. Events with three leptons are rejected if the third lepton gives with one of the other two leptons, a same-flavour opposite-sign pair whose invariant mass is within 15 GeV of the Z-boson mass and the scalar transverse momentum of the event, $H_{\mathrm{T}} > 155$ GeV. One-dimensional fit of all channels is performed giving a combined cross section $\sigma_{t\bar{t}V}$ = 380^{+100}_{-90} (stat)$^{+80}_{-70}$ (syst) fb with a significance of 3.7 standard deviations.

ATLAS has performed a search for top-quark pairs ($t\bar{t}$) produced together with a photon (γ) with transverse momentum > 20 GeV using a sample of $t\bar{t}$ candidate events in final states with jets, missing transverse momentum, and one isolated electron or muon. The dataset used corresponds to an integrated luminosity of 4.59 fb^{-1} at $\sqrt{s}$ = 7 TeV. Events are selected by requiring a high p_{T} single-lepton electron or muon trigger. The p_{T} threshold for the muon trigger is 18 GeV, the thresholds for the electron trigger are 20 GeV or 22 GeV, depending on the data-taking period. The selected events are required to contain a high p_{T} photon $p_{\mathrm{T}} > 20$ GeV, one isolated lepton (electron with $p_{\mathrm{T}} > 25$ GeV or muon with $p_{\mathrm{T}} > 20$ GeV and $\mid \eta \mid < 2.37$), jets are required to have $p_{\mathrm{T}} > 25$ GeV and containing a b-hadron within a jet is identified with a b-tagging algorithm. Details of the event selection as well as of the background and systematics treatment can be find in Ref. [77]. Taking into account the expected background the numbers of $t\bar{t}\gamma$ signal events for the electron and muon channels are determined to be 52 $\pm$ 14 and 100 $\pm$ 28, respectively. The results include statistical and systematic uncertainties. The p-value of the no-signal hypothesis is 5.73×10^{-8}. The $t\bar{t}\gamma$ process in the lepton + jets final state is observed with a significance of 5.3 σ. The $t\bar{t}\gamma$ cross section per lepton flavor, determined in a fiducial kinematic region within the ATLAS acceptance, is measured to be $\sigma^{\mathrm{fid}}_{t\bar{t}\gamma}\times$ BR = 63 $\pm$ 8(stat.) $^{+17}_{-13}$(syst.) $\pm$ 1(lumi.) fb in good agreement with the theoretical prediction.

4.5 Top-quark mass

The top-quark mass, m_{t}, is one of the SM parameters and play important role in the present particle physics. We have already mentioned how important it is for the consistency tests of the SM (indirect determination of the Higgs boson mass) and for the question of stability of the EW vacuum. In connection to the last question it is needed to clarify what is the relation between the top-quark pole mass the experimentally mass measured. In the following sections we will try to analyze this relation and to show the results of experiment.

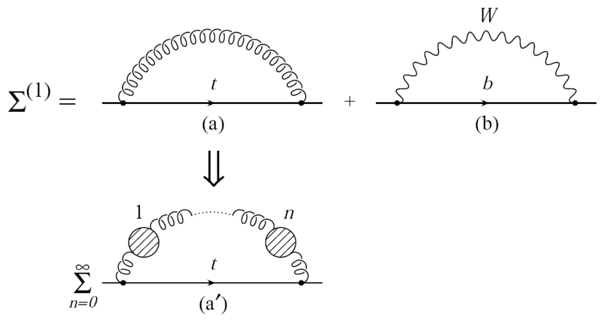

Fig. 4.14. Quark self energy in one-loop approximation -the gluon (a) and W boson (b) loop.

4.5.1 Top quark pole mass and short distance mass

Formally the top-quark mass corresponds to a pole in the full top-quark propagator. The propagator of a quark of four-momentum p is

$$D(\hat{p}) = \frac{1}{\hat{p} - m_{\mathrm{R}} - \Sigma(\hat{p})}, \quad \hat{p} = \gamma^{\mu} p_{\mu} \tag{4.13}$$

where m_{R} is a short distance mass (see below), $\Sigma(\hat{p})$ is the renormalized one-particle-irreducible quark self-energy and γ^{μ} are Dirac matrices. By the short-distance mass (see ref. [78]) we mean a running mass evaluated at a scale $m_{\mathrm{R}} >> \Lambda_{\mathrm{QCD}}$, i.e. it includes all short range loops with space size below $1/m_{\mathrm{R}}$, i.e. the loops with the "circulating" momentum above m_{R}.

The position of the pole can be extracted using the equation

$$\hat{p}_{\mathrm{pole}} = m_{\mathrm{R}} - \Sigma(\hat{p}). \tag{4.14}$$

Using leading order in α_{S} the quark self energy is $\Sigma(\hat{p}) \approx \Sigma^{(1)}(m_{\mathrm{p}})$, where $\Sigma^{(1)}(m_{\mathrm{p}})$ is the one-loop quark self-energy (see Fig. 4.14a).

Ambiguity in the pole mass comes from infrared renormalons [79], i.e. from singularities which arise from the insertion of vacuum polarization subdiagrams into the gluon propagator in the one-loop self-energy diagram (see Fig. 4.14a′). Analysis of the renormalon ambiguitiy has revealed [79, 80] that this ambiguity reads as

$$\delta m_{\mathrm{pole}} \sim \frac{8\pi}{3\beta_0} e^{-\mathrm{C}/2} \Lambda_{\mathrm{QCD}}, \tag{4.15}$$

where C is a finite renormalization-scheme dependent constant (in the $\overline{\mathrm{MS}}$ scheme $C = -5/3$) and β_0 is the one-loop QCD beta-function coefficient, $\beta_0 = 11 - (2/3)N_{\mathrm{f}}$.

For clarification of the top-quark mass issue from experimental point of view, let us consider the top-quark decay products - W boson and b-quark (see Fig. 4.15). To reconstruct the top-quark mass as an invariant mass of its decay products, its precision is limited. The reason is that in the case of b-quark its 4-momentum cannot be in principle measured precisely. Due to the confinement the b-quark should pick up at least one quark which is not from the top-quark

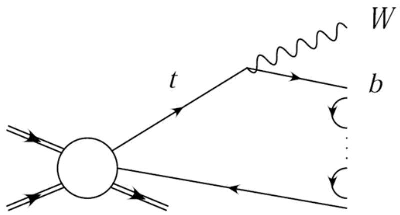

Fig. 4.15. Top quark production and its decay to W boson b-quark which hadronizes nonperturbatively.

decay but from the interaction neighborhood. As a consequence uncertainty of order of Λ_{QCD} appears in the reconstructed top-quark mass. In connection with above mentioned the question what is the relation between the pole and reconstructed masses is not fully clear. On the other hand it is well-known that short distance masses impose renormalization conditions which avoid this problem. In a perturbative expansion in the strong coupling α_{S} the pole mass $m_{\mathrm{t}}^{(\mathrm{pole})}$ can be related to the running mass $m(\mu_{\mathrm{R}})$ in the $\overline{\mathrm{MS}}$ scheme

$$m_{\mathrm{t}}^{(\mathrm{pole})} = m(\mu_{\mathrm{R}})\left(1 + \alpha(\mu_{\mathrm{R}})d_1(\mu_{\mathrm{R}})\right), \tag{4.16}$$

where coefficient $d_1(\mu_{\mathrm{R}})$ is actually known to the three-loop approximation [81]. If $\mu_R = m$ then the mass, $\overline{m} = m(m)$, is call the $\overline{\mathrm{MS}}$ mass. Using Eq. 4.16 and dependence of the top-quark production cross section on the top-quark pole mass:

$$\sigma_{pp\to t\bar{t}X} = \alpha_S^2 \sigma^{(0)}(m_{\mathrm{t}}^{(\mathrm{pole})}) + \alpha_S^3 \sigma^{(1)}(m_{\mathrm{t}}^{(\mathrm{pole})}) + \cdots . \tag{4.17}$$

Using Eq. 4.16 for the $\overline{\mathrm{MS}}$ mass, $\overline{m}$, the $t\bar{t}$ cross section can expressed through the $\overline{m}$ as follows

$$\sigma_{pp\to t\bar{t}X} = \alpha_{\mathrm{S}}^2 \sigma^{(0)}(\overline{m}) + \alpha_{\mathrm{S}}^3 \left(\sigma^{(1)}(\overline{m}) + \overline{m} d^{(1)}(\overline{m})\partial_m \sigma^{(0)}(m)\mid_{m=\overline{m}}\right) + \cdots . \tag{4.18}$$

For simplicity we have confined ourselves here to NLO but the relation between $\sigma_{pp\to t\bar{t}X}$ and $\overline{m}$ can be expressed also at the NNLO approximation (see [82]). From Eq. 4.18 it is clear that measuring the top-quark production cross section we can determine $\overline{\mathrm{MS}}$ mass or any other short range mass, where the non-perturbative effects are absent.

4.5.2 Top-quark mass measurement

The top-quark mass, m_{t}, can be reconstructed in any of the $t\bar{t}$ topologies (lepton + jets, dilepton, all jets). Different approaches are used to determine the top-quark mass. There are essentially two basic groups of the reconstruction:

- template methods [83],
- matrix elements methods [84, 85].

Template approach. The template methods are based on distributions of observables sensitive to m_t usually called signal templates. The signal templates are created using MC for different input values of m_t. An example of such a variable is a reconstructed invariant mass of b-jet, lepton and neutrino coming from the same top quark, $M_{\mathrm{top}} = M_{b\ell\nu}$. Distributions of $M_{b\ell\nu}$ for three different initial top-quark masses are shown in Fig. 4.16 (left). Distribution of the mentioned observable is created also for the background processes, it is so-called background template.

Matrix element approach. In the matrix element case, the likelihood L_{sample} to observe a sample of selected events in the detector is used. The likelihood is obtained directly from the theoretical prediction for the differential cross-sections of the relevant processes and the detector resolution and is calculated as a function of the assumed values for each the top-quark mass to be measured. The mass m_{t} is extracted from the minimisation of the full likelihood L_{sample}, which is computed as the product of likelihoods to observe each individual event.

Event selection. The first step in m_{t} reconstruction is selection of the top-quark pair candidate events. The selection is based on a hardware trigger (the first level trigger) which is implemented in hardware and uses a subset of detector information. This is followed by software-based trigger levels. In addition at reconstruction level a set of additional selection criteria is applied. The used trigger and applied selection criteria depend on the used approach. In the case of the lepton + jets channel the selection is based on single lepton (electron and muon) high transverse momentum trigger with the momentum threshold usually above 20 GeV. In addition on a software level the reconstructed events are selected using criteria designed to identify the lepton+jets final states, i.e. $t\bar{t}$ events in which one of the W bosons decays leptonically and the other hadronicaly. It means that events passing the trigger selection are required to contain exactly one reconstructed lepton, with high transverse momentum p_{T}, at least four jets with high transverse momenta and missing transverse momentum exceeding a certain threshold. The thresholds on lepton, jet and missing transverse momenta depend on the analysis type. There are also other requirements as a requirement concerning e.g. primary vertex (it should contain some minimal number of charged particles), etc. There can be also specific requirements concerning a concrete analysis. Selection of the $t\bar{t}$ event candidates in the dileptonic final state is based on a single lepton or a dilepton trigger (their combination is used) and the selected events should be characterized by the presence of two isolated leptons with high p_{T}, high $E_{\mathrm{T}}^{\mathrm{miss}}$ arising from the two neutrinos from the leptonic W boson decays, and two b-jets. In the all hadronic $t\bar{t}$ case for the selection the jet-based trigger is used and at least six high p_{T} (with threshold over 20 GeV), two of them b-tagged. The events with isolated high p_{T} lepton (electron or muon) and with high $E_{\mathrm{T}}^{\mathrm{miss}}$ are rejected.

In addition the selection of events in real analyses consists of a series of requirements on the general event quality and on the reconstructed objects, designed to select events consistent with this topology - for this see concrete analyses of ATLAS and CMC [87, 86, 53, 88, 89, 90]

Event fit. To reconstruct correctly m_{t}, concrete topology of each candidate event should be known, i.e. the event kinematics including four-momenta of all important output particles should be known and moreover it is needed to know what are the relations between the particles. In the case of lepton+jet channel we have at least four jets and we need to know which one corresponds to b-quark coming from the same (anti)top-quark decay as the lepton, which two jets are from W decay and which one corresponds to hadronic branch b-quark. Taking four jets with the highest p_{T}, we have for the lepton+jet channel twelve different jet combination and as

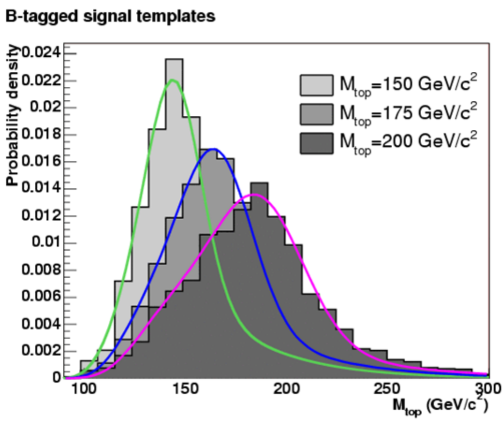

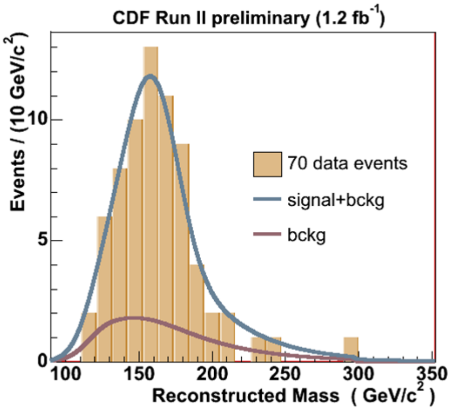

Fig. 4.16. Signal top-quark templates for three different m_t masses (left) and data fitted by sum of a signal and a background template (right).

there are two solutions for the initial value of the neutrino longitudinal momentum we have for each event 24 different topologies, if no information on b-jets is available. For events with one b-tagged jet there are six and for events with two b-tags two allowed topologies. For each of these topologies we find the reconstructed top-quark mass, $m_t^{\rm reco}$, by minimizing a χ^2 with $m_t^{\rm reco}$ as a free parameter. The kinematic fit of each event topology provide us with not only $m_t^{\rm reco}$ but also with a corresponding χ^2 and four-momenta of all reconstructed objects corresponding to $t\bar{t}$ decay products. An example of the χ^2 fit can be taken from the original CDF work [83]. The χ^2 expression contains terms for the uncertainty on the measurements of jet, lepton, and unclustered energies, as well as terms for the kinematic constraints applied to the system:

$$\chi^2 = \sum_{i=\ell,jets} \frac{\left(p_{\rm T}^{{\rm i},fit} - p_{\rm T}^{\rm i,meas}\right)^2}{\sigma_i^2} + \sum_{j=x,y} \frac{\left(p_{\rm j}^{\rm UE,fit} - p_{\rm j}^{\rm UE,meas}\right)^2}{\sigma_{UE}^2}$$
$$+ \frac{(M_{\ell\nu} - M_W)^2}{\Gamma_W^2} + \frac{(M_{jj} - M_W)^2}{\Gamma_W^2} + \frac{(M_{b\ell\nu} - M_t^{\rm reco})^2}{\Gamma_t^2} + \frac{(M_{bjj} - M_t^{\rm reco})^2}{\Gamma_t^2}. \tag{4.19}$$

The first term constrains the $p_{\rm T}$ of the lepton and four leading jets to their measured values within their assigned uncertainties; the second term does the same for both transverse components of the unclustered energy (energy corresponding to a residual interaction with respect to the $t\bar{t}$ production). The quantities $M_{\ell\nu}$, M_{jj} , $M_{b\ell\nu}$, and M_{bjj} refer to the two or three particle invariant masses as is denoted in the subscripts, e.g. $M_{\ell\nu}$ is the lepton–neutrino invariant mass: $M_{\ell\nu} = \sqrt{(p_\ell + p_\nu)^2}$, where p_ℓ (p_ν) is the lepton (neutrino) four momentum. M_W is the pole mass of the W boson, 80.42 GeV/c^2 [13], and $m_t^{\rm reco}$ is the free parameter for the reconstructed top-quark mass used in the minimization. M_{jj} is a quantity computed in the kinematic fit. Γ_W and Γ_t are the total width of the W boson and the top quark [13].

Data distribution of this sensitive observable is compared to a combination of the signal and background templates and the best agreements defines the mass (see further for an example).

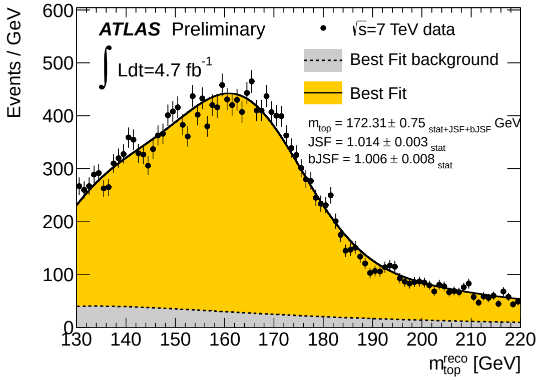

Fig. 4.17. Fitted $m_{\rm top}^{\rm reco}$ distribution in the data. The fitted probability density functions for background alone and background plus signal contributions are also shown.

An interesting example of an application of the template method is the ATLAS measurement of $m_{\rm t}$ carried out for the $t\bar{t}$ lepton+jets channel using the data sample of 4.7 fb^{-1} at 7 TeV.

$$m_{\rm t} = 172.31 \pm 0.75 \text{ (stat+JSF)} \pm 1.35 \text{ (syst) GeV}$$

The first uncertainty corresponds to a combined uncertainty of the statistics, jet energy scale and b-jet energy scale. It is so-called 3-D template method using an approach based on observables $m_{\rm top}^{\rm reco}$, $m_{\rm W}^{\rm reco}$ and $R_{\rm lb}^{\rm reco}$ [87] which are: the reconstructed top-quark mass obtained from the likelihood fit, the invariant mass of the hadronically decaying W boson and the third observable is defined as the ratio of the transverse momentum of the b-tagged jet divided by the average transverse momentum of the two light jets of the hadronic W boson decay, respectively.

For each event, to obtain the top-quark mass, $m_{\rm top}^{\rm reco}$, and to select the jets for computing $m_{\rm W}^{\rm reco}$, this analysis utilizes a kinematic fit maximizing an event likelihood. In Fig. 4.17 is shown the $m_{\rm top}^{\rm reco}$ distribution in the data together with the corresponding fitted probability density functions for the background contribution alone and background plus signal contributions. The reconstructed top-quark mass is found together with a global jet energy scale factor, and a relative b-jet to light-jet energy scale factor, and the value is found to be m_t = 172.31 $\pm$ 0.23 (stat) $\pm$ 0.27 (JSF) $\pm$ 0.67 (bJSF) $\pm$ 1.35 (syst) GeV, where the uncertainties labelled JSF and bJSF refer to the statistical uncertainties on m_t induced by the in-situ determination of these scale factors.

A similar study using the template method was carried out by CMS at $\sqrt{s}$ = 7 TeV with the selected data events corresponded to the integrated luminosity of 5.0 fb^{-1}. In this case two observables $m_{\rm t}^{\rm fit}$ and $m_{\rm W}^{\rm reco}$ corresponding to the top-quark mass from the event kinematic fit and the reconstructed W-boson mass, respectively, are used.

The top-quark mass is determined simultaneously with the jet energy scale (JES), constrained by the known mass of the W boson in $q\bar{q}$ decays, to be $m_{\rm t}$ = 173.49$\pm$0:43 (stat.+JES)$\pm$0.98 (syst.) GeV. In ATLAS and CMS the analyses on the top-quark mass determination are carried out not only in the lepton+jets channel but also in the dilepton and all hadronic channels (see in Ref. [91, 92]).

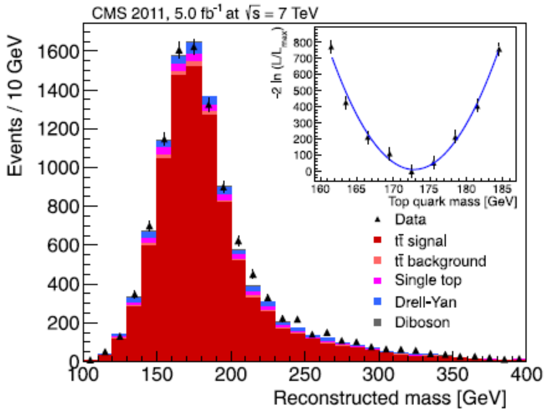

Fig. 4.18. Distribution of the reconstructed mass in data and simulation for a top-quark mass hypothesis of 172.5 GeV with the AMWT method (see text). The inset shows $-2\ln(L/L_{\max})$ versus m_t with the quadratic fit superimposed.

An example of analysis in the dileptonic mode is the analysis carried out by CMS and described in Ref. [88] and denoted as the Analitical Matrix Weighting Technique (AMWT) . The top-quark mass is measured in pp collisions at $\sqrt{s}$ = 7 TeV using a data sample corresponding to an integrated luminosity of 5.0 fb^{-1}. The measurement is performed in the dilepton decay channel $t\bar{t} \rightarrow (\ell^+\nu_l b)(\ell^-\bar{\nu}_l\bar{b})$, where $\ell = e,\ \mu$. Candidate top-quark decays are selected by requiring two isolated energetic leptons, at least two jets, and imbalance in transverse momentum. The events are selected by dilepton triggers. The mass is reconstructed with an analytical matrix weighting technique [93] using distributions derived from simulated samples. The dominant background process is DrellYan (DY) production. Single top-quark production through the tW channel as well as diboson production also mimic the dilepton signature but have much lower cross sections. The requirement on two isolated leptons makes the contribution of multijet production to be also very small. The top-quark mass is measured to be m_t = 172.50 $\pm$ 0.43 (stat.) $\pm$ 1.48 (syst.) GeV. The main source of the systematic uncertainty are the jet scale, the b-jet scale and PDFs. Fig. 4.18 shows the predicted distribution of the reconstructed masses $m_{\rm MWT}$ for a simulated top quark with mass m_t = 172.5 GeV, superimposed on the distribution observed in data. The inset shows the distribution of the $-2\ln(L/L_{\max})$ points with the quadratic fit used to measure m_t. The χ^2 probability of the fit is 0.36.

The ATLAS and CMS collaboration have measured also in the all jet mode. The ATLAS measurement carried out in a data set with 4.6 fb^{-1} at $\sqrt{s}$ = 7 TeV. Events consistent with hadronic decays of $t\bar{t}$ pairs with at least six jets in the final state are selected. The substantial background from multijet production is modeled with data-driven methods that utilise the number of identified b-quark jets and the transverse momentum of the sixth leading jet, which have minimal correlation. The top-quark mass is obtained from template fits to the ratio of three-jet to dijet mass. The three-jet mass is calculated from the three jets produced in a top-quark decay. Using these three jets the dijet mass is obtained from the two jets produced in the W boson decay. The top-quark mass obtained from this fit is thus less sensitive to the uncertainty in the energy

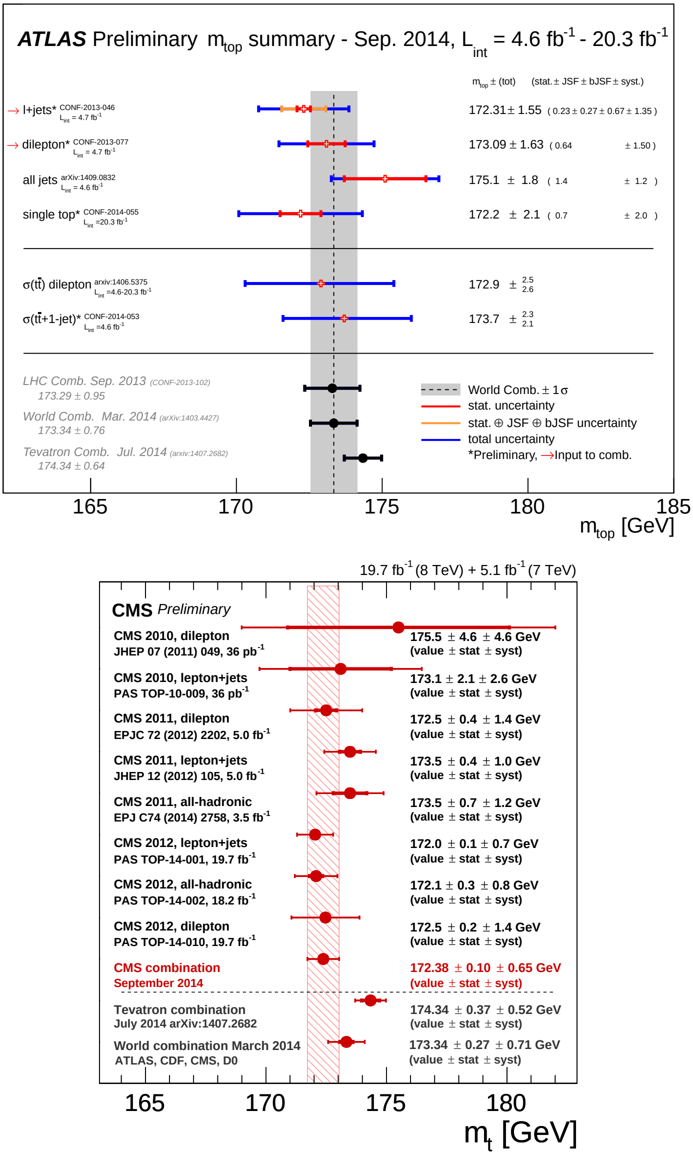

Fig. 4.19. Summary of ATLAS (left) and CMS (right) measurements of the top-quark mass at 7 and 8 TeV compared to LHC, Tevatron and world average.

measurement of the jets. A binned likelihood fit yields a top-quark mass of m_t = 175.1 $\pm$ 1.4 (stat.) $\pm$ 1.2 (syst.) GeV.

The results of the ATLAS measurements are compared with the CMS and Tevatron results in Figure 4.19 and good agreement among the obtained results can be stated.

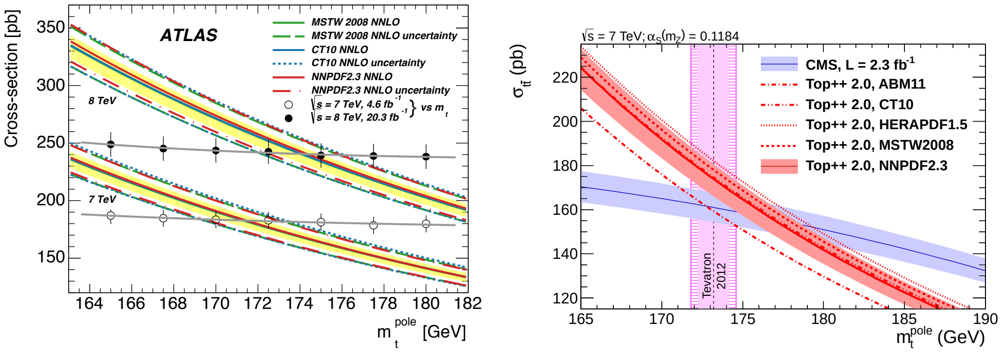

Fig. 4.20. Top quark pole mass measured by ATLAS at 7 and 8 TeV (left) and by CMS at 7 TeV (right) compared to the QCD prediction at NNLO with different PDF sets (see text).

4.5.3 Measurement of top-quark pole mass

As it has already been mentioned in Secs. 4.1 and 4.2, the top-quark pole mass plays an important role in the intrinsic tests of the SM and for the vacuum stability problem, so its precise measurement is of a great importance. In the study described in Ref. [53] the ATLAS collaboration has performed, in addition to the cross section, also a measurement of the top-quark pole mass using dependence of cross section on the pole mass $m_t^{\rm pole}$. The dependence of the cross-section predictions on $m_t^{\rm pole}$ is shown in Fig. 4.20 (left) at both $\sqrt{s}$ = 7 TeV and $\sqrt{s}$ = 8 TeV. The calculations were fitted to the parameterisation:

$$\sigma_{t\bar{t}}^{\rm th}\left(m_t^{\rm pole}\right) = \sigma_t^{\rm ref}\left(\frac{m_t^{\rm ref}}{m_t^{\rm pole}}\right)\left(1 + a_1 x + a_2 x^2\right) , \tag{4.20}$$

where $m_t^{\rm ref}$ = 172.5 GeV, and $x = \left(m_t^{\rm pole} - m_t^{\rm ref}\right)/m_t^{\rm ref}$, and $\sigma_t^{\rm ref}$, a_1 and a_2 are free parameters. This function was used to parameterise the dependence of $\sigma_{t\bar{t}}$ on m_t separately for each of the NNLO PDF sets (CT10, MSTW and NNPDF2.3) – see details in Ref. [53]. Fig. 4.20 (left) shows the predicted $t\bar{t}$ cross section at NNLO+NNLL, as a function of the top-quark pole mass, using the mentioned NNLO PDF sets, compared to the cross section measured by ATLAS assuming $m_t = m_t^{\rm pole}$. A single top-quark pole mass value, $m_t^{\rm pole}$, was derived for each centre-of-mass energy (7 and 8 TeV), giving for the CT10 PDF sets the following values:

$$m_t^{\rm pole} = 171.4 \pm 2.6 \text{ GeV } (\sqrt{s} = 7 \text{ TeV}) \text{ and } m_t^{\rm pole} = 174.1 \pm 2.6 \text{ GeV } (\sqrt{s} = 8 \text{ TeV}).$$

The main source of the top-quark pole mass uncertainty comes from theoretical uncertainties connected with the PDFs, the strong coupling constant $\alpha_{\rm S}$ and with the QCD scale choice. The experimental uncertainty main sources are the systematics of the $t\bar{t}$ cross section measurement and uncertainties of the LHC beam energy and integrated luminosity.

The CMS collaboration measured at $\sqrt{s}$ = 7 TeV in the dileptonic decay channel from data corresponding to an integrated luminosity of 2.3 fb^{-1} the inclusive cross section for top-quark pair production and compared it to the QCD prediction at NNLO + NNLL with different PDF sets to determine the top-quark pole mass, m_t^{pole}, and also the strong coupling constant, $\alpha_{\mathrm{S}}(m_Z)$ at Z boson mass, m_Z [94]. In Fig. 4.20 (right) the predicted $t\bar{t}$ cross section at NNLO+NNLL, as a function of the top-quark pole mass, using five different NNLO PDF sets, compared to the cross section measured by CMS assuming $m_t = m_t^{\mathrm{pole}}$. The uncertainties on the measured $\sigma_{t\bar{t}}$ as well as the renormalization and factorization scale and PDF uncertainties on the prediction with NNPDF2.3 are illustrated with filled bands. Using the NNPDF2.3 PDF set the measured m_t^{pole} and $\alpha_{\mathrm{S}}(m_Z)$ are:

$$m_t^{\mathrm{pole}} = 176.7^{+3.8}_{-3.4} \text{ and } \alpha_{\mathrm{S}}(m_Z) = 0.1151^{+0.0033}_{-0.0032}.$$

Similarly like in the ATLAS case, the main m_t^{pole} uncertainties come from theoretical uncertainties connected with the PDFs, α_{S} and choice of scale. Comparing the ATLAS and CMS results on m_t^{pole} good compatibility within the experimental uncertainties is seen.

An interesting method of the top-quark pole mass extraction is described in Ref. [95], where the pole mass is extracted from a measurement of the normalized differential cross section of top-quark pair production in association with one jet, $t\bar{t}$ + 1-jet, as a function of the inverse of the invariant mass, $\rho \propto 1/\sqrt{s_{\mathrm{t\bar{t}j}}}$, of the $t\bar{t}$+ 1-jet system:

$$R\left(m_t^{\mathrm{pole}}, \rho_S\right) = \frac{1}{\sigma_{t\bar{t}+1}} \frac{d\sigma_{t\bar{t}+1}}{d\rho_S} \left(m_t^{\mathrm{pole}}, \rho_S\right).$$

This process is sensitive to the top-quark mass since gluon radiation depends on the mass of the radiating quark. ATLAS applied this technique to pp collision data corresponding to an integrated luminosity of 4.6 fb^{-1} collected at $\sqrt{s}$ = 7 TeV [96]. Events are selected with the lepton+jets final state and at least one additional jet, requiring exactly one lepton (electron or muon), at least two b-tagged jets, at least three more jets not identified as b-quark jets and the presence of significant missing transverse momentum due to the neutrino which escapes detection. The differential cross section is unfolded to the parton level and normalized. The pole mass m_t^{pole} is extracted through a fit to the data with the prediction for $t\bar{t}$ + 1-jet production at NLO approximation interfaced with parton showers. The extracted top-quark pole mass is:

$$m_t^{\mathrm{pole}} = 173.7 \pm 1.5 \text{ (stat.)} \pm 1.4 \text{ (syst.)} \;^{+1.0}_{-0.5} \text{ (theo.) GeV}.$$

The statistical uncertainty (stat.) is slightly higher than the experimental one (syst.), which accounts for the imperfections in the modeling of the detector response, the background yield and the signal modeling. The theoretical error (theo.) includes the uncertainty due to missing higher orders in the perturbative NLO calculation in addition to those due to the parton distribution functions (PDFs) and the value of strong coupling constant, α_{S}, used in the calculations.

4.5.4 Measurement of the top-antitop quark mass difference

The SM is a local gauge-invariant quantum field theory in which a fundamental role plays the CPT symmetry (combination of charge conjugation (C), space reflection (P) and time reversal (T)). The CPT symmetry appears to be conserved in nature [13]. A major consequence of CPT conservation is that the mass of any particle must be equal to that of its antiparticle. Hence, the question of difference between mass of top and anti-top quark, $\Delta m_t = m_t - m_{\bar{t}}$, is very

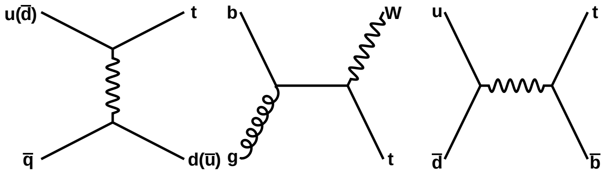

Fig. 4.21. Leading order production diagrams of single top quark: the exchange of virtual W boson in t-channel (left), the associated production of a top quark and an on-shell W boson (middle), and s-channel production (right).

actual from the early days of the top-quark physics. The difference was first measured by the Tevatron experiments. The D0 collaboration measured the mass deference Δm_t to be Δm_t = 0.8 $\pm$ 1.8 (stat.) $\pm$ 0.5 (syst.) GeV [97] and the CDF final result for this difference is: Δm_t = -1.95 $\pm$ 1.11 (stat.) $\pm$ 0.59 (syst.) GeV [98]. Both cases show no significant deviation from zero, i.e. from the SM prediction. However at LHC more stringent results are expected. The CMS collaboration has measured the top-quark mass difference using a data sample collected at $\sqrt{s}$ = 7 TeV and corresponding to the integrated luminosity of 4.96 $\pm$ 0.11 fb^{-1} [99]. The analysis was performed in the lepton + jets channel, where lepton is an electron or a muon. The top-quark mass difference measured by CMS yielded into the following value:

$$\Delta m_t = -0.44 \pm 0.46 \text{ (stat.)} \pm 0.27 \text{ (syst.)}$$

The ATLAS collaboration measured the top-quark mass difference also at $\sqrt{s}$ = 7 TeV using the data sample corresponding to the integrated luminosity of 4.7$\pm$0.2 fb^{-1} [100]. The analysis was performed in the lepton + jets channel with exactly one high p_{T} lepton (an electron or a muon) assuming two b-tags. The measured top-quark mass difference is

$$\Delta m_t = 0.67 \pm 0.61 \text{ (stat.)} \pm 0.41 \text{ (syst.)}$$

One can conclude that the LHC experiments have confirmed with higher precision the Tevatron result, that the mass difference in the $t\bar{t}$ case is compatible with the SM expectation of no difference between the top- and anti-top- quark masses.

4.6 Single-top-quark results

The single-top-quark production occurs via the EW interaction. There are three sub-processes contributing to this production at LO (see Fig. 4.21): the exchange of a virtual W boson in the t-channel, or in the s-channel, and the associated production of a top quark and an on-shell W boson. The process with the highest expected cross section at the LHC is the t-channel mode.

Among the virtues of the single-top-quark production are: (*i*) its cross section is proportional to $\mid V_{tb} \mid^2$, where V_{tb} is an element of the Cabbibo-Kobayashi-Maskawa (CKM) matrix [101] – so it enables a direct measurement of this CKM matrix element, (*ii*) charge asymmetry in production of t with respect to $\bar{t}$ is sensitive to the proton u- and d-quark PDFs, and (*iii*) it is sensitive to many models of new physics [102]. In addition, the single-top-quark processes are an important background for Higgs boson studies.

Theoretical results for single-top-quark production are based on NLO QCD and electroweak calculations [103, 104, 105, 106, 107], some of them include gluon resummations [109, 108, 110,

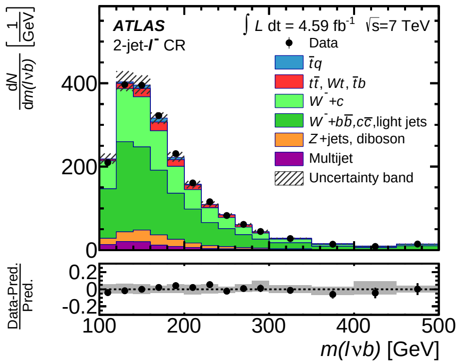

Fig. 4.22. The invariant mass $m(\ell\nu b)$ distribution for the 2-jet b-tagged sample – the signal and different backgrounds are compared.

111] and fixed order computations matched to parton showers [112, 113, 114]. In the case of the single-top-quark t-channel there are also available NNLO calculations [115]. The theoretical cross sections for the individual channels expected in the SM are summarized in Table 4.3.

Single-top-quark production was observed first in proton-antiproton collisions at the Tevatron collider (the CDF aand D0 experiments) with a centre-of-mass energy of 1.96 TeV [116,117,118, 119]. The CDF and D0 experiments measured first combined s- and t-channel production, but later they reported also s-channel process alone [120,121] and also the CDF and D0 combination.

4.6.1 Single-top-quark production in t channel

The t-channel single-top-quark production is the most abundant single-top-quark process at both the Tevatron and the LHC. An example of the ATLAS single-top-quark studies is the analysis of the t-channel process [122] using 4.59 fb^{-1} of pp collision data collected at $\sqrt{s} = 7$ TeV and using 5.8 fb^{-1} collected at $\sqrt{s} = 8$ TeV [123]. The study is based on event selection requiring one charged lepton candidate, e or μ, two or three hadronic high-p_T jets – at least one of them must be b-tagged; and missing transverse momentum $E_T{}^{\text{miss}} > 30$ GeV. The measurement of the cross section, σ_t, is based on a fit to a multivariate discriminant constructed with a Neural Network (NN) [124] to separate signal from background. The most significant background comes from from W-boson production in association with jets .
Other significant backgrounds come from multijet events and $t\bar{t}$ production. Figure 4.22 shows

Tab. 4.3. Single-top-quark production cross sections in the t-channel, Wt-channel and s-channel calculated in NLO including QCD and EW corrections at $\sqrt{s}$ = 7 and 8 TeV.

Energy	t-channel [pb]	Wt-channel [pb]	s-channel [pb]
7 TeV	$64.57\,^{+2.63}_{-1.74}$	$15.74\,^{+1.17}_{-1.21}$	$4.63\,^{+0.20}_{-0.18}$
8 TeV	$87.76\,^{+3.44}_{-1.91}$	22.37 ± 1.52	5.61 ± 0.22
source	[108]	[110]	[109]

Energy	σ_t [pb]	$\mid V_{tb} \mid$
7 TeV	68.0 $\pm$ 2.0 (stat.) $\pm$ 8 (syst.)	1.02 $\pm$ 0.07 (exp.)
8 TeV	95.1 $\pm$ 2.4 (stat.) $\pm$ 18 (syst.)	$1.04^{+0.10}_{-0.11}$ (exp.)

Tab. 4.4. Single-top-quark production cross sections (σ_t) measured by ATLAS at 7 and 8 TeV and the extracted CKM element $\mid V_{tb} \mid$.

the invariant mass of the b-tagged jet, the charged lepton, and the neutrino, $m(\ell\nu b)$, for the 2-jet b-tagged sample at 7 TeV. As follows from Figure 4.22 the signal is clearly separated from the background. Table 4.4 shows the t-channel cross sections at $\sqrt{s} = 7$ and 8 TeV inferred from simultaneous measurements in the 2-jet and 3-jet channels applying a NN-based analysis. Even at 7 TeV the significance of the observed signal corresponds to 7.2σ. The lower limit of $\mid V_{tb} \mid$at 95% C.L. is 0.75 at 7 TeV and $\mid V_{tb} \mid >$ 0.80 at 95% C.L. at 8 TeV.

In addition to the total cross section, σ_t, ATLAS has carried out within the work at 7 TeV described in Ref. [122], also a measurement of the separate t and $\bar{t}$-quark cross sections, $\sigma_t(t)$ and $\sigma_t(\bar{t})$. The separate cross sections are sensitive to the u- and d-quark PDFs and the SM expectations are

$$\sigma_t(t) = 41.9^{+1.8}_{-0.8}\text{ pb and } \sigma_t(\bar{t}) = 22.7^{+0.9}_{-1.0}\text{ pb.}$$

The multivariate technique combining several kinematic variables into one neural network discriminant was used. The obtained cross sections $\sigma_t(t)$ and $\sigma_t(\bar{t})$ are:

$$\sigma_t(t) = 46 \pm 1\text{ (stat.)} \pm 6\text{ (syst.) pb,}\quad \sigma_t(\bar{t}) = 23 \pm 1\text{ (stat.)} \pm 3\text{ (syst.) pb,}$$

assuming a top-quark mass of m_t = 172.5 GeV. The cross sections are, within uncertainties, compatible with the SM expected ones and give the ratio $R_t = \sigma_t(t)/\sigma_t(\bar{t})$ = 2.04 $\pm$ 0.13(stat.) $\pm$ 0.12(syst.) = 2.04 $\pm$ 0.18,.

The CMS collaboration has also measured the single-top-quark t-channel production at $\sqrt{s}$ = 7 TeV [125] and at $\sqrt{s}$ = 8 TeV [126] using events with leptonically decaying W bosons (muons and electrons taken as leptons). The analysis uses two complementary approaches. The first one exploits the reconstructed top-quark mass and the forward pseudorapidity distribution of the light jet recoiling against the top quark. The second approach exploits the compatibility of the signal candidates with the event characteristics predicted by the SM for electroweak top-quark production within two independent multivariate techniques – one of them is based on a NN and the other on Boosted Decision Trees (BDT) [127]. Event selection is similar as in the ATLAS case – a single isolated muon or electron and momentum imbalance due to the presence of a neutrino, with one central b-jet from the top-quark decay. An additional light-quark jet from the hard-scattering process and possibly second b-jet produced in association with the top quark. The combined result of all the approaches for the measured single-top-quark t-channel production cross section at $\sqrt{s}$ = 7 TeV is

$$\sigma_t(t) = 67.2 \pm 3.7\text{ (stat.)} \pm 3.0\text{ (syst.)} \pm 3.5\text{ (theo.)} \pm 1.5\text{ (lumi.) pb}\quad = 67.2 \pm 6.1\text{ pb,}$$

for an assumed top-quark mass of 172.5 GeV. The result is

In this analysis there was also determined the CKM element $\mid V_{tb} \mid$ assuming that $\mid V_{td} \mid$ and $\mid V_{ts} \mid$ are much smaller than $\mid V_{tb} \mid$, as $\mid V_{tb} \mid = \sqrt{\sigma_{t-\mathrm{ch}}/\sigma^{\mathrm{SM}}_{t-\mathrm{ch}}}$, where $\sigma^{\mathrm{SM}}_{t-\mathrm{ch}}$ is the

SM prediction calculated assuming $\mid V_{tb} \mid = 1$. Not assuming an anomalous Wtb coupling the extracted value of the CKM element is

$$\mid V_{tb} \mid = 1.02 \pm 0.046 \text{ (meas.)} \pm 0.017 \text{ (theo.)} ,$$

where the first uncertainty term contains all uncertainties of the cross section measurement including theoretical ones, and the second one is the uncertainty on the SM theoretical prediction. Measurement performed by CMS at $\sqrt{s}$ = 8 TeV [126], unlike that at $\sqrt{s}$ = 7 TeV [125], was performed only in the muon decay channel using the data sample of 5 fb^{-1}. The analysis has yielded the following cross section measurement:

$$\sigma_t = 80.1 \pm 5.7 \text{ (stat.)} \pm 11.0 \text{ (syst.)} \pm 4.0 \text{ (lumi.) pb.}$$

In addition, the ratio of cross sections at 7 and 8 TeV, $R_{8/7\mathrm{TeV}}$, and the CKM element $\mid V_{tb} \mid$ at 8 TeV were also extracted:

$$R_{8/7\mathrm{TeV}} = 1.14 \pm 0.12 \text{ (stat.)} \pm 0.14 \text{ (syst.) and } |V_{tb}| = 1.02 \pm 0.046 \text{ (meas.)} \pm 0.017 \text{ (theo.)}$$

The single-top-quark production cross-section measurements in the t-channel at $\sqrt{s}$ = 8 TeV performed by the ATLAS and CMS experiments and based on integrated luminosities of 5.8 fb^{-1} and 5.0 fb^{-1}, respectively have been combined [128]. The best linear unbiased estimator (BLUE) method was applied for the combination, taking into account the individual contributions to systematic uncertainties of the two experiments and their correlations. The combined single-top-quark production cross section in the t-channel at $\sqrt{s}$ = 8 TeV is

$$\sigma_{\mathrm{t-ch}} = 85 \pm 4 \text{ (stat.)} \pm 11 \text{ (syst.)} \pm 3 \text{ (lumi.) pb} = 85 \pm 12 \text{ pb.}$$

All the ATLAS and CMS measurements are in very good agreement with the SM expectations.

4.6.2 Single-top-quark production associated with W boson.

The associated tW production, unlike Tevatron, represents a significant contribution to single-top-quark production at LHC and it is a very interesting production mechanism because of its interference with top-quark pair production [103, 129], its sensitivity to new physics [102, 130, 131], and its role as a background to SUSY searches and Higgs boson studies. It should be noted that the associated Wt production at the NLO mixes with $t\bar{t}$ pair production and contribution of the $t\bar{t}$ production should be removed from the signal. All the analyses are performed using the dilepton decay channel: $pp \to Wt \to \ell\nu b\ell\nu$, where $\ell = e, \nu$. Hence, the signature of an associated Wt event is: two isolated leptons (from W bosons), one b-tagged jet from the top-quark decay and missing transverse energy corresponding to neutrino. Events with two jets (one or two b-tags) are also considered. The measured Wt production cross section are summarized along with the SM theoretical predictions in Table 4.5.

The ATLAS measurements at $\sqrt{s}$ = 7 and 8 TeV correspond to the datasets with the integrated luminosity of 4.7 fb^{-1} and 20.3 fb^{-1}, respectively. In the CMS case at $\sqrt{s}$ = 7 TeV it was 4.9 fb^{-1} and at $\sqrt{s}$ = 8 TeV it was 12.2 fb^{-1}, respectively. In all cases the absolute value of the CKM matrix element $|V_{tb}|$ is determined assuming $|V_{tb}| >> |V_{td}|$ and $|V_{ts}|$.

Energy	$\sigma_t^{\rm SM}$ [pb]	experiment	σ_t [pb]	$\mid V_{tb} \mid$
7 TeV	$16.6 \pm 0.4^{+1.0}_{-1.2}$	ATLAS	16.8 ± 5.7	$1.03^{+0.16}_{-0.19}$
		CMS	$16.0\ ^{+5.0}_{-4.0}$	$1.01^{+0.16}_{-0.14}$
8 TeV	22.4 ± 1.5	ATLAS	27.2 ± 6.1	1.10 ± 0.12(ex.)$\pm$ 0.03(th.)
		CMS	23.4 ± 5.4	1.03 ± 0.12(ex.)$\pm$ 0.04(th.)
		ATLAS+CMS	25.0 ± 4.7	–

Tab. 4.5. Single top quark in association with a W boson production cross sections (σ_t) measured by ATLAS and CMS at $\sqrt{s}$ = 7 and 8 TeV and the extracted CKM element $\mid V_{tb} \mid$; the $\sigma_t^{\rm SM}$ is the SM prediction computed at NLO in QCD, including NNLL soft gluon resummation [110].

4.6.3 Single-top-quark production in s channel

Production of top quark in this channel is of a special interest since the s-channel single-top-quark production is very sensitive to several models of new physics involving a non-SM mediator, like $\acute{W}$ or a charged Higgs boson – details can be found e.g. in Ref. [102]. First evidence of the s-channel of single-top-quark production has been announced in 2013 by the D0 collaboration in the lepton + jets channel with a data set corresponding to 9.7 fb^{-1} of integrated luminosity [121]. In 2014 has announced its evidence for the single-top-quark s-channel production also the CDF collaboration [120] using a data set that corresponds to an integrated luminosity of 9.4 fb^{-1} and selecting events consistent with the s-channel process including two jets and one leptonically decaying W boson. The Tevatron experiments have reported the first observation of single-top-quark production in the s-channel [132] – the observation is based on the combination of the CDF and D0 measurements and resulted in the measured cross section $\sigma_s = 1.29^{+0.26}_{-0.24}$ pb with the significance of 6.3 σ for the presence of an s-channel contribution to the single-top-quark production $p\bar{p}$ collision at $\sqrt{s}$ = 1.96 TeV.

At LHC in pp collisions measuring the s-channel process is more difficult due to a much smaller signal-to-background ratio in comparison with the Tevatron $p\bar{p}$ collisions – it is caused by the need for a sea anti-quark in the initial state. Theoretical calculations for the s-channel are available at approximate NNLO precision in QCD and include the contributions due to NNLL resummation of soft-gluon bremsstrahlung. For the s-channel process, the total inclusive cross-sections for pp collisions at $\sqrt{s}$ = 7 and 8 TeV are predicted to be [108]

$$\sigma_{\rm s}(7\ {\rm TeV}) = 3.20 \pm 0.06\ ({\rm scale})\ ^{+0.12}_{-0.11}({\rm PDF})\ \text{and}\ \sigma_{\rm s}(8\ {\rm TeV}) = 5.61 \pm 0.22\ ,$$

The ATLAS and CMS collaborations searched for the s-channel single-top-quark production in pp collisions at $\sqrt{s}$ = 7 (only ATLAS) and 8 TeV (ATLAS and CMS) [133, 134, 135] obtaining the more pronounced results at $\sqrt{s}$ = 8 TeV. Both the collaborations considered only leptonic decay modes of the top quark giving an electron or a muon and the signal was extracted from a likelihood fit to the distribution of a multivariate discriminant – the BDT technique was applied. Due to the above mentioned circumstances only upper limits at 95% C.L. on the s-channel production were found. The obtained results at $\sqrt{s}$ = 8 TeV are in Table 4.6.

As can be seen from Table 4.6, in both the experiments the results for the s-channel are compatible with the SM expectation.

Single-top-quark summary. The all single-top-quark results obtained by the ATLAS and CMS experiments are summarized in Fig. 4.23.

Experiment	σ_s [pb]	upper limit at 95% C.L. [pb]
ATLAS	$\sigma_s = 5.0 \pm 1.7$ (stat) $\pm$ 4.0(syst)	14.6
CMS	$\sigma_s = 6.2 \pm 5.9$ (exp.) $\pm$ 8.0(th.)	11.5

Tab. 4.6. Single-top-quark production cross sections (σ_s) measured by ATLAS and CMS at $\sqrt{s} = 8$ TeV and the cross section extracted upper limits at 95% C.L.

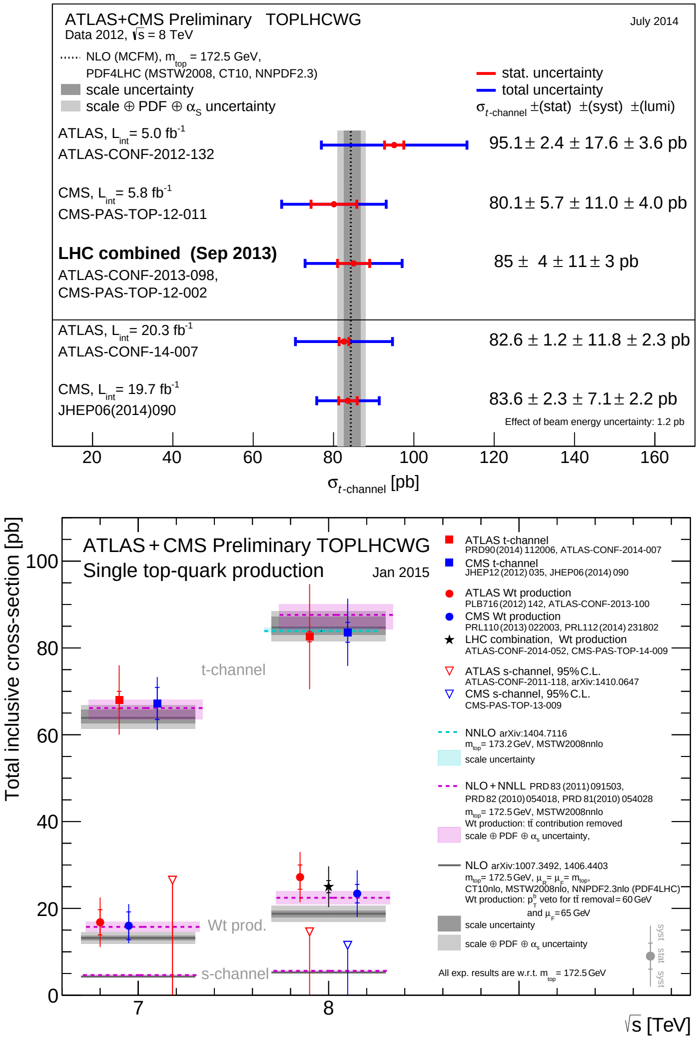

Fig. 4.23. Single-top-quark production: the ATLAS and CMS measurements performed at 8 TeV (left) and all the ATLAS and CMS measurements in all channels (right).

It can be concluded that the single-top-quark production in all channels measured at $\sqrt{s}$ = 7 and 8 TeV is within uncertainties compatible with the SM expectations.

4.7 Top-quark properties

Study of the top-quark properties enables a test of the SM predictions and search for new physics which can modify the top-quark production mechanisms, the Wtb coupling, the top-quark decays, etc.

4.7.1 W-boson helicity fractions.

The helicity fractions of the W boson produced in a $t \to Wb$ decay are defined as the partial rate for a given helicity state divided by the total decay rate: $F_{L,R,0} \equiv \Gamma_{L,R,0}/\Gamma$, where F_L, F_R, and F_0 are the left-handed, right-handed, and longitudinal helicity fractions, respectively. The W-boson helicity fraction measurements are important for the search for anomalous Wtb couplings, i.e. those that do not arise from the SM. In the SM using NNLO calculation the W boson helicity fractions are predicted to be [136]:

$$F_0 = 0.687 \pm 0.005,\ F_{\mathrm{L}} = 0.311 \pm 0.005 \text{ and } F_{\mathrm{R}} = 0.0017 \pm 0.0001.$$

The fractions F_0, F_{L} and F_{R} are extracted from angular distributions of top-quark decay products:

$$\frac{1}{\sigma}\frac{d\sigma}{d\theta^\star} = \frac{3}{4}\left(1 - cos^2\theta^\star\right) F_0 + \frac{3}{8}\left(1 - cos\theta^\star\right)^2 F_{\mathrm{L}} + \frac{3}{8}\left(1 + cos\theta^\star\right)^2 F_{\mathrm{R}}, \tag{4.21}$$

where $\theta^\star$ is the angle between the lepton and b-quark reversed momentum in the W-boson rest frame. Deviations of the measured helicity fractions from the SM predictions can be interpreted in terms of anomalous Wtb couplings [137, 138] and the most general Lagrangian with the anomalous couplings is:

$$L_{\mathrm{Wtb}} = -\frac{g}{\sqrt{2}}\bar{b}\gamma^\mu\left(V_L P_L + V_R P_R\right) t W_\mu^- - \frac{g}{\sqrt{2}}\bar{b}\frac{i\sigma^{\mu\nu}q_\nu}{M_{\mathrm{W}}}\left(g_L P_L + g_R P_R\right) t W_\mu^- + h.c. \tag{4.22}$$

where V_L, V_R, g_L, g_R are dimensionless complex coupling constants, $q = p_{\mathrm{t}} - p_{\mathrm{b}}$, where p_{t} (p_{b}) is the four-momentum of the top quark (b-quark), P_L (P_R) are left (right) chiral operator $1 - \gamma_5$ $(1 + \gamma_5)$, and h.c. denotes the Hermitian conjugate. Hermiticity conditions on the possible dimension-six Lagrangians also impose Im(V_L) = 0 [138]. The coupling constants $V_{L(P)}$ and $g_{L(P)}$ can be in general expressed as follows

$$V_L = V_{tb} + C_{\phi q}^{3,3+3}\frac{\nu^2}{\Lambda^2},\ \ V_R = C_{\phi\phi}^{33*}\frac{\nu^2}{\Lambda^2}, g_L = \sqrt{2}C_{dW}^{33*}\frac{\nu^2}{\Lambda^2},\ \ g_R = \sqrt{2}C_{uW}^{33}\frac{\nu^2}{\Lambda^2}, \tag{4.23}$$

where Λ is the scale of new physics, $\nu(= 246$ GeV) is the EWSB scale and C_X^Y are the effective operator coefficients – details can be found in Ref. [139]. In the SM and at tree level, $V_L = V_{\mathrm{tb}}$, where V_{tb} is the CKM matrix element $V_{\mathrm{tb}} \simeq 1$, and $V_R = g_L = g_R = 0$.

The $t\bar{t}$ W-boson helicity measurements were first carried out by the Tevatron experiments CDF and D0 ($p\bar{p}$ collisions at $\sqrt{s}$ = 1.96 TeV) and their final combined result is [140]:

$$F_0 = 0.722 \pm 0.081 \text{ and } F_{\mathrm{R}} = -0.033 \pm 0.046.$$

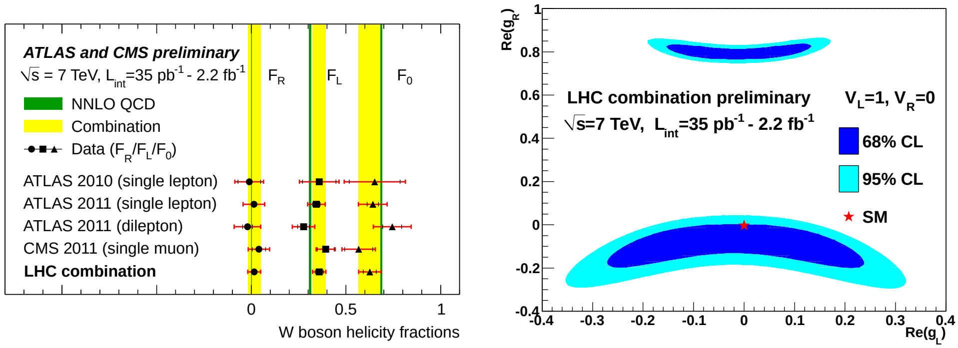

Fig. 4.24. Overview of the measurements included in the LHC combination as well as the results of the combination (see text) (left). Allowed regions for the Wtb anomalous couplings using the combined helicity fractions and assuming V_L=1 and V_R=0, at 68% and 95% C.L. (right).

The obtained Tevatron combined result is consistent with the SM expectations.

At LHC the W-boson helicity measurements have been carried out at $\sqrt{s}$ = 7 TeV (ATLAS and CMS) and at 8 TeV (CMS) in $t\bar{t}$ events as well as in single top-quark events (CMS). The ATLAS measurement of the W-boson helicity fractions has been carried out using the $t\bar{t}$ dataset of 1.04 fb^{-1} at 7 TeV and taking into account lepton+jets and dilepton events [141]. The obtained ATLAS results have been combined with the results of the CMS measurement at $\sqrt{s}$ = 7 TeV performed in the lepton+jets channel of $t\bar{t}$ events using the dataset of 2.2 fb^{-1} [142]. The individual ATLAS and CMS W-boson helicity results as well as the combined ones are shown in Fig. 4.24. The result of CMS W-boson helicity measurement in the lepton+jets of $t\bar{t}$ events using the full dataset of 5 fb^{-1} at $\sqrt{s}$ = 7 TeV is reported in Ref. [143]. In addition CMS measured the W-boson helicity at $\sqrt{s}$ = 7 TeV in the $t\bar{t}$ dilepton channel using a dataset of 4.6 fb^{-1} [144] and at $\sqrt{s}$ = 8 TeV [145] in the lepton+jets channel using the sample of 19.7 fb^{-1}. The CMS collaboration has measured the W-boson helicity also in the single top-quark channel at $\sqrt{s}$ = 7 TeV and 8 TeV [146, 147]. The all LHC W-boson helicity measurements are summarized in Table 4.7.

As it can be seen from Table 4.7, the LHC measurements of the W-boson helicity is consistent within uncertainties with the SM expectations.

Limits on anomalous Wtb couplings. Any deviation of F_0, F_L and F_R from their SM values is a sign of a new physics. Following the expressions for the helicity fractions (see Eq. 4.23) limitations on new physics contributing to the anomalous Wtb couplings can be extracted. Searching for limits on the anomalous Wtb couplings different scenarios are tried. As an example, the scenario used at the combined ATLAS and CMS result [148] assumes that V_L = 1 and V_R = 0, and assuming that the imaginary part of all couplings is 0, limits on the anomalous couplings g_L, g_R were inferred from measurements of the helicity fractions using their dependence on the couplings and these limits are shown in Fig. 4.24 (right). Once again compatibility with the SM expectations can be stated.

Energy	experiment	F_0	F_L	F_R
	$t\bar{t}$ events			
7 TeV	ATLAS (LJ)	$0.642 \pm 0.030 \pm 0.071$	$0.344 \pm 0.020 \pm 0.042$	$0.014 \pm 0.014 \pm 0.055$
	ATLAS (DL)	$0.744 \pm 0.050 \pm 0.087$	$0.276 \pm 0.031 \pm 0.051$	$-0.020 \pm 0.026 \pm 0.065$
	ATLAS (comb)	$0.670 \pm 0.030 \pm 0.060$	$0.320 \pm 0.020 \pm 0.030$	$0.010 \pm 0.010 \pm 0.065$
	CMS (DL)	$0.567 \pm 0.054 \pm 0.048$	$0.393 \pm 0.045 \pm 0.024$	$0.040 \pm 0.035 \pm 0.043$
	CMS (LJ)	$0.682 \pm 0.030 \pm 0.033$	$0.310 \pm 0.022 \pm 0.022$	$0.008 \pm 0.012 \pm 0.014$
	ATLAS+CMS	$0.626 \pm 0.034 \pm 0.048$	$0.359 \pm 0.021 \pm 0.021$	$0.040 \pm 0.035 \pm 0.043$
8 TeV	CMS(LJ)	$0.682 \pm 0.030 \pm 0.033$	$0.310 \pm 0.022 \pm 0.022$	$0.008 \pm 0.012 \pm 0.014$
	single top-quark events			
	CMS	$0.659 \pm 0.015 \pm 0.023$	$0.330 \pm 0.010 \pm 0.024$	$-0.009 \pm 0.006 \pm 0.020$

Tab. 4.7. The LHC measurement of the W-boson helicity fractions (F_0, F_L, F_R) at $\sqrt{s} = 7$ and 8 TeV using the $t\bar{t}$ events and single top-quark events, LJ $\equiv$ lepton+jets and DL $\equiv$ dilepton.

4.7.2 Spin correlation in $t\bar{t}$ events.

While the polarization of the t and $\bar{t}$ quarks in $t\bar{t}$ production is predicted to be very small, their spins are predicted to be correlated [149]. The spin-correlation value predicted by the SM can be altered by the BSM physics which can modify the production mechanism of the $t\bar{t}$ pairs. As an example is the $t\bar{t}$ production via a high-mass Z' boson [150, 151] or via a heavy Higgs boson that decays into $\bar{t}$ [152]. Measurements of the spin correlation between the top quark and the top antiquark usually rely on angular distributions of the top-quark and top-antiquark decay products. The charged leptons and the d-type quarks from the W-boson decays are the most sensitive spin analyzers, and the b quark from top-quark decay contains some information about the top-quark polarization, too. The spin correlation in $t\bar{t}$ events has been studied previously at the Tevatron. The CDF and D0 Collaborations have performed a measurement of the asymmetry by exploring the angular correlations of the charged leptons [153, 154]. The D0 Collaboration exploiting a matrix element based approach [155] has reported the first evidence for nonvanishing $t\bar{t}$ spin correlation combining the results in the dilepton and lepton+jets channels [156, 157].

At LHC the $t\bar{t}$ spin correlations have been studied by the ATLAS and CMS collaborations at both incident energies $\sqrt{s}$ = 7 and 8 TeV. The first analysis carried out by ATLAS reporting a nonvanishing $t\bar{t}$ spin correlation [158] uses a data sample of 2.1fb^{-1} collected at 7 TeV. The search was performed in the dilepton topology ($t\bar{t} \to \ell^+\nu\ell^-\bar{\nu}b\bar{b}$) with large $E_{\mathrm{T}}^{\mathrm{miss}}$ and at least two jets. The observable studied was the azimuthal angle between two leptons, $\Delta\phi$. The analysis at $\sqrt{s}$ = 7 TeV has been later improved using the data sample of 4.6 fb^{-1} [159]. In the latter analysis the dilepton and lepton+jets topologies are used and for extraction of the correlation between the top- and antitop-quark spins. Four different observables, sensitive to different properties of the top-quark pair production mechanism, are used. Using events with one or two isolated leptons in the final state, the spin correlations are measured using an angle difference, $\triangle\phi$, between directions of the lepton and one of the final-state jets or between the two leptons, respectively. Additional measurements are performed in the dilepton final state, using observables which are sensitive to different types of sources of new physics in $t\bar{t}$ production. In particular, angular correlations between the charged leptons from top-quark decays in two different spin quantization bases and a ratio of matrix elements in the dileptonic channel are also measured.

Ignoring the polarization of the pair-produced top quarks, which is in pp collisions negligible in the SM [160], the correlation between the decay products of the top quark (denoted with subscript +) and the top antiquark (denoted with subscript -) can be expressed by

$$\frac{1}{\sigma}\frac{d\sigma}{d\cos\theta_+ d\cos\theta_-} = \frac{1}{4}\left(1 + A\alpha_+\alpha_- \cos\theta_+ \cos\theta_-\right), \tag{4.24}$$

with the degree of spin correlation expressed as

$$A = \frac{N(\uparrow\uparrow) + N(\downarrow\downarrow - N(\uparrow\downarrow) - N(\downarrow\uparrow)}{N(\uparrow\uparrow) + N(\downarrow\downarrow + N(\uparrow\downarrow) + N(\downarrow\uparrow)}, \tag{4.25}$$

where N is the number of events and the arrows show orientation of lepton spin with respect to its momentum direction. The level of the spin correlation can be inferred from a fit of the data $\Delta\phi$ distribution, where $\Delta\phi$ is the azimuthal opening angle between the momentum directions of a top-quark decay product and an antitop-quark decay product in the laboratory frame. In the dilepton final state the $\Delta\phi$ between the charged lepton momentum directions, $\Delta\phi\,(\ell^+\ell^-)$, is explored. This observable is very sensitive to like-helicity gluon-gluon initial states which dominate in $t\bar{t}$ events produced in pp collisions [161] and was used in the ATLAS analysis reported in Ref. [158]. In the lepton+jets channel, $\Delta\phi$ between the lepton momentum direction and either the down-type jet from W-boson decay, $\Delta\phi\,(\ell d)$, or the b-jet from the hadronically decaying top quark, $\Delta\phi\,(\ell b)$, are analyzed. Obtained data $\Delta\phi$ distribution is then fitted to a linear superposition of the SM expected distribution (fraction $f^{\rm SM}$) and the MC uncorrelated one (1-$f^{\rm SM}$).

$$f^{\rm SM} N^{\rm SM}_{\rm t\bar{t}corr}(\Delta\phi) + \left(1 - f^{\rm SM}\right) N^{\rm SM}_{\rm uncorr}(\Delta\phi).$$

The measured degree of correlation, $A^{\rm meas}_{\rm basis}$, related to the fraction $f^{\rm SM}$ as $A^{\rm meas}_{\rm basis} = f^{\rm SM} \times A^{\rm SM}_{\rm basis}$. The subscript "basis" indicates a chosen spin basis [160, 162]. The ATLAS analysis reported in Ref. [159] uses the $\Delta\phi$ observables in both the dilepton and the lepton+jets channels. Additionally this analysis employs also three other observables:

- The *S ratio* of matrix elements M for top-quark production and decay from the fusion of like-helicity gluons ($g_{\rm R}g_{\rm R}, g_{\rm L}g_{\rm L} \rightarrow t\bar{t} \rightarrow (b\ell^+\nu)\,(b\ell^+\nu)$) with SM spin correlation and without spin correlation at LO [161].

- The $\cos(\theta_+)\cos(\theta_-)$ in helicity basis which is based on the differential distribution (see Eq. 4.24), where the top-quark direction in the $t\bar{t}$ rest frame is used as the spin quantization axis. The measurement of this distribution allows for a direct extraction of the spin correlation strength $A_{\rm helicity}$ [149], as defined in Eq. 4.25. The SM prediction is $A^{\rm SM}_{\rm helicity}$ = 0.31, which was calculated including NLO QCD corrections to $t\bar{t}$ production and decay and mixed weak-QCD corrections to the production amplitudes in Ref. [160].

- The $cos(\theta_+)cos(\theta_-)$ in "maximal" basis, based also on the angle differential distribution (Eq. 4.24), using the maximal basis as the top-quark spin quantization axis. There is no optimal axis with the spin correlation strength of 100% for the gluon-gluon fusion process, but there is a quantization axis that maximizes spin correlation on the event-by-event basis and is called the maximal basis [163]. The SM prediction is $A^{\rm SM}_{\rm maximal}$ = 0.44.

	$\Delta\phi$	S ratio	$cos(\theta_+)cos(\theta_-)_{\rm heli}$	$cos(\theta_+)cos(\theta_-)_{\rm maxi}$
$A^{\rm meas}_{\rm helicity}$	$0.37 \pm 0.03 \pm 0.06$	$0.27 \pm 0.03 \pm 0.04$	$0.23 \pm 0.06 \pm 0.07$	...
$A^{\rm meas}_{\rm maximal}$	$0.52 \pm 0.04 \pm 0.08$	$0.38 \pm 0.05 \pm 0.06$	...	$0.36 \pm 0.06 \pm 0.08$

Tab. 4.8. Summary of measurements of the spin correlation strength A in the helicity and maximal bases in the combined dilepton channel for the four different observables.

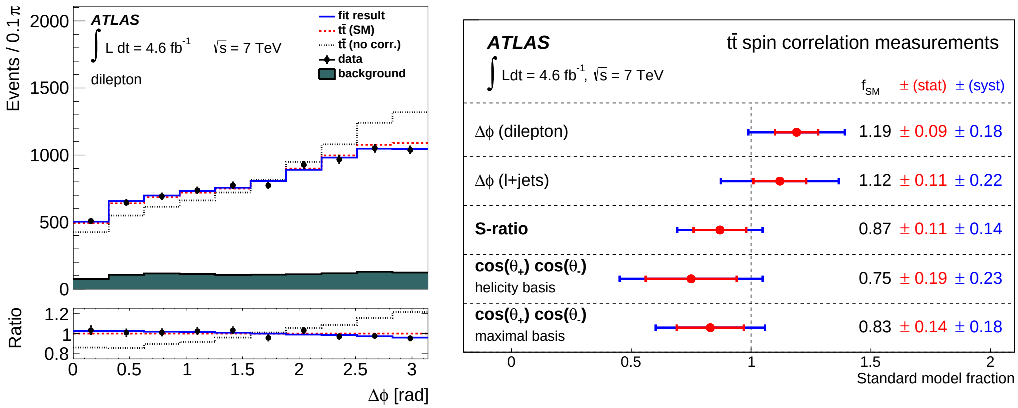

Fig. 4.25. Data distribution $\Delta\phi_{\ell\ell}$ fitted to the templates for background plus $t\bar{t}$ signal with SM spin correlation (red dashed) and without spin correlation (black dotted) (left) and summary of the spin correlation strength measurements (right).

To reconstruct the spin correlation strength, the full kinematic reconstruction of $t\bar{t}$ events is performed in the dilepton and lepton+jets modes. The measured spin correlation strength is found for all four observables and the results are summarized in Table 4.8 and in Fig. 4.25.

In the left plot of Fig. 4.25 is an example of the $\Delta\phi_{\ell\ell}$ data distribution fitted to the templates for background plus $t\bar{t}$ signal with SM spin correlation (red dashed) and without spin correlation (black dotted), while the right plot shows summary of the measurements of the fraction of $t\bar{t}$ events corresponding to the SM spin correlation hypothesis, $f_{\rm SM}$, for all four observables. Further details can be found in Ref. [159]. Taking into account the SM prediction for the spin correlation strength ($A^{\rm SM}_{\rm helicity}$ = 0.31 and $A^{\rm SM}_{\rm maximal}$ = 0.44) and that the fraction $f^{\rm SM}$ = 1, it can be concluded that the measured values are compatible within uncertainties with the SM expectations.

The CMS Collaboration has also reported measurements of the $t\bar{t}$ spin correlation and top-quark polarization at $\sqrt{s}$ = 7 TeV using dilepton final states with the dataset corresponding to 5.0 fb^{-1} [164]. The CMS measurements are carried out using angular asymmetry variables unfolded to the parton level, allowing direct comparisons between the data and theoretical predictions.

The top-quark polarization can be inferred from the single differential angular distribution of the top-quark decay width Γ is given by

$$\frac{d\Gamma}{d\cos{(\theta_i)}} = \frac{\Big(1 + \alpha_i|\vec{P}|cos(\theta_i)\Big)}{2}, \tag{4.26}$$

where θ_i is the the angle between the momentum direction of decay product i of the top (antitop) quark and the top- (antitop-)quark polarization three-vector $\vec{P}$, $0 \leq |\vec{P}| \leq 1$. The factor α_i is the spin-analyzing power, which must be between -1 and 1. At NLO, the factor α_i is predicted to be $\alpha_{\ell+}$ = +0.998 for positively charged leptons [165], α_d = -0.966 for down quarks, α_b = -0.393 for bottom quarks [166], and the same α_i value with opposite sign for the corresponding antiparticles. The top-quark polarization $P = |\vec{P}|$ in the helicity basis is given by $P = 2A_{\mathrm{P}}$, where the asymmetry variable A_{P} is defined as

$$A_{\mathrm{P}} = \frac{N[\cos(\theta^{\star}_{\ell}) > 0] - N[\cos(\theta^{\star}_{\ell}) < 0]}{N[\cos(\theta^{\star}_{\ell}) > 0] + N[\cos(\theta^{\star}_{\ell}) < 0]}, \tag{4.27}$$

where the number of events N is counted using the $\theta^{\star}_{\ell}$ (the angle of lepton direction relative to parent top(antitop)-quark direction in the $t\bar{t}$ rest frame) measurements of both positively and negatively charged leptons ($\theta^{\star}_{\ell+}$ and $\theta^{\star}_{\ell+}$), assuming CP invariance.

For $t\bar{t}$ spin correlations, CMS uses the variable based on $\Delta\phi_{\ell\ell}$:

$$A_{\triangle\phi} = \frac{N(\Delta\phi_{\ell\ell} > \pi/2) - N(\Delta\phi_{\ell\ell} < \pi/2)}{N(\Delta\phi_{\ell\ell} > \pi/2) - N(\Delta\phi_{\ell\ell} < \pi/2)}, \tag{4.28}$$

which provides discrimination between correlated and uncorrelated top- and antitop-quark spins. The second variable used by CMS is based on $\cos(\theta^{\star}_{\ell})$:

$$A_{\mathrm{c_1c_2}} = \frac{N\left(\cos(\theta^{\star}_{\ell+})\right)\left(\cos(\theta^{\star}_{\ell-}) > 0\right) - N\left(\cos(\theta^{\star}_{\ell+})\right)\left(\cos(\theta^{\star}_{\ell-}) < 0\right)}{N\left(\cos(\theta^{\star}_{\ell+})\right)\left(\cos(\theta^{\star}_{\ell-}) > 0\right) + N\left(\cos(\theta^{\star}_{\ell+})\right)\left(\cos(\theta^{\star}_{\ell-}) < 0\right)}, \tag{4.29}$$

Using the standard dilepton selection criteria (details are in Ref. [164]) and unfolding of the investigated data distributions of $\triangle\phi$ and $\cos(\theta^{\star}_{\ell})$ to parton level, the CMS collaboration has measured the spin correlations amplitude $A_{\triangle\phi}$, $A_{\mathrm{c_1c_2}}$ and polarization amplitude A_{P}. The final results are summarized in Table 4.9. The measured amplitudes, listed in Table 4.9, are compared to the predictions of MC@NLO and to theoretical NLO calculation for $t\bar{t}$ production with and without spin correlations [160, 149]. From Table 4.9 it follows good compatibility of the results

Tab. 4.9. Summary of measurements of the spin asymmetry amplitudes $A_{\triangle\phi}$ and $A_{\mathrm{c_1c_2}}$, and top-quark polarization amplitude, A_{P}. The measured results are compared with the simulation (MCatNLO) and theory (NLO) expectations. The uncertainties in the data are statistical, systematic, and the additional uncertainty comes from the top-quark p_{T} reweighting. The uncertainties in the simulated results are statistical only, while the uncertainties in the NLO calculations for correlated and uncorrelated $t\bar{t}$ spins come from scale variations up and down by a factor of 2.

Asymmetry	Data	MCatNLO	NLO (SM, corr.)	NLO (uncorr.)
$A_{\triangle\phi}$	$0.113 \pm 0.010 \pm 0.006 \pm 0.012$	0.110 ± 0.001	$0.115^{+0.013}_{-0.016}$	$0.210^{+0.013}_{-0.008}$
$A_{\mathrm{c_1c_2}}$	$-0.021 \pm 0.023 \pm 0.025 \pm 0.010$	-0.078 ± 0.001	-0.078 ± 0.001	0
A_{P}	$0.005 \pm 0.013 \pm 0.014 \pm 0.008$	0.000 ± 0.001	...	...

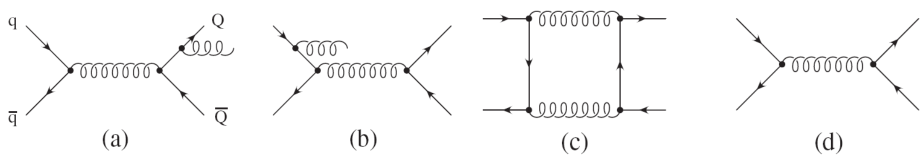

Fig. 4.26. Origin of the QCD charge asymmetry in hadroproduction of heavy quarks: interference of final-state (a) with initial-state (b) gluon bremsstrahlung, plus interference of the double virtual gluon exchange (c) with the Born diagram (d); the diagrams are taken from Ref. [181].

with the SM expectations. We can see that the $A_{\triangle\phi}$ result indicates the presence of $t\bar{t}$ spin correlations, and strongly disfavors the uncorrelated case.

Good compatibility with the SM predictions has been observed for the spin correlation strength also at $\sqrt{s}$ = 8 TeV. ATLAS has measured this strength in the dilepton final state events using a dataset corresponding to an integrated luminosity of 20.3 fb^{-1} [167]. A sensitive observable used to study the $t\bar{t}$ spin correlation was the azimuthal angle $\triangle\phi$ between the charged leptons, which are also well measured by the ATLAS detector. The $\triangle\phi$ technique is identical as the one used at $\sqrt{s}$ = 7 TeV. The measured spin correlation strength was measured at the helicity basis and the result is:

$$A^{\mathrm{meas}}_{\mathrm{helicity}} = 0.38 \pm 0.04 \text{ with the SM expectation } A^{\mathrm{SM}}_{\mathrm{helicity}} = 0.318 \pm 0.005 \text{ [160].}$$

Additionally a search was performed for pair production of top squarks with masses close to the top-quark mass decaying to predominantly right-handed top quarks and a light neutralino ($\tilde{t}_1 \rightarrow t\tilde{\chi}^0_1$), the lightest supersymmetric particle. Top squarks with masses between the top-quark mass and 191 GeV have been excluded at the 95% C.L..

4.7.3 Forward-backward asymmetry in $t\bar{t}$ events.

The measurement of the $t\bar{t}$ production charge asymmetry represents an important test of QCD at high energies and is also an ideal place to observe effects of possible new physics processes beyond the SM. Several BSM processes can alter this asymmetry [113], either with anomalous vector or axial-vector couplings (i.e. axigluons) or via interference with the SM [168, 169, 170, 171, 172, 173, 174, 175, 176, 177, 178, 179]. The $t\bar{t}$ production at hadron colliders is predicted to be symmetric under the exchange of top and antitop quark at leading order. An asymmetry arises at NLO and has its origin in radiative corrections to quark-antiquark fusion: interference of final-state with initial-state gluon bremsstrahlung ($q\bar{q} \rightarrow t\bar{t}g$) and interference of the box with the Born diagram [180, 181], see Fig. 4.26. The interference between initial state and final state radiation (ISR and FSR) results in a negative contribution, while the interference between the Born and the box diagrams leads to a positive contribution. A less significant contribution comes also from $t\bar{t}$ production involving interference terms of different amplitudes contributing to gluon-quark scattering. On the other hand, gluon fusion remains charge symmetric [181]. At the Tevatron $p\bar{p}$ collider, where $t\bar{t}$ events are predominantly produced by $q\bar{q}$ annihilation, top quarks are preferentially emitted in the direction of the incoming quark while the top antiquarks are emitted preferentially in the direction of the incoming antiquark. Therefore the $t\bar{t}$ asymmetry at the Tevatron is measured as a forward-backward asymmetry,

$$A_{\mathrm{FB}} = \frac{N(\triangle y > 0) - N(\triangle y < 0)}{N(\triangle y > 0) + N(\triangle y < 0)}, \tag{4.30}$$

where $\triangle y \equiv y_t - y_{\bar{t}}$ is the difference in rapidity between top quarks and antiquarks, and N represents the number of events with $\triangle y$ being positive or negative. The interest in this measurement has grown after CDF and D0 collaborations reported A_{FB} measurements significantly larger than the SM predictions, in both the inclusive and differential case as a function of $m_{t\bar{t}}$ and $|y_{t\bar{t}}|$. In pp collisions at the LHC, the dominant mechanism for $t\bar{t}$ production is the gg fusion process, while production via $q\bar{q}$ or qg interactions is small. Since the colliding beams are symmetric, A_{FB} is no longer a useful observable. However, $t\bar{t}$ production via $q\bar{q}$ or qg processes is asymmetric under top quark-antiquark exchange, and, moreover, the valence quarks carry (on average) a larger momentum fraction than the sea antiquarks. Hence for $q\bar{q}$ or qg production processes at the LHC, QCD predicts a small excess of centrally produced top antiquarks with respect to top quarks which are produced, on average, at higher absolute rapidities. Therefore, the $t\bar{t}$ production charge asymmetry A_{C} is defined as

$$A_{\mathrm{C}} = \frac{N(\triangle|y| > 0) - N(\triangle|y| < 0)}{N(\triangle|y| > 0) + N(\triangle|y| < 0)}, \tag{4.31}$$

where $\triangle|y| \equiv |y_t| - |y_{\bar{t}}|$ is the difference between the absolute value of the top-quark rapidity $|y_t|$ and the absolute value of the top antiquark rapidity $|y_{\bar{t}}|$. The SM prediction for the $t\bar{t}$ production charge asymmetry at $\sqrt{s}$ =7 TeV of pp collisions is $A_{\mathrm{C}}^{\mathrm{SM}}$ = 0.0123 $\pm$ 0.0005 [182]. The SM asymmetry value is computed at NLO in QCD including also electroweak corrections. The asymmetry A_{C} requires the full reconstruction of $t\bar{t}$ events and can be studied in both the lepton+jets channel and the dilepton channel. Additionally, in the dilepton channel a lepton-based charge asymmetry $A_{\mathrm{C}}^{\ell\ell}$ can be also measured. The observable $A_{\mathrm{C}}^{\ell\ell}$ is defined as an asymmetry between positively and negatively charged leptons (electrons and muons) in the dilepton decays of the $t\bar{t}$ pairs. Practically it means that for the $A_{\mathrm{C}}^{\ell\ell}$ asymmetry Eq. 4.31 can be used, but with $\triangle|\eta| = |\eta_{\ell+}| - |\eta_{\ell-}|$, where $\eta_{\ell+}$ ($\eta_{\ell-}$) is the pseudorapidity of the positively (negatively) charged lepton and N is the number of events with positive or negative $\triangle|\eta|$.

ATLAS measured the $t\bar{t}$ charge asymmetry at $\sqrt{s}$ =7 TeV in the lepton+jets channel [183] as well as in the dilepton one [184]. In the former case (lepton+jets) using a dataset of 4.6 fb^{-1}, an inclusive A_{C} measurement and measurements of A_{C} as a function of $m_{t\bar{t}}$, $p_{\mathrm{T},t\bar{t}}$, and $|y_{t\bar{t}}|$ have been carried out. To allow comparisons with theory calculations, a Bayesian unfolding procedure is applied to account for distortions due to acceptance and detector effects, leading to parton-level A_{C} measurements. The measured inclusive $t\bar{t}$ production charge asymmetry is $A_{\mathrm{C}}^{\mathrm{SM}}$ = 0.006 $\pm$ 0.010. The measured value is compatible with the SM prediction within the uncertainties. As an example in the Fig. 4.27 is shown the distribution of A_{C} as a function of $m_{t\bar{t}}$ (left) compared with the SM prediction and with an BSM model of axigluons for two value of the axigluon mass. In the dilepton channel the same asymmetries have been measured by ATLAS as in the lepton+jets channel and moreover the lepton charge asymmetry, $A_{\mathrm{C}}^{\ell\ell}$, has been investigated. The SM expectations, for the lepton charge asymmetry, based on NLO calculations are: $A_{\mathrm{C,SM}}^{\ell\ell}$ =0.0070 $\pm$ 0.0003 [182]. The measured values for the observables A_{C} and $A_{\mathrm{C}}^{\ell\ell}$ are

$$A_{\mathrm{C}} = 0.024 \pm 0.015\ (\text{stat.}) \pm 0.009\ (\text{syst.}) \text{ and } A_{\mathrm{C}}^{\ell\ell} = 0.021 \pm 0.025\ (\text{stat.}) \pm 0.017\ (\text{syst.})$$

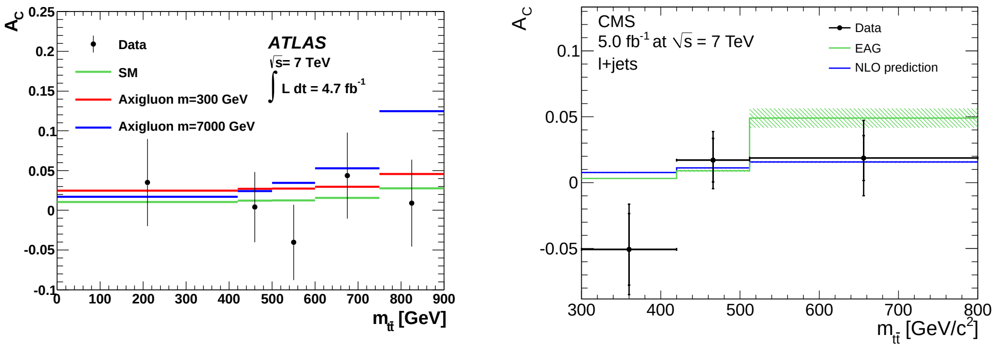

Fig. 4.27. Distributions of the asymmetry A_{C} as a function of $m_{t\bar{t}}$ after unfolding, for the electron and muon channels combined measured by ATLAS (left) and the same dependence of A_{C} measured by CMS (right). In both cases the data are compared to the SM predictions and the predictions of some BSM approaches (see text).

Similarly, CMS has also measured $t\bar{t}$ charge asymmetry at $\sqrt{s}$ =7 TeV, using a dataset of 5.0 fb^{-1}, in the lepton+jets channel [185] and the dilepton one [186]. In Ref. [185] is presented an inclusive measurement of A_{C} and three differential measurements of the $t\bar{t}$ charge asymmetry as a function of the rapidity, transverse momentum, and invariant mass of the $t\bar{t}$ system. The measurement of the $t\bar{t}$ charge asymmetry is based on the fully reconstructed four-momenta of the top quarks and antiquarks in each event. The measured value of the inclusive $t\bar{t}$ charge asymmetry is A_{C} = 0.004 $\pm$ 0.010 (stat.)$\pm$ 0.011 (syst.). An example of the charge asymmetry differential distribution, the A_{C} dependence of $m_{t\bar{t}}$ is shown in Fig. 4.27 (right).

The analysis carried out in the dilepton channel has measured the standard $t\bar{t}$ asymmetry, A_{C}, requiring the full reconstruction of $t\bar{t}$ events, and also the lepton charge asymmetry, $A_{\mathrm{C}}^{\ell\ell}$. In the case of the lepton charge asymmetry also differential asymmetries in variables $m_{t\bar{t}}$, $|y_{t\bar{t}}|$ and $p_{\mathrm{T},t\bar{t}}$ have been measured. For comparison with theory all the variables are unfolded to parton level. The measured value of of the asymmetries A_{C} and $A_{\mathrm{C}}^{\ell\ell}$ are

$$A_{\mathrm{C}} = -0.010 \pm 0.017 \text{ (stat.)} \pm 0.008 \text{ (syst.) and } A_{\mathrm{C}}^{\ell\ell} = 0.009 \pm 0.010 \text{ (stat.)} \pm 0.006 \text{ (syst.)}$$

Details on differential lepton asymmetries asymmetries can be found in [186]. The ATLAS and CMS measurements at $\sqrt{s}$ = 7 TeV in the lepton+jets channel have been combined [187]. The combined result corresponds to datasets of 4.6 fb^{-1} (ATLAS) and 5.0 fb^{-1} (CMS). The resulting combined LHC measurement of the charge asymmetry in $t\bar{t}$ events at $\sqrt{s}$ = 7 TeV is A_{C} = 0.005 $\pm$ 0.007(stat.) $\pm$ 0.006(syst.). This result for the charge asymmetry as well as the results of all other experiments at $\sqrt{s}$ = 7 TeV are consistent with the prediction from the SM and can be used to restrict BSM physics models.

The CMS collaboration has managed to measure also the $t\bar{t}$ charge asymmetry at $\sqrt{s}$ = 8 TeV, using the lepton+jets corresponding to a dataset of 19.7 fb^{-1} [188]. Similarly as in the 7 TeV case an inclusive measurement and three differential measurements of the $t\bar{t}$ charge asymmetry as a function of rapidity, transverse momentum, and invariant mass of the $t\bar{t}$ system have been investigated. Having higher statistics in comparison with the 7 TeV case, one can expect more profound manifestation of a new physics. The $t\bar{t}$ rapidity ($|y_{t\bar{t}}|$) distribution in the laboratory frame is sensitive to the ratio of the contributions from the $q\bar{q}$ and gg initial states to $t\bar{t}$ production. The charge-symmetric gluon fusion process is dominant in the central region, while $t\bar{t}$ production through $q\bar{q}$ annihilation mostly produces events with the $t\bar{t}$ pair at larger rapidities, which implies an enhancement of the charge asymmetry with increasing $|y_{t\bar{t}}|$ [189]. The $t\bar{t}$ transverse momentum ($p_{\mathrm{T},t\bar{t}}$) distribution in the laboratory frame is sensitive to the positive and negative contributions to the overall asymmetry. As we have already stated the interference between the Born and the box diagrams leads to a positive contribution, while the interference between initial state and final state radiation (ISR and FSR) diagrams gives a negative contribution. The presence of additional hard radiation implies on average a higher transverse momentum of the $t\bar{t}$ system [189]. Consequently, in events with large values of $p_{\mathrm{T},t\bar{t}}$ the negative contribution from the ISR-FSR interference is enhanced. The $t\bar{t}$ invariant mass ($m_{t\bar{t}}$) distribution is also sensitive to new physics contributions. Since the contribution of the $q\bar{q}$ initial state processes is enhanced for larger values of $m_{t\bar{t}}$ it implies that the charge asymmetry should be bigger at high $m_{t\bar{t}}$. There are new physics scenarios, where new heavy particles could be exchanged between initial quarks and antiquarks and contribute to the $t\bar{t}$ production (see e.g. Ref. [190]). The amplitudes associated with these new contributions would interfere with those of the SM processes, leading to an effect on the $t\bar{t}$ charge asymmetry, which increases with $m_{t\bar{t}}$.

The measured inclusive $t\bar{t}$ charge asymmetry along with the theoretical SM expectations is:
data: A_{C} = 0.005 $\pm$ 0.007 (stat.) $\pm$ 0.006 (syst.)
theory: $A_{\mathrm{C}}^{\mathrm{th}}$ = 0.0102 $\pm$ 0.0005 [189] and 0.0111 $\pm$ 0.0004 [182].
A comparison of the $t\bar{t}$ charge asymmetry distributions calculated from background-subtracted data to the Powheg predictions is shown in Fig. 4.28. Though a good agreement is found, it should be kept in mind that the simulation does not encompass the full SM NLO effect. The measured charge asymmetry distributions can be used to restrict new physics conceptions. As an example, one can see that in the high-mass region that the predictions from an effective field theory [191, 192] with the scale for new physics at Λ = 1.5 TeV is about 1.5 standard deviations and for Λ = 1.0 TeV 3.5 standard deviations above the data points. So this effective theory is excluded below Λ = 1 TeV at the level of 3.5 σ.

Generally it can be concluded that the $t\bar{t}$ charge asymmetry measurements at $\sqrt{s}$ = 8 TeV, similarly as at $\sqrt{s}$ = 7 TeV, are within their uncertainties consistent with the predictions of the Standard Model and no significant hints for deviations due to BSM physics contributions have been observed.

4.7.4 Flavour Changing Neutral Currents.

In the SM of particle physics, flavour-changing neutral-current (FCNC) processes, like $t \to Zq$ where q = c or u (upper quarks), are forbidden at tree level and suppressed at higher orders due to the Glashow-Iliopoulos-Maiani mechanism [193] and occur only on the loop level giving a branching fraction BR$(t \to q)$ at $O\left(10^{-14}\right)$. However some extensions of the SM, like R-parity-violating supersymmetric models [194], some technicolor models [195], and singlet quark models [196] predict enhancements of the FCNC branching fraction to the level of $O\left(10^{-4}\right)$ (for review see Ref. [197]). However a comparison of these models with data is problematic as all the mentioned models are not updated to the latest LHC results. On the other hand, a recent study [198] working with warped extra dimension models puts the branching BR$(t \to q)$ at level

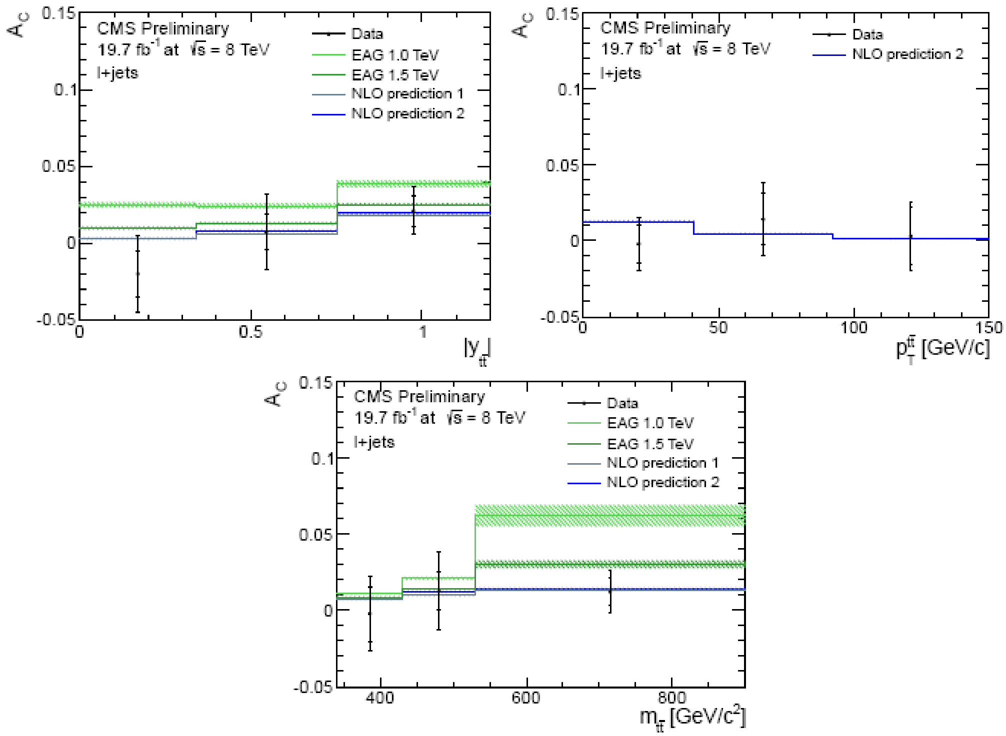

Fig. 4.28. Corrected $t\bar{t}$ charge asymmetry A_C as a function of the reconstructed $|y_{t\bar{t}}|$ (upper left), $p_{T,t\bar{t}}$ (upper right), and $m_{t\bar{t}}$ (bottom). The measured values of A_C are compared to NLO calculations for the SM (1: [189], 2: [182]) and to the predictions of a model featuring an effective axial-vector coupling of the gluon (EAG) [191, 192].

of $O\left(10^{-5}\right)$. The branching fraction is very sensitive to the Kaluza-Klein gluon scale m_{KK}, as well as to the right-handed mixing parameters. The m_{KK} scale is probed directly [199,200] at the LHC, while the right-handed couplings are only weakly constrained by B physics measurements [201].

Experimental limits on top-quark FCNC processes existing before LHC came from direct and indirect searches at the Tevatron collider [202, 203, 204, 205], and indirect searches at the LEP [206, 207, 208, 209] and HERA [210, 211, 212, 213] colliders. An improvement of these limits has already been done by the LHC experiments taking into account data sets at $\sqrt{s} = 7$ TeV and partially also at 8 TeV. The ATLAS and CMS collaborations have investigating the FNCN processes in $t\bar{t}$ channel [214,215,216] as well as in the single-top-quark channel [217,218].

The search for the FCNC processes performed by ATLAS at $\sqrt{s}$ = 7 TeV and a dataset corresponding to 2.1 fb^{-1} in the $t\bar{t}$ channel [214], is based on events in which either the top- or antitop-quark decays into a Z boson and a quark, $t \to Zq$, while the remaining top- or antitop-quark decays through the SM $t \to Wb$ channel ($t\bar{t} \to Wb + Zq \to \ell\nu b + \ell\ell q$). Only leptonic decays of the Z and W bosons were considered, yielding a final-state topology characterised by the presence of three isolated charged leptons, at least two jets, and transverse momentum

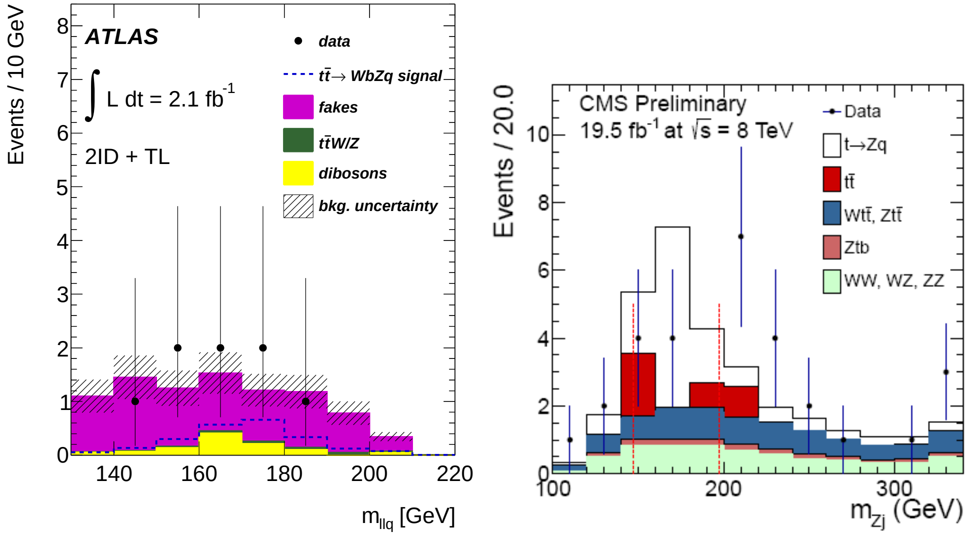

Fig. 4.29. Expected and observed m_{llq} and m_{Zq} distributions for the FCNC hypothesis in 3ℓ candidate events for ATLAS at $\sqrt{s}$ = 7 TeV (left) and CMS at $\sqrt{s}$ = 8 TeV(right) measurements, respectively.

imbalance ($E_{\mathrm{T}}^{\mathrm{miss}}$) from the undetected neutrino arising from the W-boson decay, for selection and reconstruction details see Ref. [214]. The analysis of the ATLAS data has revealed no evidence for the FNCN ($t\bar{t} \rightarrow Wb + Zq$) events. An observed limit at 95% C.L. on the $t \rightarrow Zq$ FCNC top-quark decay branching fraction was set at BR$(t \rightarrow Zq) < 0.73\%$, assuming BR$(t \rightarrow Wb)$+BR$(t \rightarrow Zq)$ = 1. The observed limit is compatible with the expected sensitivity, assuming that the data are described correctly by the SM of BR$(t \rightarrow Zq) < 0.93\%$.

A similar study aimed at the FCNC search in the $t\bar{t}$ channel carried out by CMS at $\sqrt{s}$ = 7 TeV with a dataset corresponding to 5 fb^{-1} and at $\sqrt{s}$ = 8 TeV with a dataset of 19.5 fb^{-1}, are presented in Ref. [215] and [216], respectively. Also in these studies the decay $t \rightarrow Zq$ (or $\bar{t} \rightarrow Z\bar{q}$) was assumed to have a small branching ratio (the possibility of both top quarks decaying via flavor changing neutral currents is not considered) and the analysis looked for $t\bar{t} \rightarrow Wb + Zq \rightarrow \ell\nu b + \ell\ell q$ final state events, which produce three-lepton (eee, $ee\mu$, $\mu\mu e$, $\mu\mu\mu$) final states. Neither the analysis at $\sqrt{s}$ = 7 TeV nor that at $\sqrt{s}$ = 8 TeV observed any excess of events over the SM background. Better result was obtained at $\sqrt{s}$ = 8 TeV where the branching fraction BR$(t \rightarrow Zq)$ larger than 0.07% was excluded at the 95% confidence level. The expected 95% C.L. upper limit on the BR$(t \rightarrow Zq)$ was 0.11%. In Fig. 4.29 are compared the measured and expected top-quark mass (invariant mass of $\ell\ell$+jet system) distribution for the FCNC hypothesis in 3ℓ candidate events. In the ATLAS plot (Fig. 4.29-left) the $t\bar{t} \rightarrow WbZq$ distribution is normalized to the observed limit, while in the CMS plot (Fig. 4.29-right) the $t\bar{t} \rightarrow WbZq$ distribution is normalized to 1% and added to background.

FCNC processes were also looked for in the single-top-quark channel. In searches for the anomalous single-top-quark production a much better sensitivity can be achieved than in the

FNCN decay $t \to qg$ mode, where q denotes either an up quark u or a charm quark c, as it is almost impossible to separate from generic multijet production. The most general effective Lagrangian L_{eff} for this process results from dimension-six operators and it can be written as [219, 220]:

$$L_{\text{eff}} = g_{\text{S}} \sum_{q=u,c} \frac{\kappa_{\text{qgt}}}{\Lambda} \bar{t} \sigma^{\mu\nu} T^a \left(f_L^q P_L + f_R^q P_R \right) q G^a_{\mu\nu} + h.c. \tag{4.32}$$

where the κ_{qgt} ($q = u, c$) are dimensionless parameters that relate the strength of the new coupling to the strong coupling constant g_{S}, Λ is the new physics scale – it is a mass cutoff scale above which the effective theory breaks down, T^a are the Gell-Mann matrices and $\sigma^{\mu\nu} = i/2[\gamma^\mu, \gamma^\nu]$ ($\gamma \equiv$ Dirac matrices). The $f_q^{L,R}$ are chiral parameters normalised to one: $|f_q^L|2 + |f_q^R|2 = 1$. The operator $P_L = \frac{1}{2}(1-\gamma^5)$ ($P_R = \frac{1}{2}(1+\gamma^5)$) performs a left-handed (right-handed) projection, where γ^5 represents the chirality operator. $G^a_{\mu\nu}$ is the gauge-field tensor of the gluon and t and q are the fermion fields of the top and light quark, respectively.

First searches for the FNCN at single-top-quark production were carried out at Tevatron. A search for the process $qg \to t$ was performed by CDF [221] and D0 set limits on κ_{ugt}/Λ and κ_{cgt}/Λ by analysing the processes $q\bar{q} \to t\bar{u}$, $ug \to tg$, and $gg \to t\bar{u}$ and their c quark analogues [222].

At the LHC a search for the production of single top quarks involving quarks and gluons via FCNC was also carried out. ATLAS performed a search for the $2 \to 1$ FCNC process $qg \to t$ [223]. This analysis uses data collected at $\sqrt{s}$ = 7 TeV corresponding to an integrated luminosity of 2.05 fb^{-1}. Events were selected by a single-lepton trigger with the p_{T} threshold taken at 18 GeV for muons and for electrons it was 20 GeV raised to 22 GeV for higher luminosities. At the reconstruction level electrons and muons are required to have $p_{\text{T}} >$ 25 GeV and in addition, due to presence of neutrino in the final state, also the missing transverse momentum, $E_{\text{T}}^{\text{miss}}$, is required to be over 25 GeV and to suppress events with low value of reconstructed W-boson transverse mass m_{T}^W (multijet events), a condition $m_{\text{T}}^W + E_{\text{T}}^{\text{miss}} >$ 60 GeV is required. Finally, the selected candidate events were required to have exactly one isolated lepton and one b-tagged jet. Main background comes from the W+jets processes, SM single-top-quark, $t\bar{t}$, multijet, Z+jets and diboson production. To separate signal events from background events multivariate analysis techniques were used. In this analysis a neural network approach [224] using the 11 input variables was applied. Main differences of the $qg \to t \to b\ell\nu$ process from the SM processes passing the selection cuts are:

- Single top quark produced via FCNC has almost zero transverse momentum – its p_{T} distribution is softer than the p_{T} distribution of the SM produced top quarks.

- Unlike in the W/Z + jet and diboson backgrounds, the W boson from the top-quark decay has a very high momentum and its decay products have small opening angles.

- The top-quark charge asymmetry for FCNC processes differs from the asymmetry for SM processes. The FNCN processes are predicted to produce four times more single top quarks than anti-top quarks, while for the SM single-top-quark production this ratio is not more than two.

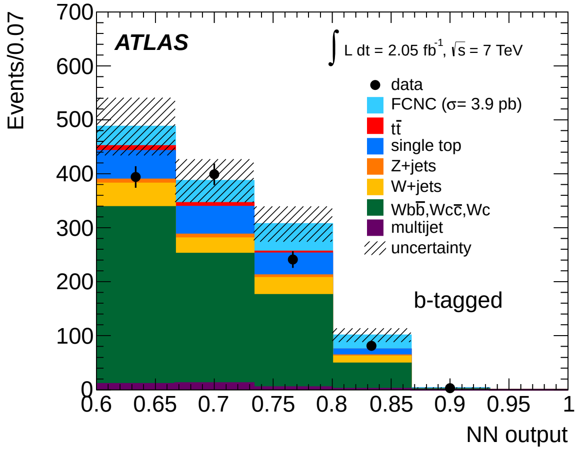

Fig. 4.30. Distributions of the neural network output: observed signal and simulated background output distribution . The FCNC single-top-quark process is normalised to the observed limit of 3.9 pb. The hatched band indicates the statistical uncertainty from the sizes of the simulated samples and the uncertainty in the background normalisation.

The analysis applied a Bayesian statistical approach using binned likelihood method to neural network output distributions for the combined electron and muon channel. Fig. 4.30 shows a comparison of distributions of the neural network output for observed signal and simulated background. The resulted upper limit on the FCNC single-top-quark production cross section at 95% C.L. was found to be 3.9 pb.

The measured upper limit on the production cross-section is converted into limits on the coupling constants κ_{ugt}/Λ and κ_{cgt}/Λ. Assuming $\kappa_{cgt}/\Lambda = 0$ the upper limit was found to be $\kappa_{ugt}/\Lambda < 6.9{\cdot}10^{-3}$ TeV^{-1} and assuming $\kappa_{ugt}/\Lambda = 0$ led to the limit $\kappa_{cgt}/\Lambda < 1.6{\cdot}10^{-2}$ TeV^{-1}. In addition, the upper limits on the branching fractions BR$(t \to ug) < 5.7{\cdot}10^{-5}$ assuming BR$(t \to cg) = 0$ and BR$(t \to cg) < 2.7{\cdot}10^{-4}$ assuming BR$(t \to ug) = 0$ were derived. The found upper limits use the NLO predictions for the FCNC single-top-quark production cross-section [225, 226] and decay rate [227].

An interesting search for FCNC processes was carried out by CMS, which studied a single-top-quark production in association with a Z boson [228]. The analysis is based on a dataset corresponding to an integrated luminosity of about 5 fb^{-1} at $\sqrt{s}$ = 7 TeV. The event selection requires three isolated leptons, electrons or muons, and of at least one jet – it corresponds to presence of two isolated leptons from Z boson, one isolated lepton and b-jet from the top-quark decay ($t \to Wb$, $W \to \ell + \nu$). The leptons are required with transverse momentum $p_{\mathrm{T}} >$ 20 GeV and jet with $p_{\mathrm{T}} >$ 30 GeV. To discriminate between signal and background a BDT technique was employed. No evidence of signal events was observed and exclusion limits at 95% C.L. on anomalous couplings were calculated from the BDT output distributions using a profile likelihood ratio method. The upper limits were calculated as functions of the κ_{gut}/Λ and κ_{Zqt}/Λ parameters. It was derived that $\kappa_{gut}/\Lambda < 0.10$ TeV^{-1}, $\kappa_{gct}/\Lambda < 0.35$ TeV^{-1}, $\kappa_{Zut}/\Lambda < 0.45$ TeV^{-1} and $\kappa_{Zct}/\Lambda < 2.27$ TeV^{-1}. The upper limits on $\kappa_{gqt/Zqt}/\Lambda$ can be converted into BR$(t \to gq)$ and BR$(t \to Zq)$ using the total NNLO top-quark width Γ_t [229] and the widths $\Gamma_{t\to gq/t\to Zq}$ of the $t \to gq$ and $t \to Zq$ decays corresponding to values of

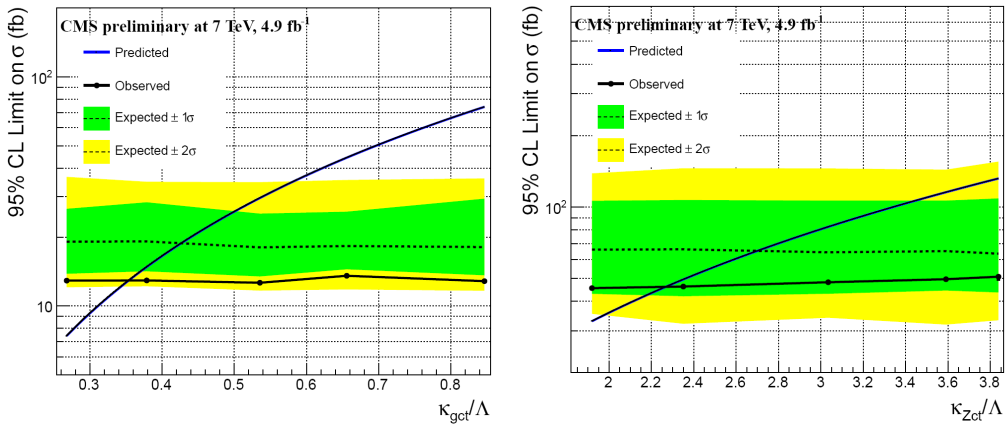

Fig. 4.31. 95% exclusion limit for the gct (left) and Zct (right) couplings as functions of the κ/Λ parameters. The blue lines shows the predicted cross-section, as calculated by MADGRAPH.

$\kappa_{gqt/\Lambda}$ and $\kappa_{Zqt/\Lambda}$. Hence, in terms of branching fractions related to rare top-quark decays, the found bounds are BR$(t \to gu) \leq 0.56\%$, BR$(t \to gc) \leq 7.12\%$, BR$(t \to Zu) \leq 0.51\%$ and BR$(t \to Zc) \leq 11.40\%$. As an example in Fig. 4.31 are shown the derived upper limits on the effective Lagrangian κ_{gct}/Λ and κ_{Zct}/Λ parameters.

Taking into account the FCNC results from the LHC and Tevatron experiments, we can conclude that no significant sign of non-SM FCNC sources has been observed so far.

4.7.5 Top-quark electric charge.

The main issue of the top-quark charge study is to distinguish between the SM scenario with decaying top quark having the electric charge of 2/3 (in units of the electron charge magnitude), $t \to W^+ b$, and the exotic one with an exotic quark having the charge of -4/3, $t_X \to W^- \bar{b}$. The study carried out by ATLAS, using the data of 2.05 fb^{-1} at $\sqrt{s}$ = 7 TeV [230], is based on exploiting of the charges of the top-quark decay products (W boson and b-quark). The charge of the W boson is determined through the charge of the lepton from its leptonic decay ($W^\pm \to \ell^\pm \nu_\ell$). The b-quark charge cannot be determined directly, but it should be correlated with an effective charge of b-jet found using a charge weighting procedure. Within this procedure the charges of tracks belonging to a b-jet cone are weighted using their momentum projection into the b-jet axis giving finally an effective b-jet charge.

$$Q_{b-\mathrm{jet}} = \frac{\sum_i^N Q_\mathrm{i} \mid \vec{j} \cdot \vec{p_i} \mid^\kappa}{\sum_i^N \mid \vec{j} \cdot \vec{p_i} \mid^\kappa}, \tag{4.33}$$

where Q_i and $\vec{p_i}$ are the charge and momentum of the i-th track, $\vec{j}$ defines the b-jet axis direction, and κ is a parameter which was set to be 0.5 for the best separation between b- and $\bar{b}$-jets mean charges using the standard MC@NLO $t\bar{t}$ simulated sample.

The observable which is used to distinguish between the SM top quark and the exotic one is $Q_\mathrm{comb} = Q_\ell \times Q_{b-\mathrm{jet}}$, where Q_ℓ and $Q_{b-\mathrm{jet}}$ are the charge of lepton and effective charge of b-jet. The lepton and b-jet should come from the same decaying quark, what is provided by

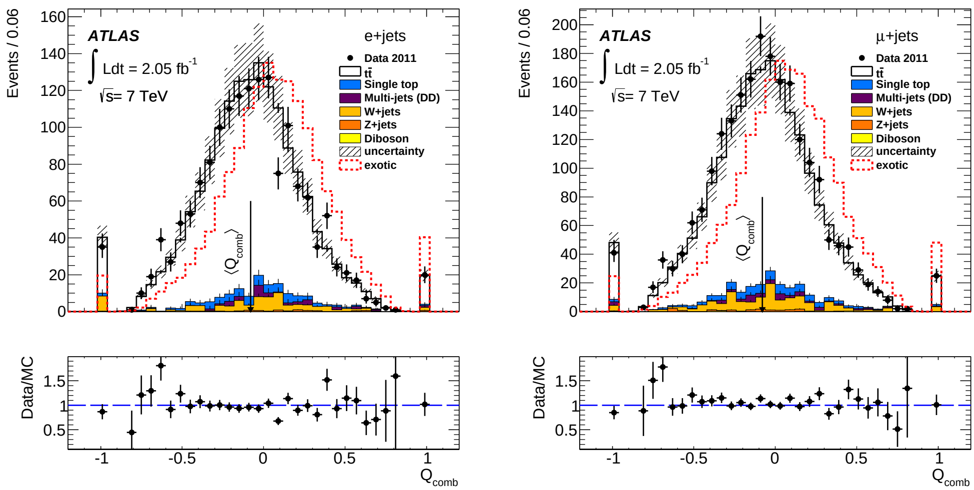

Fig. 4.32. Distribution of the combined charge, $Q_{\rm comb}$, in electron + jets (left) and muon + jets (right) final states. The full circles with error bars are data, the full black line corresponds to the SM scenario, and the dashed red line corresponds to the exotic model. The vertical line, labeled with $\langle Q_{\rm comb} \rangle$, shows the mean value of the $Q_{\rm comb}$ distribution obtained from data. Only statistical uncertainties are shown.

fulfilling a lepton b-jet pairing condition based on the lepton–b-jet invariant mass, $m(\ell, b\text{–jet})$, which should be (within resolution) less than the top-quark mass, if lepton and b-jet are top-quark decay products. The analysis was performed in the lepton + jets channel based on a single lepton (electron or muon) trigger. Event selection required only one isolated lepton, electron or muon, with transverse momentum $E_{\rm T} > 25$ GeV for electrons and with $p_{\rm T} > 20$ GeV for muons. In addition at least four jets with $p_{\rm T} > 25$ GeV, two of them b-tagged and missing transverse momentum $E_{\rm T}^{\rm miss} > 20$ GeV (35 GeV) for electron (muon) events. Finally only the selected events passing the lepton b-jet pairing condition were accepted. The observable $Q_{\rm comb}$ was reconstructed for the selected data events and for the signal ($t\bar{t}$, lepton + jets) and background (W/Z+jets, single top quark, diboson, multijets) MC events. Fig. 4.32 compares the reconstructed combined charge spectra for the data with MC expectations for signal and background after ℓb-pairing for the electron + jets (left) and muon + jets (right) final states, showing good agreement between the data and the SM expectations.

The experimentally observed mean value of the combined charge is $Q^{\rm obs}_{\rm comb}$ = -0.077 $\pm$ 0.005, which is in excellent agreement with the SM expected value: $Q^{\rm SM}_{\rm comb}$ = -0.075 $\pm$ 0.004. For the exotic model a positive value is expected: $Q^{\rm XM}_{\rm comb}$ = +0.069 $\pm$ 0.004. Taking into account all statistical and systematic uncertainties, the statistical analysis excluded the exotic model with more than 8σ C.L.

From the value of $Q^{\rm obs}_{\rm comb}$ assuming the b-quark charge of -1/3, the value of the top-quark charge was inferred: $Q_{\rm top}$ = 0.64 $\pm$ 0.02 (stat.) $\pm$ 0.08 (syst.)

The analysis performed by CMS discriminates between the SM top quark and exotic model hypotheses using the muon+jets final state of $t\bar{t}$ events [231]. The measurement is performed at $\sqrt{s}$ = 7 TeV using a dataset corresponding to an integrated luminosity of 4.6 fb^{-1}. Events

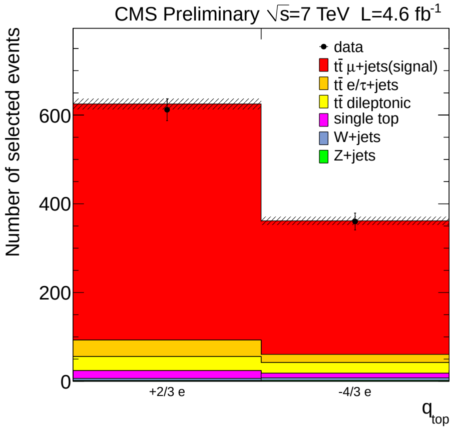

Fig. 4.33. Charge assigned to the top-quark in the selected $t\bar{t}$ events. The data (solid points with errors) are compared to the standard model ($q_{\rm top}$ = +2/3 e) prediction (histograms). The simulation is normalized to integrated luminosity. The shaded area corresponds to the statistical uncertainty on the MC prediction in each bin.

($t\bar{t}$ candidates) were selected with an isolated muon trigger and needed to contain one and only one isolated muon candidate with transverse momentum ($p_{\rm T}$) larger than 26 GeV. A veto on additional isolated leptons in the event, with $p_{\rm T} > 10$ GeV for muons and $E_{\rm T} > 15$ GeV for electrons, was applied to suppress top-pair events in dileptonic channels. The presence of at least four hadronic jets with $p_{\rm T} > 30$ GeV was required in the event. In addition, two of the jets were required to be tagged as b-jets. At least one of the two b-jets contains a soft muon within the b-jet cone $\triangle R < 0.4$. This soft muon is used to determine the charge of the initial b-quark. The charge of the remaining b-quark is then of opposite sign. A normalized asymmetry of the events categorized with a charge of either +2/3 (SM) or -4/3 (exotic model) [8] was calculated exploiting charge correlations between high-$p_{\rm T}$ muons from W-boson decays and soft muons from B-hadron decays in b-jets and can be expressed as follows:

$$A = \frac{1}{D_S}\frac{N_{\rm SM} - N_{\rm XM} - N_{\rm BG}D_B}{N_{\rm SM} + N_{\rm XM} - N_{\rm BG}}, \tag{4.34}$$

where D_S and D_B are the dilution of signal and background caused by incorrect soft muon sign (B0 oscillation and other processes), respectively, $N_{\rm BG}$ is the expected number of background events. The variables $N_{\rm SM}$ and $N_{\rm XM}$ are the number of events reconstructed with the SM top-quark charge (+2/3) and the exotic charge (-4/3), respectively (see details in Ref. [231]). The expected asymmetry A for the SM (exotic model) hypothesis is +1(-1).

Fig. 4.33 shows final distribution of the assigned top-quark charge of the selected $t\bar{t}$ events. The scenario with an exotic quark charge of -4/3 would correspond to an asymmetry (between the two categories) of A = -1. The exotic scenario can be excluded with high significance and the measured asymmetry of $A_{\rm meas} = 0.97 \pm 0.12$ (stat.) $\pm$ 0.31 (syst.) is in very good agreement with the SM expectation of A = +1. We can conclude that both experiments (ATLAS and CMS) have confirmed that the top quark is really the upper quark of the SM with an electric charge of +2/3.

[8] Charge is expressed in units of the electron charge magnitude.

5 Conclusion

The first phase of the LHC project has resulted in many significant results. The LHC experiments studying proton-proton collisions at center-of mass energy $\sqrt{s}$ = 7 and 8 TeV have discovered the Higgs boson – the last missing part of the SM which had not been confirmed before the LHC started. In addition the LHC studies have proved that the discovered boson is highly consistent with the SM Higgs-boson expectations. As very important results should be considered also the results of manifold tests of the SM which enabled considerably enlarge the kinematic region of validity of the SM. Within these tests numerous searches for new physics were performed. Up to now no evidence of physics beyond the SM has been observed. In these tests as well as at the Higgs-boson studies a significant role have played the top-quark physics processes. The precision measurements of the $t\bar{t}$ and single-top-quark production cross sections on high level have confirmed validity of the QCD and EW theory predictions. Particularly, I want to emphasize the excellent agreement between the measured total $t\bar{t}$ cross section (at $\sqrt{s}$ = 7 and 8 TeV) and the full NNLO calculations including the NNLL gluon resumations. Very good agreement between experiment and theory is also on the differential $t\bar{t}$ and single-top-quark production cross sections, but here the full NNLO calculations are still missing. Nonetheless, the measurement of differential $t\bar{t}$ cross sections as a function of the invariant $t\bar{t}$ mass considerably limited the parameter space of many extra dimension models. The precision measurement of the top-quark mass (along with the W boson mass and other EW observables) has enabled very strict intrinsic tests of the SM and has impact on such issues as is the vacuum instability. Studying the top-quark properties it was proved that the top quark is the upper quark of the third generation with the electric charge of 2/3, its spin properties are in agreement with the SM expectations and the same is true for the couplings of the top quark to other particle like W boson, b-quark or Higgs boson – within their experimental uncertainties, they are in agreement with the SM expectations. Concerning the couplings of top quark and Higgs boson, it is in agreement with the SM prediction but the uncertainties are still needed to be improved and processes like the associated production of $t\bar{t}$ with Higgs boson need more experimental data to be well established. The fact that in the LHC experiments up to now there are no significant signs of new physics means that the SM is an exceptionally successful theory and to look for the physics beyond the SM we will need higher energies and higher integrated luminosities. From this point of view the second phase of the LHC with the centre-of-mass energy increased to 13 and later 14 TeV with the assumed integrated luminosity over 100 fb^{-1}, looks very promising.

It should be also added that in addition to the excellent results of the LHC phase I, there is also a big progress in experimental reconstruction techniques and understanding of the detector systematic uncertainties. This creates good preconditions for the LHC Run II to be successful with abundance of new interesting results.

Acknowledgement

I would like to thank the members of ATLAS and CMS Collaborations for their excellent work leading to many interesting results, as well as to whole LHC accelerator team for their hard work on keeping the accelerator working. My special thanks belongs to professor Nikolaos Giocaris of National and Kapodistrian University of Athens for careful reading of the manuscript and many helpful remarks. The good working conditions of the Faculty of Mathematics, Physics and Informatics, Comenius University in Bratislava, where this work was performed, is gratefully acknowledged. I also thanks to my students Matej Melo and Oliver Majersky for their help with some technical issues.

References

[1] L. Evans, P. Bryant, *LHC Machine,* JINST **3**, p. S08001, 2008.

[2] S. Glashow, Nucl. Phys. **22**, p. 579, 1961.

[3] S. Weinberg, Phys. Rev. Lett. **19**, p. 1264, 1967.

[4] A. Salam, *Weak and electromagnetic interactions, in "Elementary particle theory: relativistic groups and analyticity",* rev. Proceedings of the Eighth Nobel Symposium, 1968.

[5] G. t'Hooft a M. Veltman, *Regularization and Renormalization of Gauge Fields,* Nucl. Phys. B **44**, p. 189, 1972.

[6] F. Englert a R. Brout, *Broken Symmetry and the Mass of Gauge Vector Mesons,* Phys. Rev. Lett. **13**, p. 321, 1964.

[7] P. W. Higgs, *Broken Symmetries and the Masses of Gauge Bosons,* Phys. Rev. Lett. **13** (1964) 508.

[8] P. W. Higgs, *Broken Symmetries, massless particles and gauge fields*, Phys. Lett. **12** (1964) 132.

[9] G. S. Guralnik, C. R. Hagen a T. W. Kibble, Phys. Rev. Lett. **13** (1964) 585.

[10] M. E. Peskin and D. V. Schroeder,An Introduction to Quantum Field Theory, The Advanced Book Program, Westview Press 1995.

[11] ATLAS Collaboration, *Observation of a new particle in the search for the Standard Model Higgs boson with the ATLAS detector at the LHC,* Phys. Lett. B **716** (2012) 1.

[12] CMS Collaboration, *Observation of a new boson at a mass of 125 GeV with the CMS experiment at the LHC,* Phys. Lett. B **716** (2012) 30.

[13] K.A. Olive et al. (Particle Data Group), Chin. Phys. C **38**, 090001 (2014).

[14] P. Fayet a S. Ferrara, *Supersymmetry,* Phys. Rep. **32**, 249 (1977).

[15] M. F. Sohnius, Phys. Rep. **128**, 39-204 (1985).

[16] A. Djouadi, Phys. Rep., **459**, 1-241 (2008).

[17] N. Arkany-Hamed, S. Dimopoulos a G. Dvali, Physics Letters B **429**, 263 (1998).

[18] L. Randall a R. Sundrum, Phys. Rev. Lett. **83**, 3370 (1999).

[19] E. Farhi a L. Suskind, Phys. Rep. **74**, 227-321 (1981).

[20] G. H. Glashow, Phys. Rev. Lett. **32**, 438-441 (1974).

[21] A. Salam, Phys. Rev. D **10**, 275-280 (1974).

[22] M. B. Green, J. H. Schwartz a E. Witten, Superstring Theory, Cambridge: Cambridge Univ. Press, 1987.

[23] G. G. Ross, *Models and Phenomenology of Superstring Theories*, CERN-TH.5109/88, 1988.

[24] J. M. Duff, *M-Theory (the Theory Formerly Known as Strings),* Int. Jour. of Modern Physics A **11**, 5623-5642, (1996).

[25] H. P. Nilles, *Supersymmetry, Supergravity and Particle Physics,* Phys. Rep. 110, 1 (1984).

[26] D. Acosta et al. (CDF Collaboration), Phys. Rev. D **71**, 032001 (2005).

[27] V. M. Abazov et al. (D0 Collaboration), Nucl. Instrum. Meth. A **565**, 463 (2006);

[28] F. Abe et al. (CDF Collaboration), Phys. Rev. Lett. **74**, 2626 (1995).

[29] S. Abachi, et al. (D0 Collaboration), Phys. Rev. Lett. **74**, 2632 (1995), hep-ex/9503003

[30] The CDF Collaboration web-page, "http://www-cdf.fnal.gov/physics/physics.html"

[31] The D0 Collaboration web-page, "http://www-d0.fnal.gov"

[32] File:cern-accelerator-complex.svg. http://commons.wikimedia.org/wiki/File:Cern-accelerator-complex.svg, 2014. Accessed 12.1.2015.

[33] ATLAS Collaboration, The ATLAS Experiment at the CERN Large Hadron Collider, JINST **3** (2008) S08003.

[34] CMS Collaboration, The CMS experiment at the CERN LHC, JINST **3** (2008) S08004.

[35] M. Davier, A. Hoecker, B. Malaescu, Z. Zhang, Eur. Phys. J. C **71**, 1515 (2011).

[36] M. Baak et al., Eur. Phys. J. C **72** (2012) 2205, DOI 10.1140/epjc/s10052-012-2205-9.

[37] Gfitter web page: "http://project-gfitter.web.cern.ch/project-gfitter/Standard_Model/index.html"

[38] ATLAS Collaboration, Phys. Rev. D **90**, 052004 (2014) [arXiv:1406.3827].

[39] CMS Collaboration, Eur. Phys. J. C **74** (2014) 3076 [arXiv:1407.0558].

[40] G. Degrassi et al., Nuovo Cim. C **037** (2014) 02, 47-53 [arXiv:1205.6497].

[41] G. Degrassi et al., JHEP **1208** (2012) 098 [arXiv:1205.6497]

[42] D. Buttazzo, G. Degrassi P. P. Giardino et al., JHEP, **1312** (2013) 089 [arXiv:1307.3536].

[43] O.V. Tarasov, A.A. Vladimirov and A.Y. Zharkov, Phys. Lett. B **93** (1980) 429; L.N. Mihaila and M. Steinhauser, Phys. Lett. B **303** (1993) 334 [hep-ph/9302208]; K.G. Chetyrkin and M.F. Zoller, JHEP, **1206** (2012) 033 [arXiv:1205.2892].

[44] F. Bezrukov et al. JHEP, **1210** (2012) 140 [arXiv:1205.2893]. D. Buttazzo et al., JHEP, **1312** (2013) 089 [arXiv:1307.3536].

[45] S.R. Coleman, Phys. Rev. D **15** (1997) 2929 [Erratum-ibid. D 16 (1977) 1248].

[46] C. Ford, I. Jack, and D.R.T. Jones, Nucl. Phys. B **387** (1992) 373 [Erratum ibid. 504 (1997) 551] [hep-ph/0111190].

[47] S.P. Martin, Phys. Rev. D **65** (2002) 116003 [hep-ph/0111209].

[48] Czarnecki et al., Nucl. Phys. B **544** (1999) 520.

[49] A. Denner and T. Sack, Nucl. Phys. B **358**, 46 (1991).

[50] M. Czakon, P. Fiedler and A.Mitov, Phys. Rev. Lett. **110** (2013) 252004 [arXiv:1303.0693].

[51] M. Cacciari, M. Czakon, M. Mangano, A. Mitov, P. Nason, Phys. Lett. B **710** (2012) 612.

[52] Phys. Rev. D **83**, 091503(R) (2011), Phys. Rev. D **82**, 054028 (2010).

[53] ATLAS Collaboration, Eur. Phys. J. C **74** (2014) 3109 [arXiv:1012.1792].

[54] CMS Collaboration, J. High Energy Phys. **02** (2014) 024; [arXiv:1312.7582]; CMS-TOP-12-007.

[55] L. Lyons, D. Gibaut and P. Clifford, How to combine correlated estimates of a single physical quantity, Nucl. Instrum. Meth. A **270** (1988) 110.

[56] ATLAS Collaboration, Eur. Phys. J. C **71** (2011) 1577, ATLAS Collaboration, Phys. Lett. B **717** (2012) 89.

[57] CMS Collaboration, Phys. Rev. D **84** (2011) 092004,
CMS Collaboration, Phys. Lett. B **720** (2013) 83.

[58] ATLAS Collaboration, ATLAS-CONF-2012-024;
ATLAS Collaboration, ATLAS-CONF-2012-131;
ATLAS Collaboration, EPJ C73 (2013) 2328;
ATLAS Collaboration, ATLAS-CONF-2012-031.

[59] CMS Collaboration, Eur. Phys. J. C **73** (2013) 2386;
CMS Collaboration, J. High Energy Phys. **05** (2013) 065;
CMS Collaboration, Eur. Phys. J. C **72** (2012) 2202;
CMS Collaboration, J. High Energy Phys. **11** (2012) 067;
CMS Collaboration, J. High Energy Phys. **06** (2012) 109;
CMS Collaboration, Phys. Rev. D **85** (2012) 112007;
CMS Collaboration, J. High Energy Phys. **07** (2011) 049;
CMS Collaboration, Phys. Lett. B **695** (2011) 424.

[60] M. Aliev et al., Comput. Phys. Commun. **182** (2011) 1034-1046.

[61] ATLAS Collaboration, Phys. Rev. D **90** (2014) 072004.

[62] J. Alwall, M. Herquet, F. Maltoni, O. Mattelaer and T. Stelzer, MadGraph 5: going beyond, JHEP **06** (2011) 128 [arXiv:1106.0522].

[63] S. Frixione, P. Nason and C. Oleari, Matching NLO QCD computations with parton showers imulations: the POWHEG method, JHEP **11** (2007) 070 [arXiv:0709.2092].

[64] S. Frixione and B. Webber, J. High Energy Phys. **0206** 029 (2002), [arXiv:hep-ph/0204244];
S. Frixione, P. Nason and B. Webber, J. High Energy Phys. **0308** 007 (2003), [arXiv:hep-ph/0305252].

[65] N. Kidonakis, Phys. Rev. D **82**, 114030 (2010), doi:10.1103/PhysRevD.82.114030. arXiv:1009.4935 [hep-ph].

[66] N. Kidonakis, The top quark rapidity distribution and forward-backward asymmetry. Phys. Rev. D **84**, 011504(R) (2011), doi:10.1103/PhysRevD.84.011504. arXiv:1105.5167.

[67] V. Ahrens et al., Renormalization-group improved predictions for top-quark pair production at hadron colliders. arXiv:1003.5827 [hep-ph] (2010).

[68] T. Sjostrand, S. Mrenna, and P. Z. Skands, PYTHIA 6.4 Physics and Manual, JHEP 0605 (2006) 026, [hep-ph/0603175].

[69] G. Corcella et al., J. High Energy Phys. **0101** 010 (2001), [arXiv:hep-ph/0011363].

[70] M. L. Mangano et al., J. High Energy Phys. **07**, 001 (2003), arXiv:0206293 [hep-ph].

[71] ATLAS Collaboration, Measurement of the differential cross-section of highly boosted top quarks as a function of their transverse momentum using the ATLAS detector in $\sqrt{s}$ = 8 TeV proton-proton collisions, ATLAS-CONF-2014-057 (2014).

[72] CMS Collaboration, Measurement of the differential cross section for top quark pair production in pp collisions at $\sqrt{s}$ = 8 TeV TOP-12-028 (2015) [arXiv:1505.04480].

[73] CMS Collaboration, Measurement of the differential ttbar cross section in the lepton+jets channel at 8 TeV, TOP-12-027 (2013).

[74] CMS Collaboration, Measurement of the Jet Multiplicity in Di-leptonic Top Quark Pair events at 8 TeV, TOP-12-041 (2013).

[75] CMS Collaboration, Measurement of missing transverse energy and other event-level observables in top pair events at $\sqrt{s}$ = 8 TeV, TOP-12-042 (2013).

[76] CMS Collaboration, Eur. Phys. J. C **74** (2014) 3060, DOI 10.1140/epjc/s10052-014-3060-7.

[77] ATLAS Collaboration, Phys. Rev. D **91**, 072007 (2015) [arXiv:1502.00586].

[78] A.H. Hoang, A. Jain, I. Scimemi and I.W. Stewart, Phys. Rev. Lett. **101**, 151602 (2008) [arXiv:0803.4214].

[79] M. Beneke and V. Braun, Nucl. Phys. B **426**, 301 (1994).

[80] M.C. Smith and S. Willenbrock, Phys. Rev. Lett. **79** (1997) 3825-3828 [arXiv:9612329].

[81] N. Gray et al., Z. Phys. C **48** (1990) 673;
K.G. Chetyrkin and M. Steinhauser, Nucl. Phys. B **573** (2000) 617, hep-ph/9911434;
K. Melnikov and T.v. Ritbergen, Phys. Lett. B **482** (2000) 99, hep-ph/9912391.

[82] U. Langenfeld, S. Moch and P. Uwer, Phys. Rev. D **80** (2009) 054009 [arXiv:0906.5273].

[83] CDF Collaboration, Phys. Rev. D **73** (2006) 032003.

[84] K. Kondo, J. Phys. Soc. Jpn. **60** (1991), p. 836.

[85] F. Fiedler, A. Grohsjean, P. Haefner,P. Schieferdecker, Nucl. Instr. and Meth. A **624**, 203 (2010).

[86] ATLAS Collaboration, Eur. Phys. J. C **73** (2013) 2261.

[87] ATLAS Collaboration, Measurement of the Top Quark Mass from $\sqrt{s} = 7$ TeV ATLAS Data using a 3-dimensional Template Fit, ATLAS-CONF-2013-046 (2013).

[88] CMS Collaboration, Eur. Phys. J. C **72** (2012) 2202

[89] CMS Collaboration, JHEP **12** (2012) 105.

[90] CMS Collaboration, Eur. Phys. J. C **73** (2013) 2494

[91] ATLAS Collaboration, *ATLAS public web page,* [Online]. Available: https://twiki.cern.ch/twiki/bin/view/AtlasPublic

[92] CMS Collaboration, *CMS public web page,* [Online]. Available: //cms.web.cern.ch/org/cms-papers-and-results.

[93] D0 Collaboration, Phys. Rev. Lett. **80**, 2063 (1998). doi:10.1103/PhysRevLett.80.2063 [arXiv:hep-ex/9706014].

[94] CMS Collaboration, Phys. Lett. B **728** (2014) 496.

[95] S. Alioli et al., Eur. Phys. J C **73** (2013) 2438 [arXiv:1303.6415].

[96] ATLAS Collaboration, ATLAS-CONF-2014-053.

[97] D0 Collaboration, Direct measurement of the mass difference between top and antitop quarks, Phys. Rev. D **84** (2011) 052005 [arXiv:1106.2063].

[98] CDF Collaboration, Measurement of the mass difference between top and antitop quarks, Phys. Rev. D **87**, 052013 (2013).

[99] CMS Collaboration, Measurement of the mass difference between top and antitop quarks, JHEP **06** (2012) 109.

[100] ATLAS Collaboration, Measurement of the mass difference between top and anti-top quarksin pp collisions at $\sqrt{s} = 7$ TeV using the ATLAS detector, Phys. Lett. B **728** (2014) 363.

[101] M. Kobayashi, T. Maskawa, Prog. Theor. Phys. **49** (1973).

[102] T. M. P. Tait, C. P. Yuan, Phys. Rev. D **63** (2000) 014018, [arXiv:hepph/0007298].

[103] A. S. Belyaev, E. E. Boos, and L.V. Dudko, Phys. Rev. D **59**, 075001 (1999).

[104] J.M. Campbell, R. Frederix, F. Maltoni and F. Tramontano, Phys. Rev. Lett. **102**, 182003 (2009).

[105] A.S. Papanastasioiu, R. Frederix, S. Frixione, V. Hirshi and F. Maltoni, Phys. Lett. B **726**, 223 (2013).

[106] R. Schwienhorst, C. -P. Yuan, C. Mueller and Q. -H. Cao, Phys. Rev. D **83**, 034019 (2011).

[107] P. Falgari, F. Giannuzzi, P. Mellor and A. Signer, Phys. Rev. D 83, 094013 (2011).

[108] N. Kidonakis, Phys. Rev. D **83**, 091503 (2011).

[109] N. Kidonakis, Phys. Rev. D **81**, 054028 (2010).

[110] N. Kidonakis, Phys. Rev. D **82**, 054018 (2010).

[111] H. X. Zhu, C. S. Li, J. Wang and J. J. Zhang, JHEP **1102**, 099 (2011).

[112] S. Frixione, E. Laenen, P. Motylinksi and B. Webber and C. D. White, JHEP **07**, 029 (2013).

[113] R. Frederix, E. Re and P. Torrielli, JHEP **1209**, 130 (2012).

[114] S. Alioli, P. Nason, C. Oleari and E. Re, JHEP **0909**, 111 (2009) [Erratum-ibid. **1002**, 011 (2010)].

[115] M. Brucherseifer, F. Caola and K. Melnikov, On the NNLO QCD corrections to single-top production at the LHC, [arXiv:1404.7116v1].

[116] V. M. Abazov et al. (D0 Collaboration), Phys. Rev. Lett. **103**, 092001 (2009).

[117] T. Aaltonen et al. (CDF Collaboration), Phys. Rev. Lett. **103**, 092002 (2009).

[118] CDF Collaboration, Phys. Rev. D **82** (2010) 112005, doi:10.1103/PhysRevD.82.112005 [arXiv:1004.1181].

[119] D0 Collaboration, V.M. Abazov, et al., Phys. Rev. D **84**, 112001 (2011).

[120] CDF Collaboration, T. Aaltonen, et al., Phys. Rev. Lett. **112** (2014) 231804 [arXiv:1402.0484].

[121] D0 Collaboration, V.M. Abazov, et al., Phys. Lett. B **726** (2013) 656 [arXiv:1307.0731].

[122] ATLAS Collaboration, Phys. Rev. D **90**, 112006 (2014).

[123] ATLAS Collaboration, ATLAS-CONF-2012-132.

[124] M. Feindt and U. Kerzel, The NeuroBayes Neural Network Package, Nucl. Instrum. Meth. A **559**, 190 (2006).

[125] CMS Collaboration, JHEP **12** (2102) 1, doi:10.1103/JHEP **12** (2012) 035.

[126] CMS Collaboration, CMS PAS TOP-12-011 (2012).

[127] Y.R. Quinlan, Int. J. Man-Mach. Stud. **28** (1987) 221.

[128] ATLAS and CMS Collaborations, Combination of single top-quark cross-section measurements in the t-channel at $\sqrt{s}$ = 8 TeV with the ATLAS and CMS experiments, ATLAS-CONF-2013-098, CMS-PAS-TOP-12-002 (2013).

[129] C. D. White, S. Frixione, E. Laenen, and F. Maltoni, J. High Energy Phys. **11** (2009) 074;
Phys. Rev. D **63** (2000) 014018, doi:10.1103/PhysRevD.63.014018 [arXiv:hep-ph/0007298].

[130] Q.-H. Cao, J. Wudka, and C.-P. Yuan, Phys. Lett. B **658**, 50 (2007).

[131] V. Barger, M. McCaskey, and G. Shaughnessy, Phys. Rev. D **81**, 034020 (2010).

[132] CDF and D0 Collaborations, Phys. Rev. Lett. **112**, 231803 (2014)

[133] ATLAS Collaboration, Search for s-channel single top-quark production in pp collisions at $\sqrt{s}$ = 7 TeV ATLAS-CONF-2011-118 (2011).

[134] CMS Collaboration, Search for s-channel single top-quark production in pp collisions at $\sqrt{s}$ = 8 TeV, CMS PAS TOP-13-009 (2013).

[135] ATLAS Collaboration, Search for s-channel single top-quark production in protonproton collisions at vs = 8 TeV with the ATLAS detector Phys. Lett. B **740** (2015) 118.

[136] A. Czarnecki, J. Korner, J. Piclum, Phys. Rev. D 81 (2010) 111503 [arXiv:10005.2625].

[137] J. Aguilar-Saavedra, Nucl. Phys. B **812** (2009) 181 [arXiv:0811.3842].

[138] J. Aguilar-Saavedra, A minimal set of top-Higgs anomalous couplings, Nucl. Phys. B **821** (2009) 215 [arXiv:0904.2387].

[139] J. A. Aguilar-Saavedra, Nucl. Phys. B **351** (2010) 90.

[140] CDF and D0 Collaborations, T. Aaltonen et al., Combination of CDF and D0 measurements of the W boson helicity in top quark decays, Phys. Rev. D **85** (2012) 071106 [arXiv:1202.5272].

[141] ATLAS Collaboration, JHEP **1206** (2012) 088.

[142] ATLAS and CMS Collaborations, Combination of the ATLAS and CMS measurements of the W-boson polarization in top-quark decays, ATLAS-CONF-2013-033, CMS PAS TOP-12-025 (2013).

[143] CMS Collaboration, Measurement of the W-boson helicity in top-quark decays from tt production in lepton+jets events in pp collisions at $\sqrt{s}$ = 7 TeV, JHEP **10** (2013) 167, doi:10.1007/JHEP10 (2013) 167

[144] CMS Collaboration, Measurement of the W helicity in top pair production with dileptons at 7 TeV, CMS PAS TOP-12-015 (2013).

[145] CMS Collaboration, Measurement of the W-boson helicity in top decays from $t\bar{t}$ production in lepton+jets events at the LHC at $\sqrt{s}$ = 8 TeV, CMS PAS TOP-13-008 (2013).

[146] CMS Collaboration, W-helicity measurement in single top events topology, CMS PAS TOP-12-020 (2013).

[147] CMS Collaboration, JHEP01(2015)053, doi:10.1007/JHEP01(2015)053

[148] ATLAS and CMS Collaborations, Combination of the ATLAS and CMS measurements of the W-boson polarization in top-quark decays, ATLAS-CONF-2013-033, CMS PAS TOP-12-025 (2013).

[149] W. Bernreuther and Z. G. Si, Nucl. Phys. B **837**, 90 (2010).

[150] R. M. Harris, C. T. Hill, and S. J. Parke [arXiv:hep-ph/9911288].

[151] M. Arai, N. Okada, K. Smolek, and V. Simak, Acta Phys. Pol. B **40**, 93 (2009).

[152] W. Bernreuther, M. Flesch, and P. Haberl, Phys. Rev. D **58**, 114031 (1998).

[153] T. Aaltonen et al. (CDF Collaboration), Phys. Rev. D **83**, 031104 (2011).

[154] V. M. Abazov et al. (D0 Collaboration), Phys. Lett. B **702**, 16 (2011).

[155] K. Melnikov and M. Schulze, Phys. Lett. B **700**, 17 (2011).

[156] V. M. Abazov et al. (D0 Collaboration), Phys. Rev. Lett. **107**, 032001 (2011).

[157] V. M. Abazov et al. (D0 Collaboration), Phys. Rev. Lett. **108**, 032004 (2012).

[158] ATLAS Collaboration, Phys. Rev. Lett. **108**, 212001 (2012).

[159] ATLAS Collaboration, Phys. Rev. D **90**, 112016 (2014), DOI: 10.1103/PhysRevD.90.112016.

[160] W. Bernreuther and Z.-G. Si, Phys. Lett. B **725**, 115 (2013).

[161] G. Mahlon and S. J. Parke, Phys. Rev. D **81**, 074024 (2010).

[162] S. J. Parke and Y. Shadmi, Phys. Lett. B **387**, 199 (1996).

[163] P. Uwer, Phys. Lett. B **609**, 271 (2005).

[164] CMS Collaboration, Phys. Rev. Lett. **112**, 182001 (2014).

[165] W. Bernreuther, A. Brandenburg, Z. G. Si, and P. Uwer, Phys. Rev. Lett. **87**, 242002 (2001).

[166] A. Brandenburg, Z. G. Si, and P. Uwer, Phys. Lett. B **539**, 235 (2002).

[167] ATLAS Collaboration, Measurement of Spin Correlation in TopAntitop Quark Events and Search for Top Squark Pair Production in pp Collisions at $\sqrt{s}$ =8 TeV Using the ATLAS Detector, [arXiv:1412.4742].

[168] O. Antunano, J.H. Kuhn and G. Rodrigo, Phys. Rev. D **77** (2008) 014003 [arXiv:0709.1652].

[169] P. Ferrario and G. Rodrigo, Phys. Rev. D **78** (2008) 094018 [arXiv:0809.3354].

[170] S. Jung, H. Murayama, A. Pierce and J.D. Wells, Phys. Rev. D **81** (2010) 015004 [arXiv:0907.4112].

[171] J. Shu, T.M. Tait and K. Wang, Phys. Rev. D **81** (2010) 034012 [arXiv:0911.3237].

[172] S. Jung, A. Pierce and J.D. Wells, Phys. Rev. D **83** (2011) 114039 [arXiv:1103.4835].

[173] A. Djouadi, G. Moreau, F. Richard and R.K. Singh, Phys. Rev. D **82** (2010) 071702 [arXiv:0906.0604].

[174] J. Aguilar-Saavedra and M. Perez-Victoria, JHEP **05** (2011) 034 [arXiv:1103.2765].

[175] I. Dorsner, S. Fajfer, J.F. Kamenik and N. Kosnik, Phys. Rev. D **81** (2010) 055009 [arXiv:0912.0972].

[176] B. Grinstein, A.L. Kagan, M. Trott and J. Zupan, Forward-backward asymmetry in tt-bar production from flavour symmetries, Phys. Rev. Lett. **107** (2011) 012002 [arXiv:1102.3374].

[177] Z. Ligeti, G. Marques Tavares and M. Schmaltz, Explaining the tt forward-backward asymmetry without dijet or flavor anomalies, JHEP **06** (2011) 109 [arXiv:1103.2757].

[178] P. Ferrario and G. Rodrigo, Phys. Rev. D **80** (2009) 051701 [arXiv:0906.5541].

[179] P.H. Frampton, J. Shu and K. Wang, Axigluon as possible explanation for $p\bar{p} \to t\bar{t}$ forward-backward asymmetry, Phys. Lett. B **683** (2010) 294 [arXiv:0911.2955].

[180] J.H. Kuhn, G. Rodrigo, Charge asymmetry in hadroproduction of heavy quarks, Phys. Rev. Lett. **81**, 49-52 (1998) [arXiv:hep-ph/9802268].

[181] J. H. Kuhn, G. Rodrigo, Charge asymmetry of heavy quarks at hadron colliders, Phys. Rev. D **59**, 054017 (1999).

[182] W. Bernreuther and Z.-G. Si, Top quark and leptonic charge asymmetries for the Tevatron and LHC, Phys. Rev. D **86** (2012) 034026 [arXiv:1205.6580].

[183] ATLAS Collaboration, Measurement of the top quark pair production chargeasymmetry in proton-proton collisions at $\sqrt{s}$ = 7 TeV using the ATLAS detector, JHEP **02** (2014) 107.

[184] ATLAS Collaboration, Measurement of the charge asymmetry in dileptonic decays of top quark pairs in pp collisions at $\sqrt{s}$ = 7 TeV using the ATLAS detector, submitted to JHEP [arXiv:1501.0738] (2015).

[185] CMS Collaboration, Inclusive and differential measurements of the tt charge asymmetry in proton-proton collisions at $\sqrt{s}$ = 7 TeV, Phys. Lett. B **717** (2012) 129.

[186] CMS Collaboration, Measurements of the tt-bar charge asymmetry using the dilepton decay channel in pp collisions at $\sqrt{s}$ = 7 TeV, JHEP **04** (2014) 191.

[187] ATLAS and CMS Collaborations, Combination of ATLAS and CMS tt-bar charge asymmetry measurements using LHC proton-proton collisions at $\sqrt{s}$ = 7 TeV, ATLAS-CONF-2014-012, CMS-PAS-TOP-14-006, https://cds.cern.ch/record/1670535 (2014).

[188] CMS Collaboration, Measurement of the tt-bar charge asymmetry with lepton+jets events at 8 TeV, CMS PAS TOP-12-033 (2013).

[189] J. H. Kuhn and G. Rodrigo, *Charge asymmetries of top quarks at hadron colliders revisited*, JHEP **1201** (2012) 063, doi:10.1007/JHEP01(2012)063 [arXiv:1109.6830].

[190] G. Rodrigo and P. Ferrario, *Charge asymmetry: A theory appraisal*, Nuovo Cim. C **33** (2010) 221, doi:10.1393/ncc/i2010-10646-5 [arXiv:1007.4328].

[191] E. Gabrielli, M. Raidal, and A. Racioppi, *Implications of the effective axial-vector coupling of gluon on top-quark charge asymmetry at the LHC*, Phys. Rev. D **85** (2012) 074021, doi:10.1103/PhysRevD.85.074021 [arXiv:1112.5885].

[192] E. Gabrielli and M. Raidal, *Effective axial-vector coupling of gluon as an explanation to the top quark asymmetry*, Phys. Rev. D **84** (2011) 054017, doi:10.1103/PhysRevD.84.054017 [arXiv:1106.4553].

[193] S. L. Glashow, J. Iliopoulos, and L. Maiani, Phys. Rev. D **2**, 1285 (1970).

[194] J. M. Yang, B.-L. Young, and X. Zhang, Phys. Rev. D **58**, 055001 (1998).

[195] G. Lu, F. Yin, , and L.Wan, Phys. Rev. D **68**, 015002 (2003).

[196] J. A. Aguilar-Saavedra, Phys. Rev. D **67**, 035003 (2003).

[197] J.A. Aguilar-Saavedra, Acta Phys. Pol. B **35** (2004) 2695.

[198] K. Agashe et al. [arXiv:1311.2028].

[199] ATLAS Collaboration, J. High Energy Phys. **09** (2012) 041.

[200] CMS Collaboration, Phys. Rev. Lett. **111**, 211804 (2013).

[201] P. J. Fox, Z. Ligeti, M. Papucci, G. Perez, and M. D. Schwartz, Phys. Rev. D **78**, 054008 (2008).

[202] CDF Collaboration, T. Aaltonen et al., Search for the flavor changing neutral current decay t $\rightarrow$ Zq in $p\bar{p}$ collisions at $\sqrt{s}$ = 1.96 TeV, Phys. Rev. Lett. **101** (2008) 192002, [arXiv:0805.2109].

[203] CDF Collaboration, Search for top-quark production via flavor-changing neutral currents in W + 1 jet events at CDF, Phys. Rev. Lett. **102** (2009) 151801 [arXiv:0812.3400].

[204] D0 Collaboration, Search for flavor changing neutral currents via quark-gluon couplings in single top quark production using 2.3 fb^{-1} of $p\bar{p}$ collisions, Phys. Lett. B **693** (2010) 81 [arXiv:1006.3575].

[205] D0 Collaboration, Search for flavor changing neutral currents in decays of top quarks, Phys. Lett. B **701** (2011) 313 [arXiv:1103.4574].

[206] OPAL Collaboration, Search for single top quark production at LEP-2, Phys. Lett. B **521** (2001) 181 [hep-ex/0110009].

[207] ALEPH Collaboration, Search for single top production in e+e- collisions at $\sqrt{s}$ up to 209 GeV, Phys. Lett. B **543** (2002) 173 [hep-ex/0206070].

[208] L3 Collaboration, Search for single top production at LEP, Phys. Lett. B **549** (2002) 290 [hep-ex/0210041].

[209] DELPHI Collaboration, Search for single top production via FCNC at LEP at $\sqrt{s}$ = 189 GeV to 208 GeV, Phys. Lett. B **590** (2004) 21 [hep-ex/0404014].

[210] ZEUS Collaboration, Search for single-top production in *ep* collisions at HERA, Phys. Lett. B **708** (2012) 27 [arXiv:1111.3901].

[211] H1 Collaboration, Search for single top quark production at HERA, Phys. Lett. B **678** (2009) 450 [arXiv:0904.3876].

[212] H1 Collaboration, A. Aktas et al., Search for single top quark production in *ep* collisions at HERA, Eur. Phys. J. C **33** (2004) 9 [hep-ex/0310032].

[213] ZEUS Collaboration, Search for single top production in *ep* collisions at HERA, Phys. Lett. B **559** (2003) 153 [hep-ex/0302010].

[214] ATLAS Collaboration, A search for flavour changing neutral currents in top-quark decays in pp collision data collected with the ATLAS detector at $\sqrt{s}$ = 7 TeV, J. High Energy Phys. **09** (2012) 139.

[215] CMS Collaboration, Search for flavor changing neutral currents in top quark decays in *pp* collisions at 7 TeV, Phys. Lett. B **718**, 1252 (2013).

[216] CMS Collaboration, Search for flavor changing neutral currents in top quark decays in proton-proton collisions at $\sqrt{s}$ = 8 TeV, Phys. Rev. Lett. **112**, 171802 (2014) [arXiv:1312.7582].

[217] ATLAS Collaboration, Search for FCNC single top-quark production at $\sqrt{s}$ = 7 TeV with the ATLAS detector, Phys. Lett. B **712**, 351 (2012).

[218] CMS Collaboration, Search for Flavor-Changing Neutral Currents in tZ events in proton-proton collisions at $\sqrt{s}$ = 7 TeV, CMS PAS TOP-12-021 (2013).

[219] M. Hosch, K. Whisnant, B. Young, Phys. Rev. D **56** (1997) 5725.

[220] E. Malkawi, T.M. Tait, Phys. Rev. D **54** (1996) 5758.

[221] CDF Collaboration, Phys. Rev. Lett. **112** (2009) 151801.

[222] D0 Collaboration, Phys. Lett. B **683** (2010) 81.

[223] ATLAS Collaboration, Search for FCNC single top-quark production at $\sqrt{s}$ = 7 TeV with the ATLAS detector, Phys. Lett. B **712** (2012) 351.

[224] M. Feindt, U. Kerzel, Nucl. Instrum. Methods A **559** (2006) 190.

[225] J. Gao, C.S. Li, L.L. Yang, H. Zhang, Phys. Rev. Lett. **107** (2011) 092002.

[226] J.J. Liu, C.S. Li, L.L. Yang, L.G. Jin, Phys. Rev. D **72** (2005) 074018.

[227] J.J. Zhang, C.S. Li, J. Gao, H. Zhang, Z. Li, et al., Phys. Rev. Lett. **102** (2009) 072001.

[228] CMS Collaboration, Search for Flavor-Changing Neutral Currents in tZ events in proton-proton collisions at $\sqrt{s}$ = 7 TeV, CMS PAS TOP-12-021, July 2013.

[229] J. Gao, C.S. Li, and H. X. Zhu, *Top Quark Decay at Next-to-Next-to Leading Order in QCD*, Phys. Rev. Lett. **110** (2013) 042001, doi:10.1103/PhysRevLett.110.042001.

[230] ATLAS Collaboration, Measurement of the top quark charge in *pp* collisions at $\sqrt{s}$ = 7 TeV with the ATLAS detector, JHEP **11** (2013) 031 [arXiv:1307.4568].

[231] CMS Collaboration, Constraints on the Top-Quark Charge from Top-Pair Events, CMS PAS TOP-11-031 (2012).

Doc. RNDr. Stanislav Tokár, CSc. born in February 1952 received his PhD degree in physics in 1984. He is associated professor at Faculty of Mathematics, Physics and Informatics, Comenius University in Bratislava. He actively participates on the CERN and Fermilab research programs as a leader of two research groups: ATLAS-Bratislava (since 1995) and CDF-Slovakia (since 2006). In 2013, he got Slovak award Scientist of the year 2013. His research interests include production of radionuclides, hadron-nuclear interactions and experimental studies of properties of the top and b quarks.